Structural and functional characterization of profilin from *Schistosoma japonicum*

Dissertation submitted to the

Department of Chemistry,
Faculty of Mathematics, Informatics and Natural Sciences
of the University of Hamburg

for the award of the degree of
Doctor in Science

Nele Vervaet

Hamburg
July 2015

The research work reported in this dissertation was carried out from October 2010 until December 2013 in the research laboratory of Prof. Dr. Inari Kursula at the Centre for Structural Systems Biology - Helmholtz Centre for Infection Research and University of Hamburg, Hamburg, Germany.

Reviewers of the dissertation

Dr. Inari Kursula (promotor)

Prof. Dr. Dr. Christian Betzel

Examiners

Dr. Inari Kursula (promotor)

Prof. Dr. Andrew Torda

Prof. Dr. Wolfgang Maison

Abstract

Schistosomiasis, also known as bilharzia, is considered the second most socio-economically devastating disease after malaria in the (sub)tropical areas. Schistosomiasis is rather effectively treated by praziquantel. However, drug and repeated infections urge the scientific community to search for potent vaccine targets from the *Schistosoma* proteome. A key to drug and vaccine development is understanding how parasite-host recognition works at the molecular level. Neodermatan flatworms contain a unique cellular organ, the syncytial tegument, which plays an important role in host infection. Cytoskeletal proteins form a major fraction of *Schistosoma* tegumental proteins and are, thus, attractive drug targets.

An important cytosolic regulator of actin dynamics in eukaryotes is profilin. In addition to actin, profilins bind to polyproline stretches and acidic phospholipids, which makes them important keys in linking signal transduction to the actin cytoskeleton. This work focused on the biochemical and structural characterization of profilin of *Schistosoma japonicum* (*Sj*Pfn). Profilins control a complex network of molecular interactions and bind different ligands through poly-L-proline repeats. Here, the ability of *Sj*Pfn to bind octaproline repeats was shown by fluorescence spectroscopy. On the contrary, no binding could be observed for proline-rich peptides derived from *S. japonicum* formin. The crystal structure of *Sj*Pfn shows a highly conserved overall fold but also several crucial differences in the peptide binding site compared to canonical profilins.

Profilins sequester monomeric actin. This main characteristic of the profilin family was confirmed for *Sj*Pfn using polymerization kinetics and cosedimentation assays. Increasing concentrations of *Sj*Pfn decrease the rate of actin polymerization by keeping actin in its monomeric, soluble form. The crystal structure of the *Sj*Pfn-actin complex showed that *Sj*Pfn binds actin to the canonical actin-binding face, but the binding site itself is remarkably unconserved. The structural and functional information obtained here, provide insight into the profilin-mediated actin dynamics in *S. japonicum* and clues on the immunogenicity of *Sj*Pfn.

Zusammenfassung

Schistosomiasis, auch als Billharziose bekannt, ist nach Malaria die sozioökonomisch verheerendste Infektionskrankheit in den (sub)tropischen Regionen. Schistosomiasis kann mit Praziquantel behandelt werden, aber Medikamentenresistenz und wiederkehrende Infektionen erfordern Entwicklung von wirksamen Impfungen gegen die Krankheit. Ein Schlüssel zur Medikamenten- und Impfstoffentwicklung ist das Verständnis, wie die Parasit-Wirterkennung auf molekularer Ebene funktioniert. Neodermatan Plattwürmer besitzen ein einzigartiges Zellorgan, das syncytial Tegument, das eine wichtige Rolle bei der Infektion spielt. Zytoskelettproteine formen eine große Fraktion von *Schistosoma* tegument und sind somit interessante Ziele für Medikamentenentwicklung.

Ein wichtiger zytosolischer Regulator der Aktindynamik in Eukaryoten ist Profilin. Außer an Aktin, binden Profiline auch an Polyprolinketten und sauren Phospholipiden, was sie zu wichtigen Schlüsseln zwischen Signaltransduktion und dem Aktinzytoskelett macht. Diese Dissertation befasst sich mit der biochemischen und strukturellen Charakterisierung von Profilin des *Schistosoma japonicum* (*Sj*Pfn). Profiline kontrollieren ein komplexes Netzwerk von molekularen Interaktionen durch Bindung an Liganden mit Poly-L-Prolinketten. Hier wurde die Fähigkeit zu binden von *Sj*Pfn Octaprolinketten gezeigt. Im Gegensatz dazu, konnte keine Bindung von Peptiden von *S. japonicum* Formin nachgewiesen werden. Die Kristallstruktur von *Sj*Pfn zeigt eine hohe Konservierung von der Gesamtstruktur, aber auch wesentliche Unterschiede in der Peptidbindungsstelle im Vergleich zu kanonischen Profilinen.

Profilin sequestriert monomeres Aktin. Diese Hauptcharakteristik der Profilinfamilie wurde für *Sj*Pfn bestätigt. *Sj*Pfn reduziert die Geschwindigkeit der Aktinpolymerisation dadurch, dass es Aktin in seiner monomeren, löslichen Form hält. Die Kristallstruktur des Actin-*Sj*Pfn-Komplex zeigt, dass das *Sj*Pfn-Aktin an die bekannte Bindungsstelle bindet, aber die Interaktionen bemerkenswert unkonserviert sind. Die strukturellen und funktionellen Informationen geben Einblick in die Profilinvermittelte Aktindynamik in *S. japonicum* und in Hinweisen auf die Immunogenität von *Sj*Pfn.

Acknowledgements

Although I kept writing these pages for the very last moment, it gives me great pleasure to thank all the people who in one way or another have helped and supported me during the last five years.

First, I would like to thank my supervisor **Inari** for her support and guidance during my stay. Your assistance, understanding and patience were of great importance for completing this work. Thank you for giving me the freedom to find my way in this PhD while at the same time guiding me through.

I was very lucky to work with nice colleagues in the research group. **Juha**, your help has been unvaluable to enable me to complete my thesis, I am very grateful. Liebe **Susanne**, I will never forget the flowers in my office the first day I started work. You made me feel at home in the lab. I have many good memories from our coffee breaks, even if they were in German ;-). I was very lucky that we could work together on the *Sj*Pfn project when I was pregnant. **Moon** and **Gopi**, thanks for showing me an example of a proper PhD attitude when I arrived in the office, I wish you all the best for the future! **Katharina** and **Manuela**, your love for Hamburg has been contagious. Thanks for the nice moments in and outside the lab. I also thank my other colleagues in the group for making my time at DESY unforgettable: Petri, Huijong, Saara, Esa-Peka and the group members in Oulu.

Ook een woordje van dank naar de collega's van **L-ProBe**. Door nog steeds elke dag het onderzoekswereldje mee te beleven, geraakte ik niet vervreemd. Dit was een grote hulp en heeft me gestimuleerd dit boekje te schrijven.

Björn, we hadden nooit gedacht dat ons Hamburgavontuur zo zou aflopen. Ik ben nog steeds heel blij dat we in September 2010 de grote stap hebben gezet en dat ik vandaag een mooi einde aan dit hoofdstuk mag breien. De afgelopen jaren zijn niet mild voor ons geweest maar hebben me laten zien dat we samen veel aankunnen. Ook al werd hij niet altijd blij onthaald, je kritische wetenschapszin heeft zeker positief bijgedragen aan mijn thesiswerk. Bedankt voor alle liefde, steun en de goede papazorgen voor onze kleine deugniet **Florian**.

Mama en **papa**, dankzij jullie onvoorwaardelijke liefde en steun sta ik hier vandaag. Bedankt om me mijn eigen weg te laten kiezen. Toen ik op kot in Gent Biochemie en

Biotechnologie wou gaan studeren, maar ook toen we besloten voor een tijdje naar het buitenland te verhuizen. Mama, dankjewel voor de manden strijk en oppasdagen zodat ik me tenvolle kon concentreren tijdens het schrijven. Papa, het was een grote hulp dat ik op verplaatsing kon komen thesissen. Bedankt voor de gezellige koffiepauzes tussendoor!

Mijn liefste zus, **Céline**, jouw aanmoedigingen zorgden steeds voor dat extra duwtje in de rug. "Gij kunt dat, gij hebt discipline!" heb ik meermaals van jou mogen horen, met resultaat. **Domien**, wees maar zeker dat we er hier eentje op zullen drinken! Ook al ben je hier niet meer fysiek aanwezig, ik weet dat je meekijkt, lieve broer. Volgens Florian is nonkel **Maarten** een ster, heel hoog in de hemel, en dat geloof ik graag! Ik draag dit boekje graag op aan jou.

Meme Paula en **meme Spoele**, jullie zijn beide sterke vrouwen waar ik naar opkijk. Bedankt voor de steun en bezorgdheid al die jaren.

Ook in Wielsbeke voel ik me intussen thuis. **Dirk, Joke, Marleen, Filip, Sarah** en **Jens**, dankjewel voor de gezellige familie-uitjes naar West-Vlaanderen. Jullie zijn intussen familie geworden, bedankt om steeds voor ons klaar te staan.

Mijn studietijd was maar half zo leuk geweest zonder de vrienden van de Biochemie. **Elke**, **Laura**, **Kristof**, **Muriel**, **Benjamin**, bedankt voor de fijne tijd samen in Gent. Ik hoop dat we elkaar blijven zien!

De gezellige kletsavonden met de Lokerse vriendinnen doen steeds meer dan deugd en waren een groot gemis in het buitenland. **Marijke**, **Sanne**, **Jene**, **Evy**, **Vanessa**, **Machteld**, **Freya**, **Anneleen** en **Margot**, na een avondje meisjesgegiechel waren m'n batterijen steeds opgeladen om er verder tegenaan te gaan!

I could not have succeeded without the invaluable support of all of you!

Nele

Table of Contents

Abbreviations and symbols

Å	Ångström (10^{-10}m)
ADF	Actin-depolymerizing factor
AI	Auto-induction
Arp2/3	Actin related protein 2/3
ATP	adenosine triphosphate
ß-ME	ß-mercaptoethanol
BLAST	Basic Local Alignment Search Tool
CD	circular dichroism
CV	column volume
ddH_2O	double-distilled water
DESY	Deutsches Elektronen-Synchrotron
DNase	deoxyribonucleic acd
DTT	dithiothreitol
EDTA	ethylenediaminetetraacetic acid
EST	Expressed Sequence Tag
EtBr	ethidium bromide
ExPASy	Expert Protein Analysis System
GST	glutathione S-transferase
HEPES	hydroxyethyl piperazineethanesulfonic acid
HPSF	high purity salt free
Hs	*Homo sapiens*
IMAC	immobilized-metal affinity chromatography
IPTG	isopropyl ß-D-1-thiogalactopyranoside
ITC	isothermal calorimetry
K_d	dissociation constant
kDa	kilodalton
LB	lysogeny broth
MES	2-(N-morpholino)ethanesulfonic acid
MS	mass spectrometry
MWCO	molecular weight cut-off
m/z	mass-to-charge ratio
NMR	nuclear magnetic resonance

OD	optical density
PAGE	polyacrylamide gel electrophoresis
PCR	polymerase chain reaction
PDB	Protein Data Bank
PEG	polyethylene glycol
PIP	phosphatidylinositol 4-monophosphate
PIP_2	phosphatidylinositol 4,5-bisphosphate
PIPES	piperazine-N,N'-bis(2-ethanesulfonic acid)
PISA	Proteins, Interfaces, Structures and Assemblies
PLP	poly-L-proline
PETRA	Positron-Electron Tandem Ring Accelerator
SAD	single-wavelength anomalous diffraction
Sc	*Saccharomyces cerevisiae*
SDS	sodium dodecyl sulphate
SEC	size exclusion chromatography
SOC	super optimal broth with catabolite repression
SEM	scanning electron microscopy
SLIC	sequence and ligation independent cloning
SMN	survival of motor neuron protein
SSM	secondary-structure matching
TAE buffer	tris-acetate-EDTA buffer
TCEP	tris(2-carboxyethyl)phosphine
TEM	transmission electron microscopy
T_m	melting temperature
Tris	tris(hydroxymethyl)aminomethane
UV	ultraviolet
v/v	volume/volume
w/v	weight/volume

Amino acids

A	Ala	alanine	C	Cys	cysteine
D	Asp	aspartate	E	Glu	glutamate
F	Phe	phenylalanine	G	Gly	glycine
H	His	histidine	I	Ile	isoleucine
K	Lys	lysine	L	leu	leucine
M	Met	methionine	N	Asn	asparagine
P	Pro	proline	Q	Gln	glutamine
R	Arg	arginine	S	Ser	serine
T	Thr	threonine	V	Val	valine
W	Trp	tryptophan	Y	Tyr	tyrosine

List of figures

List of tables

1 Introduction

1.1 Schistosomiasis

Schistosomiasis, also known as bilharzia, is caused by parasitic blood flukes of the genus *Schistosoma*. These parasites can survive extended times in the blood circulation of their host, despite its specific immune response (Pearce and MacDonald, 2002). This is made possible by diverse mechanisms that the parasite has evolved to evade the host immune responses. The mechanisms, by which the parasite evades the snail-host defence response are currently not well understood. Succesful host-evasion mechanisms of the parasite involve the unique biophysical properties of the tegument, the recruitment of host components to the surface and the essential functions of various antigens and immune-regulating factors.

The disease poses a large health and socio-economic threat to developing countries in (sub)tropical regions. The chronic aspect of schistosomiasis affects many individuals with long-standing infections in poor rural areas (Engels *et al.*, 2002). More than 240 million people in 78 tropical and subtropical coutries are affected, of which more than 90% in Africa (WHO website).

1.1.1 Treatment

Used for over 20 years, praziquantel (PZQ; 2-cyclohexylcarbonyl-1,2,3,6,7,11b-hexahydro-4H-pyrazino{2,1-a} isoquinoline-4-one) is in most parts of the world the only antischistosomal chemotherapeutic treatment, which is commercially available (Fenwick *et al.*, 2003). The drug is effective against all schistosome species and induces only some side effects, such as vomiting, sweating and drowsiness. Although treatable with praziquantel, schistosomiasis is becoming an increasingly severe problem because of increasing drug resistance, the high re-infection rates in humans and animals and the requirement of frequent administration of the drug (McManus and Loukas, 2008).

Praziquantel interferes with inorganic ion transport thereby affecting calcium homeostasis in *Schistosoma*. The drug causes an increase in the calcium influx in the

organism, which initiates the schistosomal musculature to contract. This results in paralysis, damaging the adult schistosome tegument and exposing the surface antigens to the host immune system (Salvador-Recatalà and Greenberg, 2012).

Praziquantel is not equally effective against all life stages of schistosomal species. Juvenile schistosomes are refractory to the drug and only become sensitive when eggs are deposited. The mode of action and specific molecular target of praziquantel are undefined (Salvador-Recatalà and Greenberg, 2012). One suggested mechanism explains the mode of action *via* an ion channel subunit, Ca_vß, and the alteration of the schistosomal membrane fluidity (Greenberg, 2005; Kohn *et al.*, 2001). Voltage-gated Ca^{2+} channels are potential drug targets as they initiate the contraction of the schistosomal musculature, are involved in synaptic transmission and gene expression and have enzymatic activity. However, Valle *et al.* showed that subunits of the Ca^{2+} channel did not present structural differences between schistosomes that show different susceptibilities to PZQ (Valle *et al.*, 2003). The glutathione S-transferase (GST) in *S. japonicum* (*Sj*26), was also suggested as a possible interactor of PZQ but afterwards it was shown that there was no inhibition of GST activity by praziquantel (Milhon *et al.*, 1997).

Praziquantel is too hydrophobic to assume that it traverses the lipid bilayer of the worm by passive diffusion. In this context, a mechanism in which the drug binds to a surface membrane protein carrier to enter the worm was suggested. Tallima et al. performed a study to elucidate the binding site and mode of action of praziquantel where they examined the identity of surface membrane antigens of *Schistosoma mansoni* adult parasites, which had the capacity to bind praziquantel (Tallima and El Ridi, 2007). The study revealed that PZQ binds surface membrane molecules of *ca*. 45 kDa, which were identified by sequencing as actin. Actin was shown as a poorly immunogenic molecule in schistosomes. Cytoskeletal molecules in general do not show a strong immunogenic response because they are internal molecules. Nevertheless, there are schistosomal cytoskeletal molecules, which are targeted by the host immune system. In this context, functional characterization of these molecules and their interactions is a worth strategy (Jones *et al*., 2004).

In historical endemic areas of schistosomiasis in China, chemical intervention has been applied to suppress the transmission of schistosomiasis. Beside the widespread use of

praziquantel to humans and niclosamide for snail control, also environmental changes can have an important impact in the control of the disease (Spear, 2012).

Vaccination, either alone or in combination with drug treatment, represents the best long-term hope for controlling schistosomiasis. Novel targets for drug and vaccine development remain to be defined for optimal treatment and disease prevention.

In animal models, radiation-attenuated cercariae[1] showed a huge cellular and humoral immune response (Tian *et al.*, 2010). Nowadays, remarkable efforts are made to find recombinant antigens with protective efficacy. Vaccination can be targeted either towards the prevention of schistosome infection or the reduction of the parasite reproductive rate (McManus and Loukas, 2008).

The majority of targets for the development of new vaccines are membrane proteins, muscle components or enzymes (McManus, 2005; Wu *et al.*, 2005). Antigens present in the vulnerable larval development stage seem to have considerable potential in targetting the host immune system. This can be explained by the fact that larval stages are suspected to be the target of naturally acquired immunity in humans. In contrast, chronic infection of schistosomes is caused by the presence of adult worms in the host blood stream (McWilliam *et al.*, 2014).

Attempts to develop a vaccine against *S. mansoni* using tegument proteins from the tetraspanin family to stimulate an immune response seem to be succesful (Cardoso *et al.*, 2008; Tran *et al.*, 2006). However, vaccination with *S. japonicum* orthologs of these antigens, seem to be only effective in a small percentage of the parasite (Zhang *et al.*, 2011).

Proteins from the tegument-allergen-like (TAL) family are present in all human infecting *Schistosoma* species. A boost of the immune system with TAL allergens is seen when adult worms die. In *Schistosoma mansoni*, Sm22.6 and SmTAL1-13 (Fitzsimmons *et al.*, 2012) belong to this protein family. In *S. japonicum* and *Schistosoma haematobium*, Sj22.6 and Sh22.6 (Fitzsimmons *et al.*, 2004; Santiago *et al.*, 1998) have been described. These tegumental proteins have EF-hand motifs, a common characteristic of allergens, at their N-terminus. Their C-terminus resembles a dynein light chain (DLC)-1 domain,

[1] Larval form of the parasite liberated from the snail intermediate host and capable to infect humans as its final host.

which might be involved in vesicle transport into the tegument surface. *S. japonicum* (*Sj*) DLC-1 localizes in the basal layers of the tegument during mammalian-parasite stages of *S. japonicum*. *Sj*DLC-1 is involved in the transport of membranous and discoid bodies towards the tegumental membrane (Yang *et al.*, 1999). Another component of the dynein complex is *Sj*DLC-3, which is expressed in the schistosomal epithelia in all life stages (Zhang *et al.*, 2005).

In *S. japonicum*, another worm tegumental protein with immunological potency was characterized, Ly-6-like protein. This protein is expressed in both the larval and adult worm stage of the parasite but only seems to be antigenic in the lungs after larval migration (McWilliam *et al.*, 2014).

DNA vaccination of mice with the *S. mansoni* homolog of the human filamin has an impact on the pathology and transmission of the parasite. Filamin is an actin-binding structural protein expressed in the tegument of adult worms (Cook *et al.*, 2004).

Nowadays, knowledge of vaccination strategies is mainly based on the control of haploid organisms, such as the malaria parasite (species of the *Plasmodium* genus). Although both parasites have sexual stages in their development, schistosomes are diploid when infecting their definitive host and can be homo- or heterozygous. Under certain circumstances, the heterozygocity of schistosomula can be an advantage for diploid organisms. After immunization, a protective response will only occur if the products of both alleles are recognized by the immune system, which has a direct effect on the survival of *Schistosoma*.

To reduce the zoonotic transmission of *S. japonicum* to humans, schistosomiasis japonica allows for a complementary approach involving the development of a transmission-blocking veterinary vaccine in livestock animals, particularly bovine cattle (McManus and Dalton, 2006). Bovine species are the major reservoir for *S. japonicum* infection in China, 90% of egg contamination comes from this source (Chen and Lin, 2004).

Immunization with recombinant *S. japonicum Sj*TP22.4 (Zhang *et al.*, 2012), insulin receptor 2 (You *et al.*, 2012) and UDP-glucose 4-epimerase protein (Liu *et al.*, 2012) has shown good immunogenicity in mice. Although these proteins could be potential targets for designing anti-parasite drugs or vaccines, production of highly effective immunity

for clinical use can not be guaranteed. The availability of the schistosome genome and proteome deliver a great value in the identification of new target antigens (Bergquist *et al.*, 2008).

Pathology associated with human schistosomiasis is not directly due to the adult parasite but rather to large numbers of eggs trapped in tissues during egg migration or from an embolism in organs, such as the liver, spleen or the lungs.

Eggs that are not excreted get trapped in mucosae and liver tissues, causing immune reactions that result in human schistosomiasis (Walker, 2011). Consequently, many of the symptoms of schistosomiasis are attributed to the egg-induced inflammatory response and associated fibrosis. In order to protect itself from schistosome eggs and their secreted products, the host needs to deposit a protective granulomatous matrix around the eggs, in order to sequester or neutralize the parasite antigens. Granuloma formation restrains the infection and serves as an important host-protective function, which allows the host to live with the infection for many years. Presumably, the chronic detrimental effects associated with granulomas (*e.g.* fibrosis, portal hypertension) represent a better alternative for host and parasite, than that of the host dying soon after parasite egg production due to damage of the infected tissues. The most severe public health impact of schistosomiasis lies in the high number of patients expressing moderate morbidity rather than the few patients with severe morbidity (Secor, 2005).

The specific tropism of the different *Schistosoma* species causes varying clinical symptoms and organ complications. *S. japonicum* eggs are trapped in the hepatic portal tract causing liver damage, kidney failure and infertility. *S. mansoni* causes intestinal schistosomiasis manifested by anemia, malnourishment, stunted growth, progressive liver fibrosis, portal hypertension and hematemesis in later life. *S. haematobium* resides in vessels of the bladder and causes disease symptoms like hematuria, bladder calcification, kidney damage and an increased risk of bladder cancer (Wilson *et al.*, 2006).

Understanding the immune response to schistosome infection, both in animal models and in humans, may accelerate the development of a vaccine. The immune response associated with helminthic infections is polarized to a Th2 immune response in the mammalian hosts. Significant amounts of IL-4, IL-5, IL-9, IL-10 and IL-13 are produced, together with the development of strong immunoglobulin E (IgE), eosinophil and mast

cell responses. The early production of IL-4 in naive and memory T-cells, eosinophils, mast cells, basophils, antigen presenting cells and dendritic cells play an important role in the amplification of the Th2 pathway. The persistent and chronic aspects of helminthic infections in adult hosts are caused by the parasitic development of different mechanisms to overcome the host immune response. Modulation of the immune system by infection with helminthic parasites is proposed to reduce the levels of allergic responses and to protect against inflammatory bowel disease (Kamal and El Sayed Khalifa, 2006).

1.2 Schistosoma

1.2.1 Taxonomy

Schistosomes are metazoan[1] parasitic flatworms that belong to the digenean[2] family of *Schistosomatidae* (table 1). Since this family of flatworms does not have specialized circulatory and respiratory organs, oxygen and nutrients pass through their body by diffusion. The blind digestive cavity contains only one opening for both the uptake and removal of food and faeces respectively. In order to sense and integrate environmental signals, schistosomes are equipped with a complex nervous system. The body plan of parasitic flatworms consists of two suckers, reproductive organs and a though syncitial tegument that surrounds the body surface (figure 1). The tegument acts as a direct interface between the organism and the outside environment (Rollinson and Simpson, 1987). *Schistosomatidae* are found in molluscs during their immature developmental stages and in vertebrates during the adult stage. The external environment changes depending on the developmental stage, therefore the tegumental membrane needs to be an adaptable organ of the parasite. As most *Platyhelminthes*[3] are hermaphrodites, *Schistosomatidae* are exceptional by being dioecious, meaning that they have individuals of separate sexes, a rare characteristic for parasites. Largely based on morphological descriptions on adult worms, this family comprises *ca.* 14 genera, all infecting vertebrates (mainly birds and mammals), where they inhabit the blood vascular system (Basch, 1991; Khalil LF, 2002). The genus *Schistosoma* comprises over 20 species of

[1] Multicellular, eukaryotic organisms with cells differentiated into tissues and organs.
[2] Subclass of the *Platyhelminthes*, parasitic flatworms containing a syncitial tegument, a continuous cytoplasm surrounding the entire animal.
[3] Synonymous: flatworms. Worms with no specialized circulatory and respiratory organs.

which mainly five (*S. japonicum, S. mansoni, S. mekongi, S. haematobium, S. intercalatum*) cause the human disease schistosomiasis.

Kingdom	*Animalia / Metazoa*
Phylum	*Platyhelminthes*
Class	*Trematoda*
Order	*Strigeatida*
Family	*Schistosomatidae*
Genus	*Schistosoma*

Table 1: Taxonomic classification of *Schistosoma.*

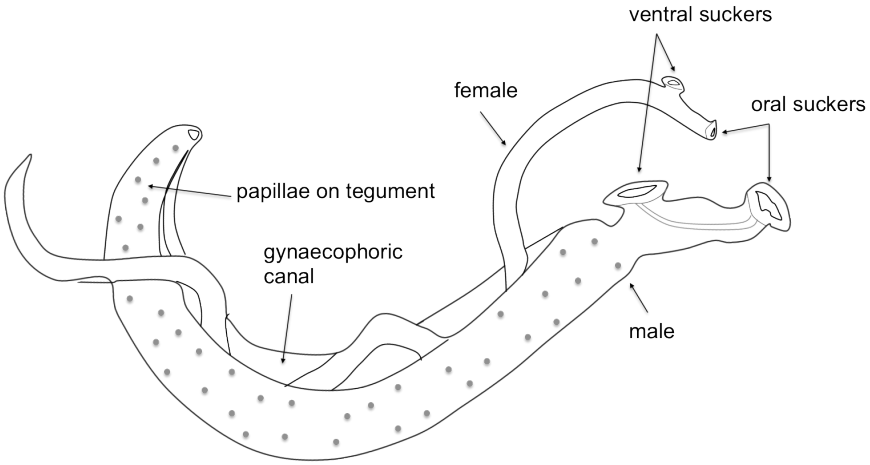

Figure 1: Morphology of *Schistosoma* species. Adult worms have a basic bilateral symmetry and are 10-20 mm in length and 0.5-1.0 mm in width. Female worms are held in the gynaecophoric canal of the male, and paired worms migrate together through the host circulation. The entire body of the adult worm is covered with a tegument. The worm contains two suckers, with which it maintains its position in the mesenteric blood vessels.

1.2.2 Subtypes

Analysis of the 18S ribosomal RNA, 28S ribosomal RNA and mitochondrial cytochrome C oxidase subunit I (COI) genes revealed the diversity and phylogenic relations of the species in the genus *Schistosoma* (Brant *et al.*, 2006).

Five main schistosome species may cause disease in humans: *S. mansoni, S. haematobium, S. japonicum, S. mekongi* and *S. intercalatum* (Southgate *et al.*, 1976; Stich

et al., 1999; Sturrock, 1993; Tchuem Tchuenté *et al.*, 2003). Schistosome infections of humans occur in regions of Africa, South America, the Middle East, Southeast Asia, China and the Caribbean islands. The geographical distribution of the various schistosome species is related to the ecosystem, in which their respective intermediate hosts live, see table 2 (Gryseels *et al.*, 2006). Civilization driven ecological changes (such as irrigation and the migration of infected human populations) further contribute to the epidemiology of schistosomiasis (Muller, 1995).

Species	**Geographical distribution**	**Intermediate host**
S. mansoni	Africa, the Middle East, the Caribbean, Brazil, Venezuela and Suriname	*Biomphalaria* species
S. hematobium	Africa, the Middle East	*Bulinus* species
S. japonicum	China, Indonesia, the Philippines	*Oncomelania* species
S. mekongi	Several districts of Cambodia and the Lao People's Democratic Republic	*Neotricula* aperta
S. intercalatum	Rain forest areas of central Africa	*Bulinus* species

Table 2: Geographical distribution and intermediate hosts of *Schistosoma* species (WHO).

Schistosoma infections in humans are mainly associated with chronic hepatic and intestinal fibrosis[1] (McManus and Loukas, 2008). However, *S. haematobium* infections cause fibrosis, narrowing and calcification of the urinary tract.

Unlike other human schistosome species, *S. japonicum* is zoonotic[2], infecting mammals of the orders *Primates*, *Rodentia*, *Insectivora*, *Artiodactyla* and *Carnivora* (He, 1993). The whole genomes of *S. japonicum* and *S. mansoni* have been recently published in Nature (Berriman *et al.*, 2009; *Schistosoma japonicum* Genome Sequencing and Functional Analysis Consortium, 2009). The analysis of the parasite sequence reveals a wealth of information, which helps to elucidate the mechanisms of the host-parasite interaction.

[1] The development of fibrous connective tissue as a reparative response to injury or damage

[2] A zoonotic disease is a disease that can be passed between humans and other animal species.

The genome of *S. japonicum* contains seven pairs of autosomes and one pair of sexual chromosomes, with an estimated 397 Mb, containing primarily 13 469 protein-coding sequences that account for 4% of the genome. The sequencing of the *S. mansoni, S. japonicum* and *S. haematobium* genomes, which are the three most pathogenic *Schistosoma* species, enabled the systematic dissection of both the parasite biology and identification for possible drug targets against the parasite (Webster *et al.*, 2010). A substantial level of the *S. japonicum* genome undergoes alternative splicing events, suggesting a complicated transcriptional and post-transcriptional regulatory mechanism employed by the parasite (Piao et al., 2014).

1.2.3 General biology

1.2.3.1 Life cyle

The various species of *Schistosoma* have complex digenic life cycles, during which they use freshwater snails as an intermediate host and mammals, including humans, as the definitive host (McManus and Loukas, 2008).

Throughout their life cycle (figure 2), trematodes[1] undergo striking morphological and physiological changes. The parasite is adapted to both a parasitic and free-living mode, which allows movement between the intermediate and final hosts. The parasite uses host nutrients, neuroendocrine hormones and signalling pathways for its growth, development and maturation. Therewith *S. japonicum* can perceive physiological signals from the fresh water or human host, allowing its adaptation to the current environment, such as fresh water or the tissues of its intermediate and mammalian hosts (*Schistosoma japonicum* Genome Sequencing and Functional Analysis Consortium, 2009).

Eggs are released within the definitive host's vasculature by female parasites and are emitted in water *via faeces* (*S. mansoni* and *S. japonicum)* or urine (*S. haematobium*). Hatched eggs release *miracidia* and these free-swimming larvae use cilia to move towards a compatible intermediate snail host. This swimming behaviour towards snail components is mainly driven by light (photokinetic) and possibly by chemical cues (chemokinetic). When the larvae penetrate the intermediate host, the *miracidia*

[1] A class within the phylum Platyhelminthes including two groups of parasitic flatworms, known as flukes.

differentiate into a mother sporocyst and produce daughter sporocysts by asexual reproduction. Daughter sporocysts develop into *cercariae*, which are free-living parasites that swim towards a suitable definitive host. This process is influenced by water turbulence and certain skin chemicals, and continues until the cercarial glycogen reserves are depleted, typically after a few hours. A single *miracidium* results in a few thousand *cercariae*, of which each one is capable of infecting a mammalian host. During infection, the *cercariae* produce proteases, allowing the penetration of the skin of the host. The *cercariae* shed their forked tail and transform structurally and physiologically into *schistosomula*. *Schistosomula* remain several days in the skin, after which they enter the systemic circulation and migrate to the liver, where they mature into adults. Following sexual maturation, pairs of female and male schistosomes migrate against the blood stream to the site of egg deposition. The *schistosomulae* migrate through several tissues to their residence in the veins. Adult worms in humans reside in the mesenteric venules in various organs, which seem to be specific for each species. *S. japonicum* is more frequently found in the superior mesenteric veins draining the small intestine. *S. mansoni* resides more often in the superior mesenteric venules draining the large intestine. *S. haematobium* finally passes to the vesical venules around the bladder, but can also be found in the rectal venules. When this final location is reached, *schistosomula* mature and unite. Adult male and female worms are intimately associated, the male body forms a groove, in which the longer and thinner female is held (figure 1) (Gryseels *et al.*, 2006; Ross *et al.*, 2002).

The production of eggs starts 4-6 weeks after infection and can last for up to 15 years. The eggs progressively move towards the lumen of the intestine (*S. mansoni* and *S. japonicum*) or the bladder and ureters (*S. haematobium*), and are eliminated with the host excreta (McManus and Loukas, 2008).

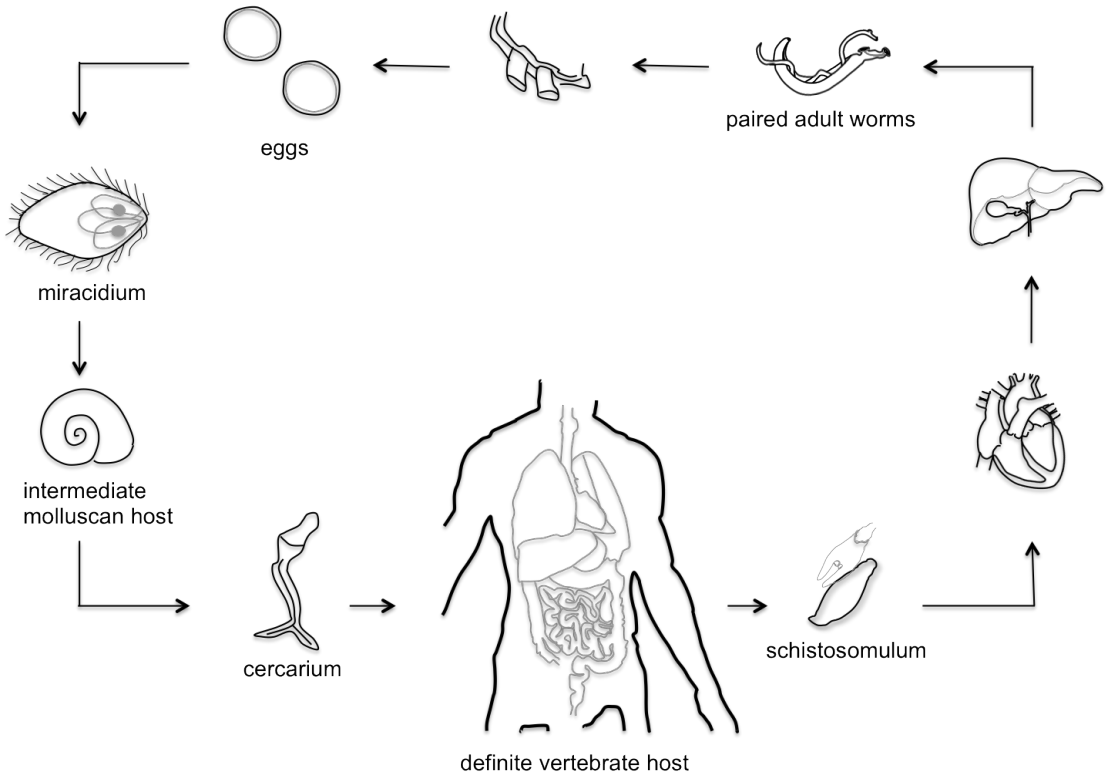

Figure 2: Digenic life cycle of *Schistosoma.* Parasitic eggs are released in the water via the *faeces* or urine of the vertebrate host. Eggs hatch *miracidiae*, free-swimming *larvae* able to penetrate the intermediate molluscan host. In freshwater snails, the larval multiplication takes place. *Miracidiae* develop into a sporocyst and produce daughter sporocysts and *cercariae*, which leave the snail. Free-swimming *cercariae* penetrate human skin and by losing their tail, they transform into *schistosomulae*. *Schistosomulae* migrate through the venous circulation to the lungs and *via* the heart into the circulation. Maturation into adult worms occurs in the liver, where the worms unite and migrate together to mesenteric vessels, where females lay eggs. Eggs retained in tissues will cause chronic schistosomiasis, while others are excreted via the *faeces* or urine. The eggs released into the water restart the cycle.

1.2.3.2 Tegument

The tegumental[1] outer surface of the *Schistosoma* parasites is a unique double-membrane structure that covers the entire surface of the worm, forming the major contact interface between the parasite and its host. Schistosomes are complex multicellular eukaryotes that have co-evolved with their mammalian hosts so that adult worms are typically able to survive several years in the vascular system of immune competent hosts (von Lichtenberg, 1987). To circumvent host immune effectors, schistosomes have evolved adaptations, resulting in the secretion of compounds that

[1] derived from tegere (Latin), meaning "to cover"

affect the host and protect the parasite itself. These secreted products suppress the host immune responses and make part of an immune refractory barrier called the tegument (Pearce and MacDonald, 2002).

The tegument of *S. japonicum* is a syncytium[1] of fused cells surrounding the entire worm with a single continuous double-bilayer membrane, called the membranocalyx (Wilson and Barnes, 1974). During the intra-mammalian-stage of the parasites, the host-interactive surface consists of two outer-surface membranes with a multilaminate appearance. This unusual organisation of the tegument is considered to be an adaptation for survival in the bloodstream and is not seen in trematodes inhabiting other environments. The tegument of *S. japonicum* was extensively analysed by scanning and transmission electron microscopy (SEM/TEM). These experiments revealed that the lipid bilayers overlaying the syncytium form many surface pits, substantially enlarging the surface area of the schistosome (figure 4). The excess of plasma membrane is probably removed by internalization. The function of tegumental folds and pits are suggestive of a highly absorptive surface, but may also be necessary for tegumental flexibility (Hockley, 1973). In contrast to the male, the female parasites have a very limited surface area with shallow grooves (Gobert *et al.*, 2003). Differences between the sexes in the topology of schistosomes are due to their different roles.

The underlying syncytial matrix contains some mitochondria and many vesicular structures, such as discoid bodies and multilamellar bodies. Discoid bodies are the precursors of the inner apical membrane, whereas the multilaminate vesicles are the precursors of the membranocalyx (figure 3), from which the latter is only present in the blood flukes. The cytoskeleton is also located in the matrix and connects the tegument membrane with the basal lamina (figure 3). The tegumental cytoskeleton also forms the basis of the spines on the surface of schistosomes, which ensures sufficient flexibility of the schistosomal interface (Gobert *et al.*, 2003; Jones *et al.*, 2004). The different layers of the basal lamina (lamina lucida, lamina densa and lamina reticularis) separate the syncytium from a layer of muscle cells and play a role in connecting the underlying muscle and parenchymal tissue (figure 3). Beneath the muscle layer, nucleated cell bodies are found which exclusively contain protein synthesising machinery and the Golgi apparatus. The 'cytons' are connected to the tegument by cytoplasmic connections and produce membrane bodies, which move along these connections to the syncytium

[1] a multinucleate mass of cytoplasm not separated into cells

to replace the outer-surface membranes (Braschi, 2006). In schistosomes, the body organs are embedded in solid parenchymal matrices rather than in a body cavity.

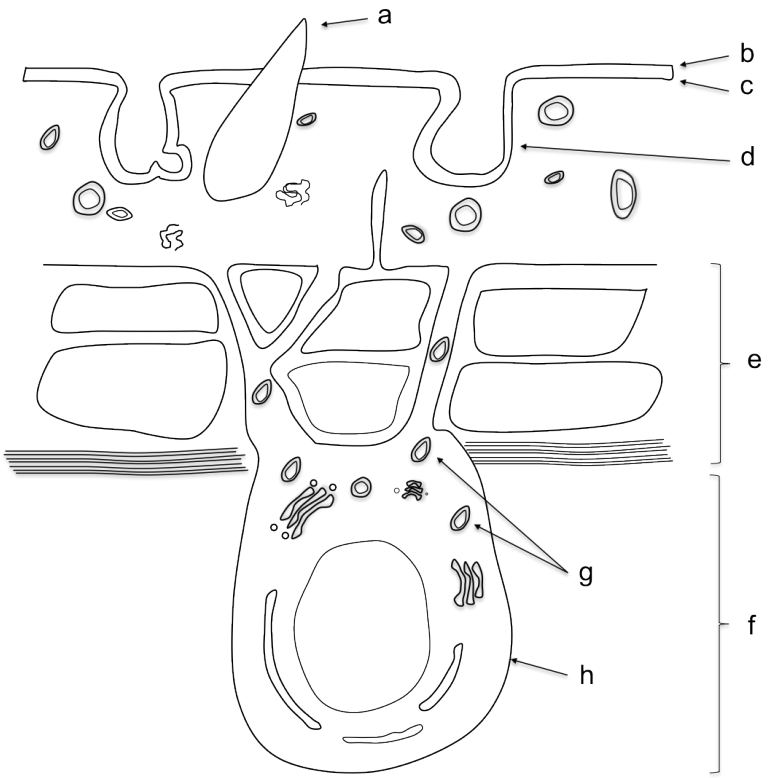

Figure 3: Details of the tegument of *Schistosoma* adult parasites. The tegumental layer covering *Schistosoma* species in their adult stage is composed of *a)* tegumental spines, *b)* membranocalyx, *c)* plasma membrane, *d)* surface pits, *e)* muscle layer with circular and longitudinal muscle cells, *f)* parenchymal tissue, *g)* vesicles and *h)* cell bodies.

The tegument is enriched in lipids and proteins that are unique for schistosomes, potentially important for fulfilling yet unknown functions (Van Hellemond *et al.*, 2006). Moreover, differences in tegumental structures occur between different *Schistosoma* species. The tegument surface contains surface enlarging spines with prominent tubercles in *S. mansoni*. These spines are smaller in *S. haematobium* while in *S. japonicum* only present in males. The interface between the external environment and the cytoplasm of the tegument is formed by a multilaminated membrane in all three species (figure 3). Also the tegument thickness (1 to 3 µm; Wilson and Barnes, 1974), which is defined as the distance from the basal lamina to the apical edge of the syncytium, is comparable for the three major human infecting schistosomes (Gobert *et al.*, 2003; Hockley and McLaren, 1973; Leitch *et al.*, 1984).

The multiple bilayer structure of the apical membrane is suspected to play an important role in the parasite evasion of the host immunological responses (Hockley and McLaren,

1973). Maintenance of the integrity of the tegumental membranes is considered to be essential. The outer and inner membranes of the tegument are expected to differ in biophysical composition (Kusel and Gordon, 1989). As opposed to the outer membrane, the inner membrane forms a rigid resistant layer against components that can cause damage (Kusel and Gordon, 1989). The parasite avoids immune-mediated damage from the host by reducing the antigenicity of the outer surface. This major immunological defence system is performed by a high rate of membrane turnover (Skelly and Wilson, 2006) and the incorporation of host molecules to the surface in adult schistosomes. Invaginations of the surface layer and basal lamina may provide the ability to avoid the host immune response by internalising host antibodies (Skelly and Wilson, 2006; Threadgold and Hopkins, 1981). The ability of the parasite to rapidly internalise proteins at its surface has implications for the development of vaccines and may also explain how these parasites are able to avoid the host immune system for long periods of time.

As the initial contact between the parasite and the host occurs at the tegument, its components are major antigens for the host immune response. Tegumental products are presumably shed into the host bloodstream, and antibodies against tegumental proteins and carbohydrates can be detected in the serum of infected animals (Cutts and Wilson, 1997; Köster and Strand, 1994; Nyame *et al.*, 2004; van Remoortere *et al.*, 2001). It is known that tegumental epitopes recognized by the host may be shared with other life stages in schistosomes but it remains, however, unclear whether the tegument itself is a strong primary focus of anti-parasite immunity (Skelly and Wilson, 2006). Since these functions are crucial for the survival of the parasite, tegumental proteins are interesting targets for both drug and vaccine development.

The tegument has an important role in the uptake of nutrients. This concept is supported by two different properties of the parasite. Components that are abundant in the blood of the host are taken up by the tegument rather than the intestinal epithelium. For the uptake of glucose and amino acids, the tegument of *Schistosoma* contains multiple transporter proteins. The glucose transporter SGTP4 is localised within the apical membranes of the tegument and is only expressed in the mammalian stage of the parasite life cycle (Skelly and Shoemaker, 1996). Next to a carrier-mediated system, amino acids produced by the host during digestion are also taken up by passive diffusion (Cornford and Oldendorf, 1979). Schistosomes only acquire cholesterol from the host, as they do not synthesise it *de novo*. After uptake by passive diffusion at

distinct regions of the parasite surface, cholesterol is redistributed throughout its body (Marr *et al.*, 2002). A third feature, which illustrates the role of the tegument in the nutritional uptake, is the presence of small vesicles, which appear to bud-off from the external apical membrane at the base of the tegument folds. These vesicles may be an indication of endycytosis (Gobert *et al.*, 2003). As discussed in the life cycle, *Schistosoma* occurs in paired male and female individuals, therefore nutrients are easily transferred between united schistosomes (Gupta and Basch, 1987).

In addition to host recognition, invasion and nutrient uptake, the tegument is also responsible for nutrient excretion, osmoregulation, sensory reception, and signal transduction (Jones *et al.*, 2004).

1.3 The actin cytoskeleton

The work reported in this dissertation focused specifically on the structural and biochemical characterization of profilin from *S. japonicum*. Since profilin is an important protein in the regulation of the actin cytoskeleton in the cell, the composition and function of the cytoskeleton is briefly described in this paragraph.

1.3.1 Composition

The cytoskeleton is an intracellular network of protein fibers located in the cytoplasm of the cell. It is characterized as a dynamic structure and plays a role in many cellular processes (see next section). The cytoskeleton has three main structural components: microfilaments, microtubules and intermediate filaments (Lodish *et al.*, 2000a).

Microfilaments are composed of monomeric actin wound in a helical shape. In eukaryotes, actin exists in two forms: monomeric, globular G-actin molecules, which are able to polymerize to filamentous F-actin. These linear filaments have a defined polarity and undergo treadmilling, a process where the filament is constantly renewed with G-actin monomers that are added to the growing ('barbed' or 'plus') end of the filament (figure 4) (Wegner, 1976). At the other side of the filament ('pointed' or 'minus' end), G-actin molecules are removed. The process of treadmilling keeps the filament length approximately constant. Myosin molecules bind actin filaments and generate contractile forces by 'walking' along the microfilaments (Lodish *et al.*, 2000b).

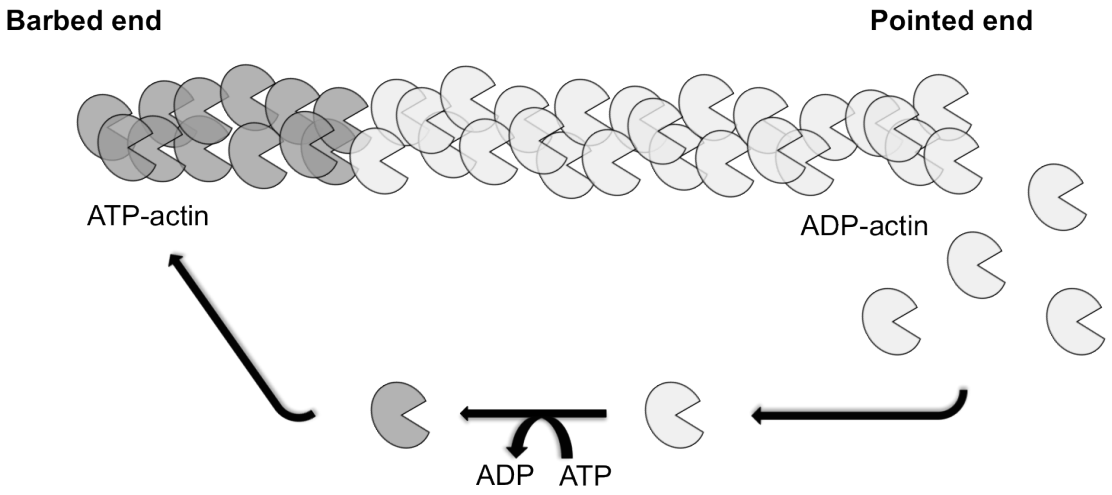

Figure 4: Treadmilling of actin filaments. Treadmilling maintains the filament length and occurs through association of ATP-actin monomers at the barbed end and dissociation of ADP-actin at the pointed end of the filament.

Microtubules are polymers of tubulin dimers and form long, hollow cylinders that are the structural components of the cell. They make up the centrioles and are thereby involved in the formation of the spindle apparatus during mitosis and meiosis. The motion of flagella and cilia are maintained by microtubules. Microtubules also serve as tracks for the transport of vesicles and organelles inside the cell. Similarity to microfilaments, microtubules bind nucleoside triphosphates in order to be able to polymerize, a property that is not seen in intermediate filaments (Sadava *et al.*, 2013).

Intermediate filaments are only found in animal cells. They form a so-called "coiled coil", of which the N- and C-terminus are non-helical regions and show huge variation in length and sequence across different families. Intermediate filaments are made up of polymerized fibrous subunits and are more stable than actin filaments. They are the only cytoskeletal component that are cell- or tissue specific and can be divided into five different subtypes, which are summarized in table 3 (Eriksson *et al.*, 2009).

Type I	acidic keratin	epithelium
Type II	basic keratin	epithelium
Type III	vimentin	fibroblast, endothelium
	desmin	muscle cells
	fibrillary acidic protein	glial cells of the central nervous system
Type IV	neurofilament proteins	neurons
Type V	lamin	nucleus

Table 3: Intermediate filaments families.

1.3.2 Functions

Although the cytoskeleton can be found in all domains of life and is composed of similar proteins, its structure, function and dynamics change among different organisms or cell types. It fulfills a plethora of functions in the cell, a property that emerges from the interaction with a lot of associated proteins. The cytoskeleton is involved in many signaling pathways of the cell, coordinates endo- and exocytosis (Perrin *et al.*, 1992), plays a role in cell division (Sanger, 1977), cell motility (Stossel, 1993) and in the intracellular transport of vesicles and organels (Witke, 2004). The cell cytoskeleton also performs an important function in the immune system. Actin is involved in migration and chemotaxis of immune cells (Lambrechts *et al.*, 2004; Van Haastert and Devreotes, 2004), phagocytosis (Castellano *et al.*, 2001), the presentation of antigens (Gordy *et al.*, 2004) and the production of reactive oxygen and nitrogen species (ROS and RNS, respectively) by macrophages and neutrophils (Su *et al.*, 2005; Webb *et al.*, 2001). The role of the cytoskeleton in all these mechanisms lies in the integration of diverse signals from the cellular environment.

Specialized structures such as flagella, cilia and lamellipodia are also composed out of cytoskeletal structures.

1.3.3 The cytoskeleton in *Schistosoma* species

Schistosomes possess all major components of a microtubular and actin-based cytoskeletal system. Cytoskeletal molecules are well represented in the transcriptome of *Schistosoma* and play an important role in the adaptation to their symbiotic lifestyle. The cytoskeleton of schistosomes shows a lot of similarities with that of other *Eukarya*, with some adaptations that are unique for helminths, especially those involved in the host-parasite interplay.

Microfilaments are found in the muscle cells and tegument of schistosomes. Moreover, actin has been identified as the main component of schistosome spines (Cohen *et al.*, 1982). In the tegumental spines, actin is present in high concentrations in the form of crystalline arrays consisting of filaments with identical polarity (Cohen *et al.*, 1982; Zhou and Podesta, 1989). These filaments are linked with the apical and basal plasma membranes of the distal cytoplasm. Beside actin, also actin-related motor proteins are largely responsible for the modulation of the tegument surface. Paramyosin and myosin are associated to the schistosomal muscle layer (Gobert *et al.*, 1997; Y. Zhang *et al.*, 1998). Microtubules form a peripheral network by forming cytoplasmatic bridges that connect cell bodies with the syncytium, providing routes for anterograde transport of vesicles towards the apical membrane (Patrick J. Skelly and Alan Wilson, 2006). Beside their important role in the host-parasite interactions, the cytoskeleton also plays an important role in the defense against the host immune system. A surface associated form found in *S. mansoni*, SCIP-1, seems to bind the Fc domain of human antibodies. By binding these region of the host antibodies which are produced as a humoral response towards cytoskeletal proteins, the antibodies are blocked (Deng *et al.*, 2003; Parizade *et al.*, 1994). This is a one major strategy of the parasite to evade a host immune response.

Beside the known proteins involved in the formation of a peripheral network (table 4), also newly identified cytoskeletal components are present in schistosomes that are associated with the tegument (tegument-associated proteins or TAP). Due to the fact that they are not homologous to other known proteins and uniquely present in schistosomes makes it more difficult to elucidate their function. In *S. mansoni*, a 20.8 kDa protein was identified and shows sequence identity with the known schistosomal dynein light chain in the cytoplasm (Hoffmann and Strand, 1996). Dyneins are large, multisubunit (heavy, intermediate, and light chains), molecular motors involved in various types of microtubule-based motility. Another protein, the Sj22.6 TAP from *S.*

japonicum showed immunogenicity in mice by inducing an IgE response in infected animals but was not able to provide protection in mice (Li *et al.*, 2000).

microfilaments	actin	
	actin-related proteins	actin-related protein 1/2/3/6/11
	actin-binding proteins	actin-depolymerizing factor (ADF), cofilin, α-actinin, calponins, capping protein, supervillin, troponin, tropomyosins, myosin, smoothelin, spectrin, profilin
	motor proteins	myosin, myosin kinases and associated proteins, paramyosin
	others	adducin, annexins, cortactin, fascin, gelsolin, thymosin β4
microtubules	tubulin	α- and β-form
	microtubule-associated proteins	tubulin-epsilon, stathmin-like protein, MAPs-XMAP, EMAP2, Tektin
	centrosomal proteins	katanin, tubulin-γ
	microtubule-associated motor proteins	dynein light chains, kinesin motor domain, dynactin
intermediate filaments	lamin	
	filarin	
other cytoskeletal proteins	dyna-drome 150 kDa	
	titin	

Table 4: Summary of cytoskeletal proteins in *Schistosoma*. Table based on Jones et al. (2004) where the protein identification is derived from annotated schistosome EST databases and published full-length genes and ESTs.

It has been reported that several tegumental cytoskeletal proteins provoke interleukin (IL)-mediated immune responses in their mammalian hosts (Jones *et al.*, 2004; Pearce and MacDonald, 2002). Also *Sj*Pfn was seen to localize mainly in the tegument and induces the production of IL-12 (Zhang *et al.*, 2008). Somewhat in analogy, actin and actin-binding proteins in apicomplexan parasites, such as *Plasmodium*, are localized in a unique membrane structure, also referred to as the inner membrane complex, close to the surface of the parasite. It has been suggested that during invasion, these parasites utilize the actin filament system of the host (Gonzalez *et al.*, 2009).

1.3.4 Actin

Actin belongs to a highly conserved family of proteins found in all eukaryotes. It is a 42 kDa protein and makes up 5% of the total protein amount in eukaryotes. Actin consists of two lobes clasping an ATPase pocket (Kabsch *et al.*, 1990) and can bind one ATP molecule (figure 5). After incorporation in the filament, ATP is hydrolysed to ADP and P_i. After hydrolysis, actin can exchange bound ADP for ATP, which alters the conformation of the protein. The actin monomer contains a small domain and a large one, which are each divided in two more subdomains, carrying numbers 1 to 4 in figure 5. The binding of ATP, along with Mg^{2+}, occurs within a deep cleft between subdomains 2 and 4. To be functional in the cell, actin depends on the presence and binding of actin-binding proteins as well as on other signaling pathways (Rho family of GTPases) (Rajakylä and Vartiainen, 2014).

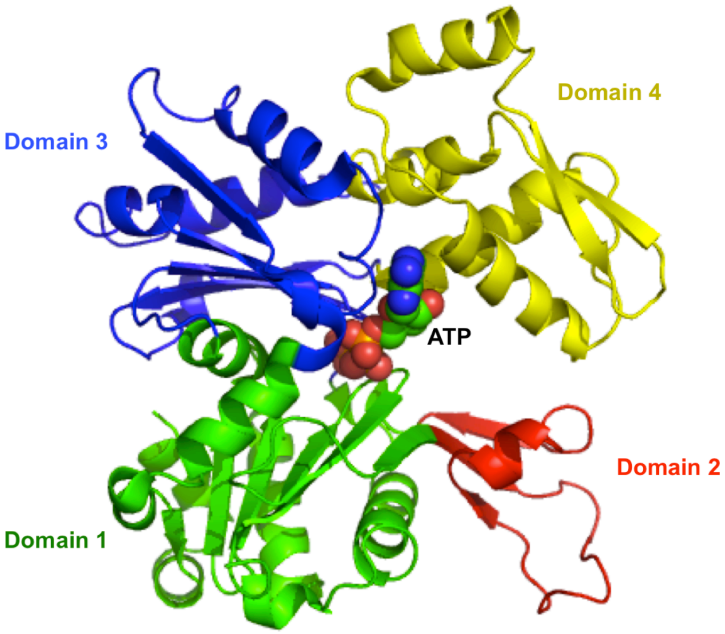

Figure 5: Structure of monomeric actin bound to ATP. Actin consists of a small and a large domain each subdivided in two subdomains, numbered from 1-4. ATP is bound in the central ATPase cleft.

Most eukaryotic species contain multiple genes encoding different isoforms of actin (Herman, 1993). However, some parasitic *Protozoa* contain only one actin gene and express the protein product only in a low level. Blasting human actin against the *S. japonicum* database results in different putative actin genes. Actin is present in the musculature of schistosomes as well as in the tegument. In *S. mansoni*, it occurs predominantly in the spines and tubercles (Matsumoto *et al.*, 1988).

1.3.5 Formation of actin filaments

At a critical G-actin concentration, ATP-actin monomers polymerize spontaneously in a head-to-tail fashion to form long double helical filaments (figure 6). The actin filament has polarity, which means that all actin monomers are oriented in the same way, with their cleft towards the pointed filament end.

The ends of actin filaments differ from each other both in structural and dynamical properties. As discussed above, actin filaments undergo treadmilling, a process where ATP-actin is added on the fast-growing 'plus' end and where ADP-actin is lost from the slow-growing 'minus' end (figure 6). This keeps the microfilaments in a steady-state by controlling the length and activity of the F-actin.

When comparing *in vitro* and *in vivo* conditions of actin, large differences are present. Within the cell, the concentration of G-actin is thousand times higher than the critical concentration needed for polymerisation. Subsequently, the turnover of dynamic structures *in vivo*, is 100 times faster than observed *in vitro*. This can be explained by the interaction with actin-binding proteins (Theriot and Mitchison, 1991).

The process in which actin filaments are formed, can be divided in three phases: nucleation, elongation and steady-state of the filaments (Cooper, 2000). The first stage in *de novo* filament formation is nucleation. Until the formation of three associated monomers, filament formation is thermodynamically unfavourable (Sept and McCammon, 2001). Actin-binding proteins, which assist in the nucleation stage, are crucial to rapidly overcome the unfavourable lag phase. New filaments can form *de novo* and by branching from or severing of existing filaments (Winder and Ayscough, 2005). Once nucleated, ATP-actin monomers are incorporated at the barbed end and the actin filaments extend, which is referred to as the elongation stage. ATP bound in the central cleft of actin becomes hydrolysed when the filament matures, and phosphate is released (Winder and Ayscough, 2005). From the pointed side of the filaments, ADP-actin is disassembled. New ATP-actin molecules are generated by a process called nucleotide exchange of the released ADP-actin monomers, which can then be used again for polymerization (Porta and Borgstahl, 2012). Tight regulation of the availability of actin monomers is needed and this is mainly achieved by the actions of a group of highly conserved actin-monomer-binding proteins, discussed below. These proteins are involved in the binding of ADP-actin released from filaments ends, facilitating the nucleotide exchange of ADP for ATP and delivering the monomers to the barbed end to start new rounds of polymerization (Winder and Ayscough, 2005). The organization of actin into networks is crucial to both the shape and function of the cell (Cooper, 2000).

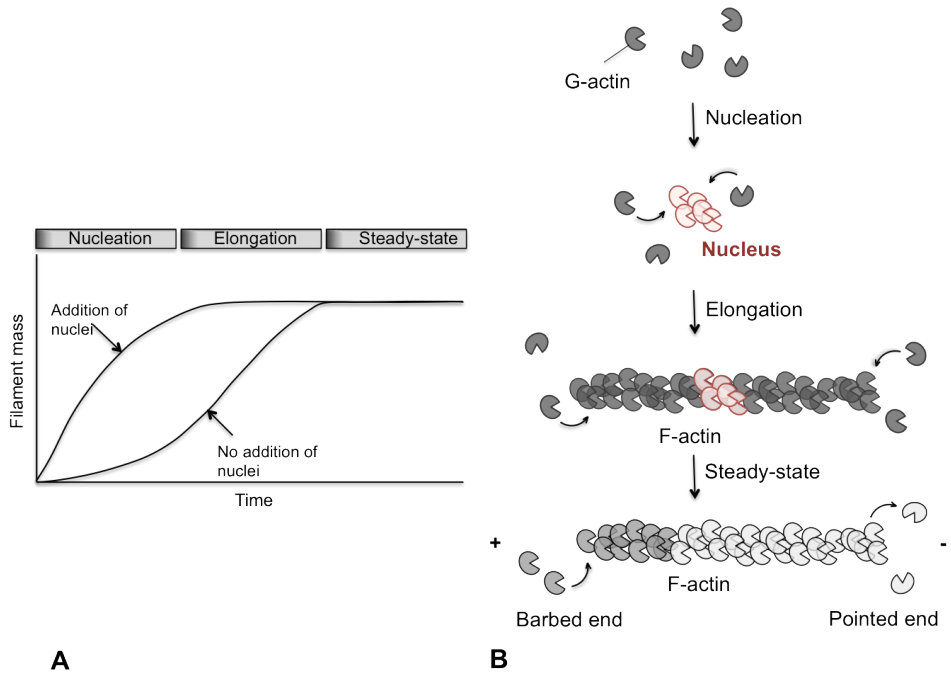

Figure 6: Formation of actin filaments *in vitro*. A pool of monomeric G-actin aggregates slowly until a stable nucleus is formed. The nucleus elongates by addition of monomers to both ends, where the barbed end (+) elongates faster than the pointed end (-) of the filament. When a steady-state phase is reached, the filament dynamics enter a state of equilibrium. The assembly and disassembly of monomers from the respectively + and – end is balanced. The steady-state is known as treadmilling. Althoug actin monomers will polymerize spontaneously in solution when their concentration is higher than the critical concentration, these aggregates are highly unstable. Additional proteins named 'nucleators' promote the formation of a stable actin nucleus.

1.3.6 Actin-binding proteins

Actin networks can be regulated through actin-binding proteins that play a role in filament assembly, length, cross-linking and dynamics. Perturbation of these proteins *in vivo* causes a serious impact on the actin architecture. Table 5 gives a schematic overview of the different actin-binding proteins and their function.

Monomer binders	Profilin, thymosins, twinfilin, Srv2/CAP, WASP, verprolin/WIP, Arp2/3, formins
Bundlers and crosslinkers	Fimbrin, scruin, villin, espin, fascin, α-actinin
Crosslinkers	Filamin, spectrin, transgelin
Cytoskeletal linkers	Spectrin, plectin, BPAG, MACF, MAP2, tau
Myosins	
Rulers and stabilisers	Adducin, caldesmon, calponin, nebulins, tropomyosins
Capping and severing	CapZ, formins, tensin, Arp2/3, tropomodulin, gelsolin, fragmin, villin, ADF/cofilin, AIP1
Branch formation	Arp2/3, WASP/SCAR/WAVE
Sidebinders and signallers	IQGAP, Abp1, cortactin, coronin, drebrin, ENA/VASP
Anchors to membranes and membrane proteins	α-actinin, annexin II, α-catenin, BPAG, dystrophin, ERM proteins, plectin, spectrin, Sla2, talin, tensin, utrophin, vinculin

Table 5: Overview and functions of actin-binding proteins, adapted from (Winder and Ayscough, 2005).

1.3.6.1 ADF/Cofilin family

Members of the actin-depolymerizing factor (ADF)/cofilin family exist in multiple isoforms and are the best characterized proteins that drive depolymerisation of F-actin (Maciver and Hussey, 2002). ADFs are named by their ability to depolymerize F-actin and cofilins due to cosedimentation with F-actin. In general, both proteins elevate the levels of monomeric actin by binding filaments. They are small (15-19 kDa), highly conserved proteins and are expressed in virtually all eukaryotic cells. Members of the

ADF/cofilin family play a central role in actin turnover (Bamburg, 1999). They function by binding ADP-F-actin and promote dissociation of ADP-actin monomers from the pointed end of the filament. It is common to regard ADF and cofilin as synonyms, although these proteins are encoded by different genes and are distinctly different (dos Remedios *et al.*, 2003). In mammals and birds, only one isoform of ADF is known, whereas for cofilin, two are known. ADF and cofilin have different expression patterns in human tissues.

1.3.6.2 Profilin family

Profilins belong to a multigenic family and are differentially expressed in different eukaryotic organisms. These small (12-16 kDa) proteins consist of biochemically and functionally different isoforms, which are involved in different cellular mechanisms. Profilins are among the most highly expressed proteins in the cytoplasm (Buss *et al.*, 1992). In view of this dissertation, where profilin from *S. japonicum* is the main topic, the function and structure of profilins are discussed in more detail in section 1.4.

1.3.6.3 Gelsolin superfamily

Proteins of the gelsolin superfamily all contain large (120 amino acids) related repeating segments in their primary sequence (Kwiatkowski *et al.*, 1986). Villin and gelsolin contain six of the large gelsolin repeats, while 3 of these are present in severin and fragmin. Gelsolin disassembles F-actin structures by severing actin filaments (Selden *et al.*, 1998). When bound to the actin filament, gelsolin changes its conformation and causes a kink in the actin filament. The protein remains attached to the barbed end of the filament after severing. At this moment, gelsolin serves as a capping protein, preventing reannealing or elongation of short filaments (Sun *et al.*, 1999). Afterwards, gelsolin can be released from the barbed end, which allows the filaments to rebuild. In this way, gelsolin can be seen as a promotor of actin polymerisation (Sun *et al.*, 1999).

1.3.6.4 Thymosins

Proteins from the tymosin family sequester monomeric actin to provide a large pool of G-actin in the cell that can be released to allow rapid filament extension. These proteins clamp actin (e.g. thymosin-ß) to prevent incorporation into filaments (Hertzog *et al.*,

2004; Irobi *et al.*, 2004). Appropiate signals in the cell can rapidly release thymosin binding, which results in a massive increase in the amount of actin available for polymerisation.

1.3.6.5 DNase I

DNase I cleaves single- and double- stranded DNA at the phosphodiester bond and releases thereby polynucleotides with 5'-phosphate and 3'-OH groups. DNAse I has a wide tissue distribution and requires Ca^{2+} and Mg^{2+} to be active. During apoptosis, DNase I plays a role in the fragmentation of DNA (Peitsch *et al.*, 1993). Beside its endo- and deoxyribonuclease function, this enzyme also binds actin monomers. A possible explanation of the interaction between DNase I and actin might be the storage of DNase I in an inactive form to prevent damage of the genetic information (Lazarides and Lindberg, 1974). On the other hand, Dnase I is an inhibitor of actin polymerisation as it can interrupt actin:actin contacts in filaments (Hitchcock *et al.*, 1976; Holmes *et al.*, 1990; Lazarides and Lindberg, 1974; Schutt *et al.*).

1.3.6.6 Capping proteins

Capping proteins cap the barbed end of filaments and block thereby the addition of new monomers (Narita *et al.*, 2006). This causes a decrease in the overall length of the filament. The CapZ capping protein is such a protein that inhibits polymerization (Caldwell *et al.*, 1989). By contrast, proteins that cap the pointed end cause a reduction in the loss of monomers, which results in a fast extension of the filament. An example of this class of proteins are tropomodulins, which prevent the dissociation of actin monomers (Rao *et al.*, 2014).

1.3.6.7 The Arp2/3 complex

The Arp2/3 complex binds G-actin and forms thereby a stable trimer which operates as a nucleus for the growth of a filament (Winder and Ayscough, 2005). The Arp2/3 complex includes two actin-related proteins, Arp2 and Arp3, and five smaller proteins. Bound to G-actin, Arp2/3 functions a capping protein and encourages rapid growth of the filament at the pointed end of the growing filament (Winder and Ayscough, 2005). When binding at the side of an excisting actin filament, the Arp2/3 complex can start the

formation of a new filament branch (Amann and Pollard, 2001). *In vivo*, the activity of Arp2/3 is enhanced by the interaction with other proteins like WASP and SCAR/WAVE proteins (Higgs and Pollard, 1999; Pollitt and Insall, 2009).

1.3.6.8 Formins

Formins are a family of large multi-domain proteins, important in the nucleation of actin polymerization (Goode and Eck, 2007). These proteins are found at the barbed end of actin filaments and remain bound to the filament as actin monomers are added at the plus ends. Bound formin prevents binding of plus-end capping proteins to actin filaments. Formins are characterized by the presence of two formin homology (FH) domains: the filamentous actin binding FH2 domain and the proline-rich FH1 domain (Wallar and Alberts, 2003). Formins bind to actin filaments and, on the other hand, to proline-rich sequence binding proteins, such as profilins, SH3 domains and WW domains (Zigmond, 2004). Xu *et al.* showed that the FH2 domain is involved in the addition of actin monomers to the barbed end of a filament (Xu *et al.*, 2004).

1.4 Profilin

Profilins are small proteins that are highly conserved among eukaryotes. In many organisms, there are different isoforms of the protein, different gene products or splice forms that are tissue specifically expressed. The presence of multiple isoforms with different biochemical characteristics allows for better fine-tuning of signaling pathways (Lambrechts *et al.*, 2000). Profilin was initially discovered as an inhibitor of actin polymerization, as it was copurified with monomeric actin from calf spleen (Carlsson *et al.*, 1976, 1977). Profilins are a large family of proteins of which the name originates from 'PRO-FILamentous actin' (Tilney *et al.*, 1983) as they were originally described to keep actin in a pro-filamentous form.

Profilins have been identified in lower eukaryotes, (in)vertebrates, plants and are also present in *Vaccinia* virus (Machesky and Poland, 1993). All profilins possess a closely related tertiary structure. The profilin polypeptide is folded into a central ß-pleated sheet composed of 5-7 antiparallel ß-strands (figure 7). The core is on one side, flanked by the N- and C-terminal α-helices and on the opposite side by another α-helix

connected with an additional α-helix or a small ß-strand (figure 7). Other actin-binding proteins like severin (Schnuchel *et al.*, 1995), villin (Markus *et al.*, 1994) and gelsolin (PMcLaughlin and Weeds, 1995) share similar characteristics in their structure.

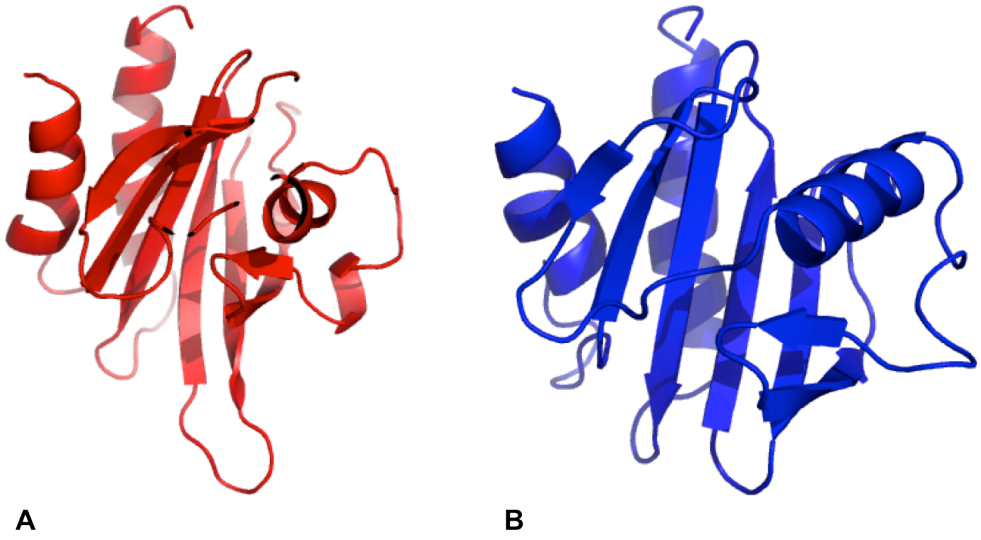

Figure 7: Comparison of the structural organization of human and *Arabidopsis thaliana* profilin. The canonical profilin fold consists of a central antiparallel ß-sheet sandwiched between the N- and C-terminal α-helices on one side and another α-helix connected with an additional α-helix (*A*; human profilin I) or an additional ß-strand on the opposite site (*B*; *Arabidopsis thaliana* profilin).

The importance of profilins was demonstrated as profilin-deficient mutants show impaired cell proliferation and differentiation mechanisms (Magdolen *et al.*, 1988). The complete deletion of profilin has severe consequences on the viability of mice (Witke *et al.*, 2001) and *Drosophila* (Verheyen and Cooley, 1994).

Different mechanisms cause the multifunctionality of profilins. Post-translational modificiations alter the Ser and Thr residues by phosphorylation and on the level of the genetic information, single nucleotide and sequence polymorphisms exist which result in the formation of profilins with different charge and size (Jimenez-Lopez *et al.*, 2012). Profilin II in mice for example originates from alternative splicing events during gene expression. Although being very similar, structure determination of profilins by NMR and X-ray diffraction determined six isoforms of profilin (Di Nardo *et al.*, 2000).

Profilins are mainly detected in the cytoplasm, however, they are able to enter the nucleus by diffusion because of their small size. In mammalian cells, a profilin-specific exportin recognizes the profilin-actin complex and transports it out of the nucleus

actively (Stüven *et al.*, 2003). The level of profilin and actin is therefore tightly controlled in the nucleus. It has been described that profilin 1 associates with ribonuclear particles in the nucleus, which suggests a role for profilin 1 in pre-mRNA processing (Skare *et al.*, 2003). Interaction of profilin 1 and 2 with the survival of motor neuron protein (SMN), a nuclear factor which is mutated in spinal muscular atrophy, adds a potential nuclear role of these proteins. SMN is involved in the regulation of splicing events (Sharma *et al.*, 2005).

1.4.1 Ligand binding sites on profilin

Profilins have the capacity to bind three classes of ligands: *1)* they are found to form complexes with G-actin (Schutt *et al.*, 1993) and actin related proteins (Machesky *et al.*, 1994), *2)* bind to polyphosphoinositides (Lassing and Lindberg, 1985) and *3)* interact with poly-L-proline (PLP) (Mahoney *et al.*, 1997). Among different species and isoforms, the affinity for the different ligands can differ.

Profilins are small monomeric (G) actin-binding proteins that also bind various filamentous (F) actin-binding regulatory proteins. Profilins bind globular actin in a 1:1 stoichiometric complex with an affinity in the micromolar range. Remarkably, the N-terminal region of profilin involved in actin binding is not conserved. Depending on the profilin/G-actin ratio, the ionic environment in the cell and the interaction with other actin-binding proteins, profilins play a duplex role by both promoting and inhibiting actin polymerization in the cell (see below) (Lodish *et al.*, 2000a).

In addition, profilins bind to membrane phospholipids and have been suggested to participate in membrane-trafficking and signalling events (Witke, 2004). Although the affinity for phosphatidylinositol 4,5-bisphosphate (PIP_2) is more refined, profilin also has affinity for other phosphatidylinositol lipids like phosphatidylinositol 3,4-bisphosphate and phosphatidylinositol 3,4,5-trisphosphate (Lu *et al.*, 1996). There are two binding areas involved in the binding of PIP_2 in profilins. The first region involves a hydrophobic patch, which is also involved in the interaction with actin, the other one overlaps with the PLP site (see below) at the C-terminus of profilin. This causes competition between PIP_2 and PLP ligands to bind profilin. *Via* the interaction of profilin with PLP stretches and PIP_2, profilin mediates membrane-cytoskeleton communication by transmitting the signal in the plasma membrane *via* different transduction cascades

to rearrange the cytoskeleton (Jimenez-Lopez *et al.*, 2012). By binding profilin, phosphoinositides sequester profilin in an inactive form, from where it can be released by action of the enzyme phospholipase C.

Binding of other actin regulatory proteins by profilin is mediated by the property of profilins to bind a variable number of proline-rich sequence repeats which can be presented as a peptide or as a sequence motif in proteins. Profilins have affinity for PLP of at least 8 to 10 prolines, which may be interrupted by single glycine residues. A plethora of proteins with PLP stretches are bound showing a high variability with respect to their cellular localization, structural organisation and function (Jockusch *et al.*, 2007). These PLP containing proteins function in the organisation and motility of the cytoskeleton, storage, transport and transcription. Members of these PLP ligand families are able to bind both profilin and profilin-actin complexes. Ena/VASP, formin, WASP/WAVE families are examples of large multidomain proteins with a central PLP motif flanked by a G-actin and frequently also by a F-actin-binding site (Jockusch *et al.*, 2007). It is through the PLP binding domain that profilin can be seen as a "hub" that interacts with many proteins, thereby controlling a complex network of molecular interactions (Witke, 2004). These interactions are of great importance in processes related to microfilament nucleation and elongation. The affinity of profilins for PLP depends also on the presence of posttranslationally phosphorylated tyrosine residues. Also, the phosphorylation of Ser92 by Protein Kinase C increases the affinity for G-actin and PLP while the interaction with PIP2 is not altered by this event (Sathish, 2004).

The affinity of profilins for their ligands differs between profilins from different species and isoforms. This is shown in splicing variants of mice which do not bind G-actin and in *Vaccinia virus* were profilin does not bind PLP (Jimenez-Lopez *et al.*, 2012).

1.4.2 The role of profilin in actin polymerization

In this section, we will focus on the role of profilin in actin polymerization dynamics as in this work our aim was to study the role of *S. japonicum* profilin on actin dynamics. Profilins are among the most important proteins regulating actin dynamics (Yarmola and Bubb, 2006) by stabilizing the pool of unpolymerised actin in cells (Carlsson *et al.*, 1977).

Profilin interacts with subdomains 1 and 3 of actin (Schutt *et al.*, 1993). The conformation of actin bound to profilin can be either in an open or closed state (Porta and Borgstahl, 2012). The crystal structures of unbound profilin versus bound with actin are almost identical. The conformation of actin, which changes a lot after profilin binding to its barbed end, determines the main differences in crystal structure, namely the rotation of the small domain relative to the large domain results in different conformations of actin. Comparison of the open versus closed state of the actin-profilin interactions shows reorganisation events in different regions of the complex when binding with profilin. Actin undergoes large rearrangements of domains such as the rotation in the orientation of subdomain 2 and changes in the N-terminus. The nucleotide bound in the central cleft of actin becomes more solvent exposed in the open state (Chik *et al.*, 1996), and the hydrogen bonding between ATP and the surrounding residues is less extensive (Porta and Borgstahl, 2012). Also the actin C-terminus undergoes significant changes in conformation upon open-to-close transition, *e.g.* the local conformation change in the hydrophobic pocket surrounding Cys374 (*Bos taurus* numbering) (Chik *et al.*, 1996).

Profilin controls *de novo* actin polymerization by two mechanisms. First, by increasing the rate of nucleotide exchange and second by decreasing the critical concentration required for filament elongation at the barbed end. Profilin facilitates nucleotide exchange by binding subdomains 1 and 3 from actin and thereby modulating the opening of the nucleotide cleft. Thanks to the ability of profilin to recharge actin with ATP, any ADP-actin subunit released from the pointed filament end is rapidly converted to ATP-actin (figure 8) (Witke, 2004). Because profilin and cofilin act at opposite ends of a filament, they can enhance filament turnover at the same time, with profilin providing ATP-actin at the barbed end, while cofilin dissociates ADP-actin from the pointed end (Didry *et al.*, 1998). When ATP is bound to actin, profilin inhibits the hydrolysis of ATP. This causes actin monomers to maintain in a state where they have a high affinity for the growing end of filaments (Ampe *et al.*, 1988). Profilins are the main buffer of the actin pool in the cell and promote polymerization by transporting G-actin to the barbed end of filaments (figure 8). The assembly of F-actin from profilin-actin is possible because of the coupling to ATP hydrolysis. After association with the barbed end, the actin-bound ATP gets hydrolyzed and the interaction between profilin and actin becomes weaker. Profilin dissociates from the filament and generates thereby a free barbed end for further growth. Profilin has a low affinity for the pointed ends of the filament. After delivering a monomer to the growing end of the filament, PIP and PIP_2 stimulate the

dissociation of profilin from actin. This implicates that profilin plays a role in the transmission of cell signals between the membrane and the actin cytoskeleton (Goldschmidt-Clermont *et al.*, 1990).

In contrast to what described in previous paragraph, profilins can also inhibit filament polymerization by sequestering monomeric actin in the cytosol. This decreases the concentration of free actin monomers that are available for filament elongation. The dual activities of profilin in actin assembly shows that profilin function is dependent on the presence of other actin-binding proteins (Perelroizen *et al.*, 1994, 1996).

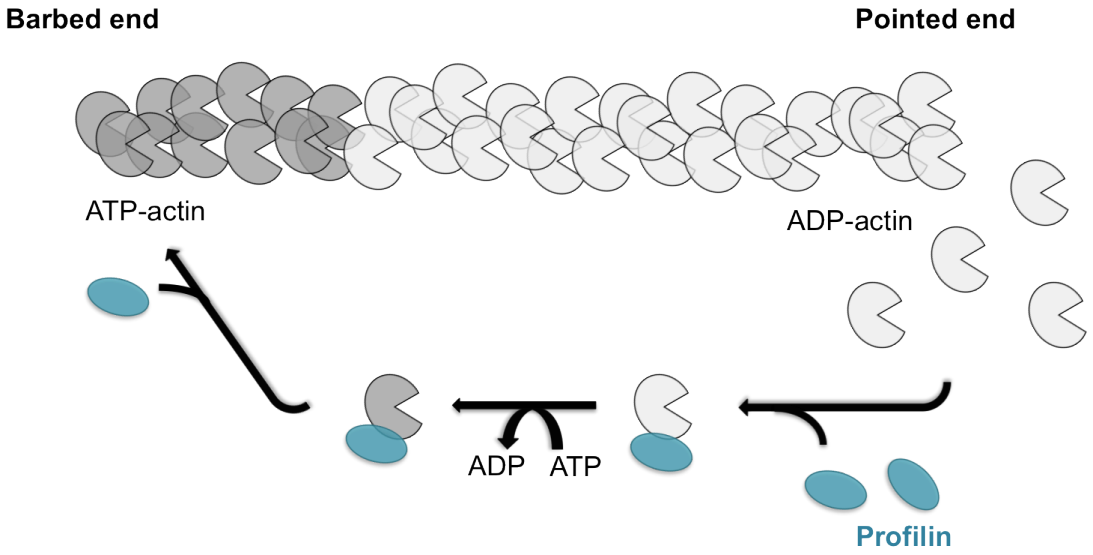

Figure 8: Effect of profilin on actin filament formation. Profilin has different functions in the regulation of actin polymerization. First, profilins can bind ADP-actin monomers, which are released from the – end of the filament and increase the rate of nucleotide exchange 1000-fold compared to the rate in case of diffusion. Second, the profilin-ATP-actin complex can interact with the barbed end, thereby releasing profilin when ATP-actin is added to the growing filament. Third, the sequestration of actin monomers by profilin decreases the concentration of free actin monomers that are available for filament elongation.

1.4.3 The role of profilin in signal transduction

The actin filament system plays an important role in signal cascades, the activation of which is crucial for fundamental cellular mechanisms. Intermediate products of signal transduction pathways and changes in actin assembly and architecture are controlled by each other with great precision by different events at the microfilament site. Regulation

of the architecture of the actin cytoskeleton in response to extracellular signals is an important mechanism by which cells control their morphology and motility (Higgs and Pollard, 2001). Profilins play a complex role in these processes and bind ligands, which play a role in various signal transduction pathways (Schlüter *et al.*, 1997).

The capacity of profilins to bind not only actin but also polyphosphoinositides created the concept that profilins combine the signalisation of PIP signalling with the regulation of the microfilament system. The lipid metabolism must also be taken into account when considering the functions of profilin in the cell (Lassing and Lindberg, 1985).

The formin-related profilin ligands connect the microfilament system with the GTPase-related signaling cascade, which is also linked to the PIP signaling pathway (Schlüter *et al.*, 1997). The small GTPases of the Rho family are crucial in the regulation of microfilament-based processes such as cell morphology, adhesion and cytokinesis (Schlüter *et al.*, 1997). The formin-related proteins are probably downstream effectors of Rho in this cascade.

1.4.4 Exploring the profilin family: characteristics in different organisms

Phylogenetic comparison of profilins shows that two profilin subfamilies originated very early from one ancestor. After separation, one group contains vertebrate and viral profilins whereas the non-mammalian profilins form another group and include profilin IV from vertebrates. The explanation for the viral profilins to follow changes in vertebrate profilins lies in the evolutionary pressure for a viral profilin to exist in the vertebrate host cell. On the other hand, plant profilins form a more closely related group in the non-mammalian profilin branch (Arasada *et al.*, 2007).

Profilins can be divided into four classes depending on their origin: plants, mammals, other eukaryotes and viruses. Between the different classes of profilins sequence homology is low (30%) but within a class homology is much higher (50 to 80%).

1.4.4.1 Profilin in lower eukaryotes

Lower eukaryotes contain one, two and occasionally even three genes as seen in the free living amoeba *Dictostelium discoideum* (Arasada *et al.*, 2007; Haugwitz *et al.*, 1991). The sequences of profilins I and II from *D. discoideum* are 55% identical and have similar characteristics (Haugwitz *et al.*, 1991). Although mutations in these profilins do not cause severe defects, double mutants showed malfunction in cytokinesis, pinocytosis, motility and development. *D. discoideum* profilin III shows only minor expression and represents 0.5% of total profilin even though it has the characteristics of a typical profilin. Beside profilins, *D. discoideum* contains an almost complete set of actin-binding proteins. Three *D. discoideum* profilin isoforms are closer related to the mammalian and viral profilins than to the majority of other profilins from lower organisms (Arasada *et al.*, 2007). Another amoeba, *Acanthamoeba castellanii* contains three profilin isoforms with either acidic (profilin IA and IB) or basic (profilin II) properties and different subcellular localisations (Bubb *et al.*, 1998). Vinson et al. determined the structure of *A. castellanii* profilin I in solution using NMR (Vinson *et al.*, 1993).

1.4.4.2 Profilin in higher eukaryotes

Higher eukaryotes contain higher numbers of profilin genes. In mammals, four discrete profilin genes have been identified (*Pfn1-4*) which are diversified in sequence and expression. The Pfn1 gene is known as the ubiquitous isoform profilin 1 (Schlüter, 1997), the Pfn2 gene exists in two splice variants, of which profilin 2a is primarily expressed in neuronal cells and profilin 2b mainly in the kidney (Di Nardo *et al.*, 2000). Pfn3 and Pfn4 encode respectively for kidney- and testis-specific variants (Hu *et al.*, 2001; Obermann *et al.*, 2005).

Profilin 1 was the first isolated profilin from the mammalian thymus (Carlsson *et al.*, 1977). In mice, profilin 1 is present in all embryonic stages and is present in nearly all cell types and tissues except for skeletal muscle (Witke *et al.*, 1998). Profilin 1 is involved in the regulation of the cytoskeletal architecture and dynamics and plays a role in the maintenance of the cell structure. The high expression of the profilin 1 isoform in proliferating cells suggests a role in cell growth and division. Disruption of the profilin 1 gene causes death in the embryological stage in mice (Witke *et al.*, 2001). When the gene is overexpressed, an abnormal stabilisation of microfilaments is observed. In human, the

affinities of profilin 1 and 2 for PLP and PIP_2 are equal, while the affinity of profilin 1 for actin is 4-5 times higher compared to profilin 2 (Gieselmann *et al.*, 1995).

A second profilin gene was discovered by sequencing cDNA library clones from human brain (Honoré *et al.*, 1993). Further studies showed expression of profilin 2 in the developing nervous system, differentiated neurons (Witke *et al.*, 2001), brain (Di Nardo *et al.*, 2000), skeletal muscles and kidney (Honoré *et al.*, 1993). In mice, the profilin 2 transcript can be spliced alternatively to produce a minor form of profilin 2, profilin 2b, in mouse brain. This protein differs in the last 32 amino acids and has a low affinity for actin and poly-L-proline (Di Nardo *et al.*, 2000).

Profilin 3 was isolated from rat kidney and binds actin (Hu *et al.*, 2001). Although isolated in the kidney, the main expression pattern of profilin 3 in mice seems to be in testis (Braun *et al.*, 2002; Obermann *et al.*, 2005).

Profilin 4 shares only 30% of its amino acid sequence with other profilins but is nevertheless significantly well aligned with the profilin domain. Like profilin 3, this isoform interacts specifically with the actin cytoskeleton of developing male germ cells at distinct time points and subcellular locations. Profilin 4 is expressed earlier than profilin 3 during spermatogenesis and functions in the generation of acrosomes and spermatid nuclear shaping (Obermann *et al.*, 2005). The presence of profilins during sperm development shows that actin plays an important role in the function of testis and is regulated by a number of actin-interacting proteins (Vogl, 1989).

The structure of yeast profilin was determined by X-ray diffraction and showed also a global fold, which is similar to other profilins (Eads *et al.*, 1998). Analogous to the lower eukaryote *D. discoideum*, mutations in the ligand binding site of yeast profilin cause impaired cytokinesis and are lethal, showing the importance of profilin in this organism (Haugwitz *et al.*, 1991; Lu and Pollard, 2001). *C. elegans* has three profilins, which show tissue specific expression. The three profilins show low to intermediate similarity to each other and have different biological functions. Gene knockout studies of profilins 2 and 3 showed they are not essential (Polet *et al.*, 2006).

1.4.4.3 Profilin in Planta

In plants, the number of profilin genes is highest, both mono- and dicotyledones contain up to ten different profilin genes (Ren and Xiang, 2007). While some of these genes may be pseudogenes, others give rise to two classes of proteins isoforms. There are ubiquitous forms which are constitutively expressed in all tissues, others are restricted to reproductive tissues, and their expression is strictly regulated during development (Kandasamy *et al.*, 2002). In *Arabidopsis*, 4 profilin genes encode for 4 isoforms of which profilins I and II are expressed in all plant organs and profilins III and IV are only present in floral tissues (Thorn *et al.*, 1997). Plant profilins function in a comparable way as profilins in mammals. Giehl et al. showed that birch pollen profilin functions in the same way on the polymerization of actin from animals, as do mammalian profilins (Giehl *et al.*, 1994). On the other hand, nucleotide exchange experiments did not confirm a role for *Arabidopsis* profilin I and II on α-actin in vitro (Perelroizen *et al.*, 1996). This function is however fulfilled by mammalian and *Acanthamoeba* profilins (Mockrin and Korn, 1980).

Profilins are highly immunogenic molecules in many organisms and are among the most prominent allergens in plants (Gadermaier *et al.*, 2013; Plattner *et al.*, 2008; Santos and Van Ree, 2011). Profilin is the major allergen present in birch, grass, and other pollen. The interaction patterns for actins, PLP and PIP_2 have been identified in plant profilins but the affinity differs between species and isoforms. Plant profilins are human allergens and are involved in 20-30% of type I allergies (Thorn *et al.*, 1997). Type I hypersensitivities are characterized by rhinitis, conjunctivitis and bronchial asthma affect 15% of the population of industrialized countries (Valenta *et al.*, 1993).

A major structural difference between plant and other profilins is the presence of a solvent-filled pocket located near the actin-binding surface. This specific binding site is a unique plant-specific structural feature and represents most likely the immunogenic site of plant profilins.

1.4.4.4 Profilin in other eukaryotes

S. japonicum possesses one profilin-like protein, which has been characterized as a potential vaccine candidate (Zhang *et al.*, 2008). Zhang and colleages identified profilin

from *S. japonicum* as a protein localized in the tegument of adult worms. During the different stages of the parasite life cycle, profilin was differentially expressed. Up to date, no profilins have been characterized in other *Schistosoma* species infecting humans.

The structure of profilin from *Plasmodium falciparum* has been determined, presenting the first profilin structure of a pathogenic parasite (Kursula *et al.*, 2008a). *Plasmodium* species cause malaria and use the microfilament system as their active motor in parasite locomotion and host cell entry. Profilin present in this parasite possesses biochemical features of eukaryotic profilins but is structurally different as it contains an unique minidomain (Kursula *et al.*, 2008a).

Profilin from the related apicomplexan parasite *Toxoplasma gondii* is known to be involved in parasite motility, host cell invasion, immune evasion and virulence in mice. It has been shown that *Toxoplasma* profilin is not needed for the survival and growth of the parasite, but is essential for the gliding motility (Plattner *et al.*, 2008). In addition, it was shown that profilin is responsible for the toll-like receptor (TLR)-11-dependent IL12 immune response during *Toxoplasma* infection in mice. A similar immune response could not be detected for *Plasmodium* profilin, which probably reflects the different host specificities of these two (otherwise very homologous) parasites. In the case of toxoplasmosis, keeping the parasite levels in the host moderate, minimizes the host immune response against the parasite. This on its turn keeps the host viable and capable of spreading the parasite.

1.4.4.5 Profilin in viruses

Vaccinia virus contains a profilin, which is closely related to mammalian profilins. This DNA-virus uses and modifies actin for morphogenesis and forms specialized actin bundles in the release of virions. The viral profilin is located in the cytoplasm and is not essential for infection, as it is not an integral component of virions. The profilin expressed is not required for actin-associated events like intracellular virus movement, formation of specialized microvilli or release of mature virions (Blasco *et al.*, 1991). Unlike mammals, *Vaccinia* virus profilin has a weak affinity for actin monomers and seems to have a more prominent role in the phosphoinositide metabolism than in actin assembly. The protein binds PIP_2 and phosphatidyl-4-monophosphate with a higher

affinity than actin. *Vaccinia* virus is the only profilin described that does not bind poly-L-proline (Machesky *et al.*, 1994).

2 Objectives

The current thesis work was set to characterize profilin from *S. japonicum* to be able to compare its function and structure with other profilins. This study was focused on both functional and structural characterization of *Sj*Pfn alone and in complex with actin.

Does *S. japonicum* express a canonical profilin?

*Sj*Pfn has a fairly low sequence identity to canonical profilins, and from the sequence it was not clear, whether it possesses the characteristic functional properties of profilins. We aimed to purify and crystallize the parasitic profilin to be able to get insight in the structure of *Sj*Pfn. Analysis of the protein fold was expected to give a better understanding of the structural features that make profilin such a highly immunogenic molecule.

Can *S. japonicum* profilin regulate actin dynamics *via* interactions with poly-L-proline ligands?

To study the functional characteristics of *Sj*Pfn, we wanted to perform different biophysical experiments to analyse the interaction of *Sj*Pfn with different repeats of poly-L-proline present in other actin regulatory proteins. This will broaden the view of the regulation of actin filament dynamics in *Schistosoma*.

How does *Sj*Pfn interact with actin?

We investigated the binding of *Sj*Pfn to actin by performing both biochemical and biophysical experiments. The goal was to analyse the interaction in detail to elucidate the role of *Sj*Pfn in actin cytoskeleton remodeling. In addition, the effect of *Sj*Pfn on actin polymerization was considered. We aimed solving the actin-*Sj*Pfn structure to get more insight in the structure-function relationships in the regulation of actin polymerization in *S. japonicum*.

3 Materials

3.1 Laboratory equipment

Equipment	Manufacturer
ÄKTA explorer, ÄKTA purifier	GE Healthcare, Sweden
Analytical balance	Sartorius, Germany
Astacus distillation unit	MembraPure, Germany
Avanti J26-XP centrifuge	Beckman Coulter, USA
CERTOMAT® IS benchtop incubator	Sartorius, Germany
CFX96 RealTime System	Bio-Rad, Germany
ChiraScan Plus spectrophotometer	Applied Photophysics, UK
DynaPro NanoStar™	Wyatt, Germany
Electrophoresis unit	Bio-Rad, Germany
Gel documentation system	PEQ Lab, Germany
Genie vortex	Scientific Industries, Germany
Heraeus™ FRESCO21™ centrifuge	Thermo Scientific, Germany
Laminar air flow chamber	Kojair Tech Oy, Finland
Mastercycler® gradient	Eppendorf, Germany
MiniDAWN™ TREOS detector	Wyatt, Germany
Multitron Pro shaker	Infors, Germany
Nanodrop 2000 spectrophotometer	Thermo Scientific, Germany
Optilab® T-rEX refractometer	Thermo Scientific, Germany
pH meter	Mettler Toledo, Germany
Sonopuls Sonifier	Bandelin, Germany
Systec VX150 autoclave	Systec, Germany
Tabletop centrifuge 5810-R	Eppendorf, Germany
TECAN infinite M200 fluorometer	TECAN, Germany
Thermomixer comfort	Eppendorf, Germany
Tube rotator	Stuart, UK
VARIOMAG® magnetic shaker	Thermo Scientific, Germany

3.2 Laboratory consumables

Consumable	Supplier
Amicon-Ultra centrifugal filter units	Millipore, Ireland
Assay plates (96-well)	Greiner Bio-One, Germany
Dialysis membranes	Carl Roth, Germany
Disposable plastic cuvettes	Carl Roth, Germany
Erlenmeyer flasks	Schott Duran, Germany
Falcon tubes	Greiner, Bio-One
Gravity-flow columns	Bio-Rad, Germany
Inoculation loops	Greiner Bio-One
Low 96-well clear plate	Bio-Rad, Germany
Microcentrifuge tubes	Eppendorf, Germany
Microseal adhesive films	Bio-Rad, Germany
Mini-PROTEAN^{R} TGX™ precast gels	Bio-Rad, Germany
Polymerase chain reaction (PCR) tubes	Brand, Germany
Pipette tips	Sartorius, Germany
Plastic Petri dishes	Sarstedt, Germany
Plastic syringes	Braun Melsungen, Germany
Serological pipettes	Greiner Bio-One, Germany
Slide-A-Lyzer mini dialysis units	Thermo Scientific, Germany
Syringe filters	Millipore, Germany
Vivaspin 20 concentrators (MWCO: 10 & 30K)	Sartorius Stedium Biotech, Germany
PD-10 columns	GE Healthcare, UK

3.3 Chemicals

Chemicals used in this study were of analytical grade and were purchased from Carl Roth (Germany), Sigma Aldrich (Germany), Roche Diagnostics (Germany), Calbiochem (Germany), GE Healthcare (Sweden) and AppliChem (Germany), unless stated otherwise.

3.4 Kits, spin columns and reagents

QIAprep^{R} Spin mini-prep kit	Qiagen, Germany
QIAquick^{R} Gel Extraction kit	Qiagen, Germany
QIAquick^{R} PCR purification kit	Qiagen, Germany
Quick-Load DNA Ladder	New England Biolabs, Germany
PageRuler prestained protein ladder	Thermo Scientific, Lithuania

3.5 Growth media and antibiotics

LB medium	Carl Roth, Germany
Ampicillin	Carl Roth, Germany
Kanamycin	Carl Roth, Germany

3.6 Bacterial strains and vectors

Bacterial strains:

Cloning strain:

NEB5α	New England Biolabs, Germany

Expression strains:

BL21 (DE3)	New England Biolabs, Germany
BL21 CodonPlus (DE3) RIPL	Agilent Technologies, Germany
Rosetta (DE3)	Novagen, Germany

Vectors:

p-GEX-4T-1-sj15	Zhong-dao Wu's group, Sun Yat-sen University, Guangzhou, China
pETNKI-his-SUMO3-LIC	Protein facility of the Netherlands Cancer Institute, Amsterdam, The Netherlands

3.7 Enzymes, substrates and nucleotides

cOmplete Mini Protease Inhibitor Cocktail tablet	Roche Applied Science, Germany
KpnI	New England Biolabs, Germany
PCR primers	Eurofins MWG, Germany
Phusion^{R} high-fideltiy PCR master mix	Thermo Fisher Scientific, Germany
SYPRO Orange dye	Molecular Probes, Germany
T4 DNA polymerase	New England Biolabs, Germany
Thrombin restriction grade	Merck Millipore

3.8 Materials for chromatography

Resins:

Ni-NTA agarose	GE Healthcare, Sweden

Columns:

GSTrap FF (1ml) column	GE Healthcare, Sweden
HisTrapFF (1ml) column	GE Healthcare, Sweden
HiLoad 16/60 Superdex 200 column	GE Healthcare, Sweden
HiLoad 16/60 Superdex 75 column	GE Healthcare, Sweden
Superdex 200 10/300 GL	GE Healthcare, Sweden
Superdex 75 10/300 GL	GE Healthcare, Sweden

3.9 Growth media

3.9.1 Lysogeny broth medium

The lysogeny broth (LB) medium is the most widely used, nutritionally-rich medium for the growth of bacteria. The composition of LB medium (Bertani, 1951), used in this study, is given below:

Tryptone	1.0% (w/v)
Yeast extract	0.5% (w/v)

NaCl	1.0% (w/v)

The medium was prepared in double-distilled water (ddH_2O) and sterilized using an autoclave at 121°C for 15 min, and stored at 4°C until use.

3.9.2 Auto-induction medium

The auto-induction (AI) medium, introduced by William Studier (Studier, 2005), allows spontaneous induction of protein expression, in isopropyl ß-D-1-thiogalactopyranoside (IPTG)-inducible *E. coli* strains, when the cells reach high density close to saturation phase. The medium contains a limited amount of glucose, which prevents uptake of lactose until it is depleted. The glucose is metabolized during the initial phase of bacterial growth and depleted in mid to late log phase. At this stage, lactose is taken up by the cells and converted to the natural inducer, allolactose, by ß-galactosidase. Allolactose causes the release of lactose repressor from its binding sites in DNA and induces the expression of T7 polymerase, which in turn induces the expression of target proteins (Studier, 2014). The ZYM-5052 auto-induction medium was used in this study and its final composition is given below:

ZY medium:	
Tryptone	1.0%
Yeast extract	0.5%

50X M:	
Na_2HPO_4	25 mM
KH_2PO_4	25 mM
NH_4Cl	50 mM
Na_2SO_4	5 mM
$MgSO_4$	2 mM

50x 5052:	
Glycerol	54 mM
Glucose	2.8 mM
α-lactose	5.6 mM

1000 X Trace metals:

$FeCl_3$	50 mM
$CaCl_2$	20 mM
$MnCl_2$	10 mM
$ZnSO_4$	10 mM
$CoCl_2$	2 mM
$CuCl_2$	2 mM
$NiCl_2$	2 2 mM
Na_2MoO_4	2 mM
Na_2SeO_3	2 mM
H_3BO_3	2 mM

First, 1 l of ZY medium was prepared in distilled water and the medium was sterilized in an autoclave. The 50x 5052 solution was made up to 100 ml with distilled water and mixed overnight to completely dissolve the sugars. The 50x M solution was made in a volume of 100 ml with distilled water and autoclaved.

3.9.3 SOC medium

Super optimal broth medium with catabolite repression was used after heat-shock transformation in *E. coli*. The addition of a nutrient rich bacterial growth medium instead of LB after heat-shock results in a higher transformation efficiency.

tryptone	2% (w/v)
yeast extract	0.5% (w/v)
NaCl	10 mM
KCl	2.5 mM
Glucose	20 mM
$MgCl_2$	10 mM

To ensure sterility, the medium was autoclaved at 121°C for 15 min. Glucose and $MgCl_2$ can be autoclaved separately to prevent the Maillard reaction.

3.10 Buffers and solutions

3.10.1 Buffers for agarose gel electrophoresis

1X Tris-acetate-EDTA (TAE) buffer	40 mM tris(hydroxymethyl)aminomethane (Tris), 1 mM ethylenediaminetetraacetic acid (EDTA), pH 8.0
6X DNA loading buffer	10 mM Tris-HCl (pH 7.6) 0.03% (w/v) bromophenol blue 0.03% (w/v) xylene cyanol 60 mM EDTA 60% glycerol

3.10.2 Buffers and solutions for SDS-PAGE

1X sodium dodecyl sulphate (SDS) running buffer	25 mM Tris, 192 mM glycine, 0.1% (w/v) SDS
6X SDS loading buffer	375 mM Tris (pH 6.8), 12% (w/v) SDS, 60% glycerol, 600 mM dithiotreitol (DTT), 0.06% (w/v) bromophenol blue
Coomassie staining solution	0.05% (w/v) Coomassie brilliant blue, 10% (v/v) acetic acid and 25%
Destaining solution	10% (v/v) acetic acid

3.10.3 Buffers for GST-tagged affinity chromatography

Buffer A (lysis buffer)	50 mM Tris (pH 8), 150 mM NaCl, 10% glycerol, 5 mM DTT, 25 µg/ml DNase, 6.25 mM $MgCl_2$, 10 mM imidazole and 1x cOmplete Mini Protease Inhibitor Cocktail tablet
Buffer B (equilibration buffer)	50 mM Tris (pH 8), 150 mM NaCl, 10% glycerol, 5 mM DTT
Buffer C (wash buffer)	50 mM Tris (pH 8), 500 mM NaCl, 10% glycerol, 5 mM DTT
Buffer D (elution buffer)	50 mM Tris (pH 8), 150 mM NaCl, 10% glycerol, 5 mM DTT, 30 mM reduced glutathione
Buffer E (dialysis buffer)	100 mM Hepes (pH 7), 50 mM NaCl, 5 mM DTT

3.10.4 Buffers for immobilized-metal affinity chromatography

Buffer A (lysis buffer)	100 mM HEPES (pH 7), 150 mM NaCl, 5 mM β-ME, 25 µg/ml DNase, 6.25 mM $MgCl_2$, 10 mM imidazole and 1x cOmplete Mini Protease Inhibitor Cocktail tablet
Buffer B (equilibration buffer)	100 mM HEPES (pH 7), 50 mM NaCl, 5 mM ß-ME and 10 mM imidazole
Buffer C (wash buffer)	100 mM HEPES (pH 7), 150 mM NaCl, 5 mM ß-ME
Buffer D (elution buffer)	100 mM HEPES (pH 7), 50 mM NaCl, 5 mM ß-ME, 300 mM imidazole

3.10.5 Buffers for size exclusion chromatography

3.10.5.1 SEC GST-SjPfn

Buffer 1 100 mM HEPES (pH 7), 50 mM NaCl and 5 mM DTT

3.10.5.2 SEC His-SUMO-SjPfn

Buffer 1 100 mM HEPES (pH 7), 150 mM NaCl and 5 mM ß-ME

3.10.6 Buffers for actin purification from muscle acetone powder

Buffer A 5 mM Tris (pH 8), 0.2 mM $CaCl_2$, 0.2 mM ATP, 0.5 mM DTT

3.11 Bioinformatic tools used

The bioinformatic tools described below where used to predict a plethora of properties from the nucleotide and amino acid sequence of the expression constructs studied. In this manner we were able to predict characteristics from the sequence such as sequence similarity, structural and functional homology to families of proteins, conserved sequence patterns in the course of evolution, secondary and tertiary structural features and regions of flexibility and disorderness.

3.11.1 ProteinCCD

Protein Crystallographic Construct Design (ProteinCCD) is available online at http://xtal.nki.nl/ccd. This tool is a meta-web server collecting information from prediction servers concerning secondary structure, disordered regions, coiled coils, flexible linkers and transmembrane domains. Although mainly used to design multiple truncation constructs to be used for protein expression and crystallization (Mooij *et al.*, 2009), Protein CCD was used in this study to calculate the parameters (G+C content, melting temperature) of the oligonucleotides designed for PCR amplification.

3.11.2 T-Coffee

T-Coffee (Tree-based Consistency Objective Function For alignment Evaluation) is an opensource package to align nucleic acids and protein sequences (Notredame *et al.*, 2000). T-Coffee generates multiple alignments via a library of pair-wise alignments and uses a progressive-alignment strategy to find the best fit multiple sequence alignment. The combinational use of local and global alignments in this tool is a remarkable improve for the accuracy of the alignment (Notredame *et al.*, 2000).

3.11.3 ClustalW

Clustal is a family of widely used computer software for multiple sequence alignment (Higgins and Sharp, 1988). Clustal Omega is the latest version of Clustal and makes use of seeded trees and HMM profile-profile techniques to perform multiple alignments. In the first step, the computer program performs a pairwise alignment that it uses to create a guide tree. This tree is then used to carry out a multiple alignment (Higgins and Sharp, 1988).

3.11.4 BLAST

BLAST (Basic Local Alignment Search Tool) is a widely used bioinformatics program for sequence searching (Johnson *et al.*, 2008; Notredame *et al.*, 2000). A BLAST search compares DNA or protein sequence information with a library or database of sequences. The software identifies library sequences that resemble the query sequence above a certain treshold (Johnson *et al.*, 2008). According to the query sequence, different types of BLAST searches can be performed. The nucleotide (Blastn) and protein blast (Blastp) algorithms search nucleotide and protein databases respectively (Johnson *et al.*, 2008).

3.11.5 ExPASy tools

The Expert Protein Analysis System (ExPASy) provides access to different software tools and databases in different domains of life sciences (Artimo *et al.*, 2012). In this study, the translate tool was used to translate a nucleotide sequence into a protein sequence.

ProtParam was used to calculate the molecular weight, theoretical isoelectric point, hydrophobicity and the extinction coefficient from a protein.

3.11.6 Espript

Espript (Easy sequencing in PostScript) was used to analyse multiple sequence alignments. This program starts from information from aligned sequences to obtain sequence similarities and secondary structure information (Robert and Gouet, 2014).

3.11.7 PISA

The publicly available tool PISA implements a method to identify macromolecular complexes in crystals (Krissinel and Henrick, 2007). The program provides a systematic approach based on physical-chemical models of macromolecular interactions and chemical thermodynamics. PISA was used to analyse the molecular interface of the protein complex, solved in this study by X-ray diffraction.

3.12 Software used for protein structure determination

3.12.1 Coot

The molecular graphics application COOT (Crystallographic Object-oriented toolkit) was used to build and validate atomic models into three dimensional electron density maps obtained by X-ray diffraction. The software uses three dimensional computer graphics to display and manipulate atomic models of macromolecules (Emsley *et al.*, 2010). Beside model building, Coot was also used to superimpose threedimensional structures of profilins via secondary structure matching (SSM). This tool fits the secondary structure elements of one protein to those of the other and places hereby the molecules in the same position and orientation so that the differences may be clearly seen (Emsley *et al.*, 2010). The superimposed structures were then analysed to make a structure-based alignment.

3.12.2 PyMol

PyMol is a molecular visualisation program to make high quality three dimensional images of proteins (The PyMOL Molecular Graphics System, Version 1.2r3pre, Schrödinger, LLC). This program was used to look at molecular structures and to make publication quality pictures of proteins. Coordinate files obtained from the Protein Data Bank can be imported in PyMol which makes it easy to get insight in the available protein structures. Using the high quality images of proteins in PyMol, the secondary structure of profilins were analysed.

3.12.3 Phenix package software

After X-ray data collection, PHENIX (Python-based Hierarchical Environment for Integrated Xtallography) was used for the determination and refinement of the macromolecular crystal structures. Within the package, Phenix.autosol and phaser were used to solve the structures with anomalous signal and molecular replacement respectively. The AutoSol program automatically performs heavy atom location, phasing, density modification and initial model building. Phaser is a program for experimental phasing with maximum likelihood methods. Different cycles of refinement were executed using the Phenix.refine program. In this program, likelihood based refinement is performed with the possibility to refine different positional parameters.

3.12.4 XDS Program Package

The X-ray Detector Software (XDS) program is the main program within the XDS Program Package. This program was used to proces single-crystal monochromatic diffraction data (Wolfgang Kabsch, 2010). XDS processes a sequence of adjacent, nonoverlapping rotation images collected from a single-crystal at a fixed X-ray wavelength. The program derives automatically the reflecting range, spot width, crystal orientation, symmetry and cell parameters from the data images and delivers a list of corrected integrated intensities of the reflections occurring in the data images.

4 Methods

This section provides a general description of the experimental procedures used in the study. Case-specific modifications are reported wherever necessary.

4.1 Sequence and ligation independent cloning

The *Sj*Pfn cDNA (S. M. Zhang *et al.*, 2008) was cloned into a prokaryotic expression vector using a sequence- and ligation-independent cloning (SLIC) method (Li and Elledge, 2012). SLIC uses T4 DNA polymerase, this enzyme is a 3' → 5' exonuclease and creates single stranded overhangs in both vector and insert. These are then annealed by *in vitro* homologous recombination. Transformation of the constructs in *E. coli* finally generates recombinant expression of the protein of interest (Li and Elledge, 2012). The following sub-sections detail the steps followed in this study to clone target DNA fragments into the vector of choice by using the SLIC method.

4.1.1 Design of primers

Primers were designed (table 6) and their properties, such as the G+C content and melting temperatures, were calculated using ProteinCCD.

Construct	**Designed primers**
Vector: forward primer	5'-AGCACCACCACCACCACCAC
Vetor: reverse primer	5'-CCCTCCCGTCTGCTGCTGGA
Insert: forward primer	5'-TGTTCCAGCAGCAGACGGGAGGGATGAGCGCT-GATAGTTGGG
Insert: reverse primer	5'-GTGGTGGTGGTGGTGGTGCTTTAGTAACCCATT-CGCTCGTAATG

Table 6. Primers used for PCR amplification of target DNA fragments.

The primers were synthesized and delivered by Eurofins MWG GmbH, Ebersberg (Germany) in lyophilized form with high-purity salt-free (HPSF)-purified quality. The

primers were dissolved in ddH_2O to a final concentration of 100 pmol/µl and frozen at -20°C until use.

The pETNKI-hisSUMO3-LIC vector, provided by the Netherlands Cancer Institute (NKI), was used for SLIC-based sub-cloning. As indicated by its name, the vector includes an N-terminal hexa-histidine tag and a 3C protease-cleavable site. The 3C protease cleavage site enables removal of the affinity tag following initial purification of the protein from a soluble lysate. The vector also contains and kanamycin resistance marker.

4.1.2 Plasmid purification

The template plasmids and the cloning vector were purified from overnight bacterial cultures by the alkaline lysis method using the QIAprep spin mini-prep kit, according to the instructions of the manufacturer.

4.1.3 Amplification of target genes

The pETNKI-hisSUMO3-LIC vector and the coding region of *Sj*Pfn were amplified *in vitro* by the polymerase chain reaction (PCR) (Mullis *et al.*, 1986) with the primers described in table 6. The recombinant plasmid pGEX-4T-1-sj15 that contains the *S. japonicum* profilin gene was used as template.

Following is the mixture of reagents used for each PCR reaction:

Template plasmid	0.01 µg
Forward insert primer	0.5 µM
Reverse insert primer	0.5 µM

Phusion^R High-Fidelity Mastermix was added to the above and the reaction volume was adjusted to 50 µl. The Phusion^R High-Fidelity Mastermix is a mixture of 0.04 U/µl Phusion^R DNA polymerase, 200 µM of each deoxynucleotide and an optimized reaction buffer. Following are the conditions used in the thermal cycle:

Initial denaturation	98°C for 45 s
	98°C for 10 s
Annealing cycle	68°C for 20 s
	72°C for 1 min 35 s

The annealing cycle was repeated 30 times

Extension	72°C for 5 min

After the PCR reaction, DpnI was added to the PCR products to digest the template DNA.

4.1.4 Agarose gel electrophoresis

During agarose gel electrophoresis, an electric field is applied to an agarose gel which allows negatively-charged DNA molecules to migrate through the porous matrix according to their size. This technique was used to analyse the size and purity of the amplified DNA fragments or purified plasmid DNA molecules. Dependent on their size, the migration of DNA molecules towards the positive pole of the electrophoresis chamber will differ where smaller fragments will move faster than larger molecules. Ethidium bromide (EtBr), a fluorescent dye that intercalates with DNA double strands, was added to the melted agarose to visualize the DNA bands under a short-wavelength UV light source. DNA samples were mixed with 6X gel loading buffer and then loaded into the slots on a 1.2% agarose gel. To determine the size of the DNA fragments, a marker lane was also included. An electric current of 100 V was applied to the gel in order to start the migration of the DNA molecules.

4.1.5 Gel extraction of DNA fragments

Extraction of the PCR products from the agarose gel was performed by following the QIAquick gel extraction kit protocol. The excised DNA bands were solubilized and when applied to a spin column, the DNA in the sample adsorbs to the silica membrane. Impurities are washed away before pure DNA elutes from the column. This purification method eliminates nucleotides, agarose, EtBr and other impurities present in the sample.

4.1.6 Linearization of the vector by KpnI digestion

0.5 µg of the vector (pETNKI-hisSUMO-LIC) was linearized by restriction digestion with the KpnI enzyme using the enzyme concentration, incubation temperature and duration as prescribed by the manufacturer.

4.1.7 T4 DNA polymerase treatment of insert and vector

To create single-stranded overhangs, the resulting constructs were treated separately with T4 polymerase at 20 °C for 20 min. The reaction was terminated by adding a 1/20 volume of 500 mM ethylenediaminetetraacetic acid (EDTA) followed by inactivation of the T4 polymerase by incubation at 75 °C for 20 min.

4.1.8 Annealing

The T4 DNA polymerase-treated insert and vector were were mixed in a 1:5 molar ratio. The annealing reaction was performed at 65 °C for 10 min, and the reaction mixture was subsequently slowly cooled to room temperature in a PCR machine to improve the annealing efficiency.

4.1.9 Transformation of *E. coli* cells

An aliquot of heat-competent NEB5α cells (50 µl) was thawn on ice and mixed with 1 µl of the recombinant plasmid. Before exposing the cells to a heat shock of 45 s at 42 °C, an incubation period of 30 min on ice was applied. Afterwards, the cells were immediately placed on ice for 2 min. 500 µl of SOC medium were added to the cells, and the mixture was incubated at 37°C for 45 min with shaking. The cells were plated out on an LB agar plate supplemented with appropriate antibiotic(s) and incubated overnight at 37°C.

4.1.10 Colony PCR

The presence of the correct recombinant plasmid in a bacterial clone was analysed via colony PCR. A single colony was picked from the LB agar plate and used as a DNA template during the PCR reaction, using the reaction mixture described in section *4.1.3.* The amplified products of the colony PCR were analysed by agarose gel electrophoresis. Afterwards, the plasmids corresponding to positive transformants were isolated from the bacterial cultures.

4.1.11 Plasmid sequencing

The purified plasmids were sent to Eurofins MWG GmbH (Ebersberg, Germany) for DNA sequencing. The standard vector forward and reverse primers were used in sequencing. The sequences were compared to the original gene sequences available on the NCBI database by using Blastn. The DNA sequences were translated to protein sequences by the use of the ExPASy translate tool, and the comparison of protein sequences to the database was performed by using Blastp. Only the plasmids that showed 100% sequence identity to both reference sequences were considered for further experiments.

4.2 Recombinant expression and purification of SjPfn

4.2.1 *E. coli* cell strains used for expression screening

The following *E. coli* strains were used to test the heterologous overexpression of the constructs.

BL21 (DE3)

Genotype: fhuA2 [lon] ompT gal (λ DE3) [dcm] ΔhsdS λ DE3 = λ sBamHIo ΔEcoRI-B int::(lacI::PlacUV5::T7 gene1) i21 Δnin5

Properties: BL21 (DE3) is an *E. coli* B strain that carries the λ DE3 lysogen. It is deficient in proteases lon and ompT and minimizes proteasomal degradation. This strain is widely used for high-level expression of recombinant proteins that are not toxic to *E. coli*.

BL21 CodonPlus (DE3) RIPL

Genotype: F-ompT hsdS(rB- mB-) dcm+ Tetr gal λ(DE3) endA The [argU proL Camr] [argU ileY leuW Strep/Specr]

Properties: This strain of *E. coli* is engineered to include extra copies of the tRNA genes, argU, ileY, leuW and ProL. These genes encode tRNAs that often limit the translation of heterologous proteins in *E. coli.* The addition of

such tRNAs improves the expression levels of heterologous proteins that are otherwise poorly expressed in conventional BL21 strains.

Rosetta (DE3)

Genotype: F^-ompT $hsdS_B(r_B^-m_B^-)$ gal dcm(DE3) pRARE (Cam^R)

Properties: Rosetta (DE3) is a derivative of the conventional BL21 strain and is specifically constructed to improve the expression of eukaryotic proteins that contain rare *E. coli* codons. This strain expresses six rare tRNAs for the codons AUA, AGG, AGA, CUA, CCC and GGA.

4.2.2 Optimization of growth conditions and cell lysis

The expression of the recombinant proteins from plasmids pETNKI-hisSUMO3-SjPfn and pGEX-4T-1-*Sj*Pfn was tested in all three bacterial strains described in the previous paragraph. For each strain, a single colony was picked and an overnight culture at 37°C was set up in LB medium supplemented with kanamycin. In order to analyse the expression level and solubility of the expressed protein, different growth conditions were applied to small volumes of *E. coli* cells (typically, 5 ml). Different autoinduction medium cultures were inoculated with 2% of the overnight primary culture and grown at either 18°C or 25°C for a certain incubation period (24, 36 or 48h). The cells were harvested by centrifugation. The pellets were flash-frozen and stored at -80°C until further use. The pellets were lysed as described in 4*.2.6*, and the resulting yields of soluble protein were compared to find out the optimal growth conditions.

Harvested cell pellets were thawn and resuspended in lysis buffer. The cells were lysed *via* the freeze-thaw method because of small volumes. The cell suspensions were immersed in liquid N_2 for 30 s, and the frozen cells were transferred immediately to a water bath at 42°C for thawing. Following lysis, the cell debris was removed by centrifugation at 35 000 g for 30 min at 4 °C. Samples were taken from both soluble and insoluble fractions of the cell lysate and analysed on SDS-PAGE.

4.2.3 Sodium dodecyl sulphate polyacrylamide gel electrophoresis

Sodium dodecyl sulphate polyacrylamide gel electrophoresis (SDS-PAGE) is a technique to separate proteins according to their size (Laemmli, 1970). The protein sample is mixed with sodium dodecyl sulphate (SDS), which denatures the protein by binding to the protein. This results in linear unfolded protein molecules, which are negatively charged and will travel in an electrical field independent of their structure and charge. When the SDS gel is placed in an electrical field, proteins will migrate towards the positive electrode through the effect of molecular sieving. Staining of the protein gels with Coomassie brilliant blue afterwards will visualize the protein bands. The size of the protein can be deduced by comparison of the migration of a protein marker, which is run in parallel with the protein samples.

SDS-PAGE was run using mini-PROTEAN^{R} precast gels and a Bio-Rad electrophoresis sytem. The samples were mixed with SDS sample buffer and heated at 95 °C for 5 min. Electrophoresis was performed at a constant voltage (150-180V). The gels were stained with Coomassie blue staining solution for 30 min on an orbital shaking platform and placed in a destaining solution for 20 min.

4.2.4 Quantification of proteins

Protein concentrations were determined by measuring the light absorption at 280 nm using a Nanodrop spectrophotometer and by applying the working principle of the Lamber-Beer law (Beer, 1852):

$$c = A / (\varepsilon . l)$$

Where, c is the molar concentration of the protein ($mol.l^{-1}$)
l is the pathlength of light (cm)
A is the absorption
ε is the molar extinction coefficient of the protein ($l.mol^{-1}.cm^{-1}$)

4.2.5 Confirmation of protein identity by mass spectrometry

The identification of the purified proteins was performed by tryptic peptide mapping using mass spectrometry. This method determines the masses of biomolecules by

measuring the mass-to-charge (m/z) ratio of the respective ions (Fenn *et al.*, 1989). In this study, the mass spectrometric analyses of the samples were carried out at the Biocenter Oulu Proteomics Core Facility, Department of Biochemistry, University of Oulu (Oulu, Finland).

4.2.6 Large-scale expression of recombinant *Sj*Pfn

4.2.6.1 GST-SjPfn

GST-*Sj*Pfn was recombinantly expressed in *E. coli* BL21(DE3) cells, which were grown at 18 °C in 1 l autoinduction medium (Studier, 2005) supplemented with 100 µg/ml ampicillin. The cells were harvested after 36 h by centrifugation at 4 °C and 3000 g for 30 min. The cell pellets were stored at -80 °C until further use. The cell pellets were resuspended in 50 ml buffer A, after which the cells were disrupted by sonication and the lysate was clarified by centrifugation. The supernatant containing the protein of interest was used for purification.

4.2.6.2 His-SUMO3-SjPfn

Recombinant polyhistidine-SUMO3-*Sj*Pfn (His-SUMO3-*Sj*Pfn) was expressed in *E. coli* BL21(DE3)-RIPL cells. Transformed cells were grown at 25 °C in 1 l autoinduction medium (Studier, 2005) supplemented with 50 µg/ml kanamycin. After 36 h, the cells were harvested by centrifugation at 4 °C and 3000 g for 30 min, and the cell pellets were frozen at -80 °C until further use. The cell pellets were thawn and subsequently resuspended in lysis buffer. The cells were disrupted by sonication and the lysate was clarified by centrifugation. The supernatant containing the protein of interest was used for purification.

4.2.7 Affinity purification of proteins

Affinity chromatography is a separation method for protein mixtures based on a highly specific interaction between an immobilized ligand and its binding partner. The purification of the protein of interest is based on the interaction of the protein with a covalently bound component on the stationary phase of the chromatographic column. In

this study, two variants of affinity purification were used to purify the protein of interest.

4.2.7.1 GST tagged proteins

Glutathione S-transferase (GST) is a 26 kDa protein that can be expressed as a fusion protein to the N-terminus of target proteins. These tagged proteins are easily purified in a one-step procedure by affinity chromatography on immobilized glutathione (Smith and Johnson, 1988). The GST tag adds about 220 amino acids to the protein of interest and has a positive influence on its expression efficiency and protein solubility. The functional GST protein forms a dimer. Reduced glutathione, the tripeptide Glu-Cys-Gly, can be immobilized through its sulfhydryl group to sepharose beads. Binding is most efficient near neutral physiological pH and mild conditions to preserve the structure and enzymatic function of GST. When the protein mixture is loaded on the column, the GST-tagged protein will be retained while the proteins without affinity for reduced glutathione will pass the column easily (Simons and Vander Jagt, 1977). Unspecific interactions with the stationary phase are washed away before the protein of interest is eluted from the column by adding excess amounts of reduced glutathione. GST has a higher affinity for free glutathione compared to immobilized glutathione and this will result in the elution of the GST-tagged protein from the column (Harper and Speicher, 2011).

GSTrapp FF columns (1 ml) are prepacked columns suitable for the purification of GST-tagged *Sj*Pfn cloned into a pGEX vector. Columns were stored in 20% ethanol and before use, the columns were first extensively washed with 20-25 column volumes (CV) filtered and degassed ddH_2O to remove ethanol. Impurities were washed away with 50 mM glutathione (15-20 CV). The matrix was equilibrated with 50 ml of buffer B. The supernatant of the cell lysate was applied to the column and binding of the lysate (20 ml) was allowed for 4 h at 4 °C with the use of a pump at a constant flow rate of 0.250 ml/min. The column was then washed extensively with buffer B (20 CV) and buffer C (25 CV) at a flow rate of 0.5 ml/min to wash off any impurities. A second wash with buffer B (20 CV) was performed before elution. The protein of interest was eluted with buffer D in 1 ml fractions (0.25 ml/min) in order to monitor the extent of purity at different stages of elution. The eluted fractions were resolved using SDS-PAGE. The concentration of the pooled fractions containing the fusion protein was measured using

a Nanodrop 2000 spectrophotometer and the samples were dialysed against buffer E overnight at 4°C.

4.2.7.2 Hexa-histidine tagged proteins

Immobilized-metal affinity chromatography (IMAC) is based on the ability of histidine and cysteine residues to form stable interactions with divalent metal cations such as Ni^{2+}, Co^{2+}, Zn^{2+} and Cu^{2+} (Porath *et al.*, 1975). After elimination of unbound and aspecific bound contaminants from the column, the protein of interest can be eluted competitively by the use of high concentrations of imidazole.

In this study, a hexa-histidine tag was cloned at the N-terminus of the protein. When expressed recombinantly, polyhistidine-tagged proteins can be purified from a protein sample using a chromatographic column on which Ni^{2+} is covalently bound as the initial purification step. A HisTrap FF sepharose column (1 ml) charged with Ni^{2+} was first extensively washed with 5-10 CV of filtered and degassed ddH_2O to remove ethanol in which the matrix was stored. The matrix was equilibrated with 5 CV of buffer B containing 10 mM imidazole to remove nonspecifically bound proteins. The supernatant of the cell lysate was applied onto the column with the use of a pump at a constant flow rate of 0.5 ml/min. The column was then washed extensively with buffer C to wash off any impurities. Elution of the protein of interest was performed with buffer D in 1 ml fractions in order to monitor the extent of purity at different stages of elution. The eluted fractions were resolved using SDS-PAGE. The pooled fractions containing the fusion protein were concentrated to a volume of 2.5 ml and applied onto a PD-10 desalting column to remove the imidazole in the buffer.

4.2.8 Cleavage of the affinity tag

4.2.8.1 Cleavage of the GST tag

The affinity purified protein was digested with thrombin restriction grade (Merck Millipore) in order to cleave the N-terminal GST tag. The amount of thrombin, temperature and length of incubation had to be optimised and was most effective for GST-*Sj*Pfn by adding 4U enzyme per mg of protein. Cleavage was performed overnight at room temperature. In order to avoid unwanted proteolysis at secondary sites, the extent

of thrombin digestion was analysed by SDS-PAGE. The protein was then concentrated to 1 ml by using Vivaspin 20 concentrators with a cut-off (MWCO) of 10 kDa and centrifuged at 3220 g (4°C).

4.2.8.2 Cleavage of the hexa-histidine tag

The N-terminal 6xHis-SUMO3 tag was cleaved using 1 µg/ml recombinant SENP2 protease for 2 h at room temperature (20°C). The cleaved proteins were passed through a Ni-NTA column to remove the SUMO3 tag and any uncleaved fusion proteins. The protein was then concentrated to 500 µl by using Vivaspin 20 concentrators with a cut-off (MWCO) of 10 kDa and centrifuged at 3220 g (4°C).

4.2.9 Size exclusion chromatography

Final purification was performed by size-exclusion chromatography using a Superdex 75 10/300 GL or HiLoad 16/600 Superdex 75 column. 8 mg of the protein were applied onto the preparative grade column, pre-equilibrated with the SEC buffer using an ÄKTApurifier or an ÄKTAexplorer (GE Healthcare Life Sciences). A constant flow rate of 1 ml/min was applied at equilibration, sample injection and fractionation. SEC separates molecules based on their hydrodynamic volume, which is often proportional to the molecular weight (Porath and Flodin, 1959).

Absorbances at 280 and 260 nm were recorded in order to monitor the elution of the protein and the prescence of any nucleic acid impurities. The gel filtered protein was collected as 1 ml fractions. The collected fractions were resolved by SDS-PAGE. Pure protein was flash-frozen in liquid nitrogen and stored at -80°C until use.

4.3 Purification of muscle actin from acetone powder

Pig skeletal muscle α-actin was isolated from muscle acetone powder following the protocol by Pardee and Spudich (Pardee and Spudich, 1982). To extract actin, the acetone powder was grinded, added to buffer A and stirred on ice for 30 min. The extraction was performed under depolymerizing conditions at low salt concentrations (less than 2 mM K^+ or Na^+ and 0.2 mM Mg^{2+}). The extract was then filtered through several layers of sterile cheesecloth and centrifuged at 10 000 - 20000 g for 1 h at 4°C to get rid off the hydrated acetone powder. Contamination was avoided by wearing latex gloves. After pipetting the supernatant in a new tube, actin was induced to polymerize

by increasing the salt concentration to 50 mM KCl, 2 mM $MgCl_2$ and adding ATP to a concentration of 1 mM. Polymerization of the actin solution could be observed by a visible increase in the solution viscosity during the incubation step of 2 h at 4°C. Afterwards, KCl was slowly added to 0.6 M in the stirring solution. The polymerized actin was then ultracentrifuged at 80 000 g for 3 h at 4 °C to sediment the filamentous actin. After discarding the supernatant, the intact F-actin pellet was rinsed thoroughly with buffer A. Resuspension of the F-actin pellet was performed by gentle homogenization in 3 ml of cold buffer A per gram of acetone powder that was extracted originally. Purified actin was stored up to one week in dialysis against buffer A at 4 °C, the buffer was changed daily in order to replenish the ATP and DTT. Before use, the actin was centrifuged at 80 000 g for 3 h to remove non-depolymerized actin. The supernatant was saved and the protein concentration was determined at 290 nm using the nanodrop spectrophotometer.

4.4 Analysis of folding by synchrotron radiation circular dichroism spectroscopy

Circular dichroism (CD) spectroscopy was performed to analyse the folding state of the purified protein (Adler *et al.*, 1973). This technique measures the difference in absorption of left-handed polarized light versus right-handed polarized light which arise due to structural asymmetry (Beychok, 1966). The absence of regular structure does not show a CD intensity, while an ordered structure results in a spectrum, which can contain both positive and negative signals. Secondary structure elements can be determined by CD spectroscopy in the far-UV spectral region (190-250 nm) (N. Greenfield and Fasman, 1969; Holzwarth and Doty, 1965). At these wavelengths the chromophores are the peptide bond and the aromatic side chains. The chromophores are optically the most active groups present in a protein molecule and will interact with polarized light in a chiral environment (Adler *et al.*, 1973). The signal arises when the chromophore is located in a regular, folded environment. Different structural elements have characteristic CD spectra and give rise to a characteristic shape and magnitude of the CD spectrum (Greenfield, 2006). The CD signal can estimate the fraction of the molecule that is in each secondary structure type rather than the specific determination, of which residues are involved in the α-helical or β-portion (Whitmore and Wallace, 2008).

4.4.1 Preparation of samples

Protein samples for CD were purified by size exclusion chromatography and prepared to a concentration of 0.2 mg/ml. Optically active materials in the sample, except for the protein, were eliminated to prevent signal interference. Before measurements, the protein sample was dialyzed into CD buffer (50 mM NaF, 20 mM sodium phosphate buffer pH 7 and 1 mM Tris-(2-Carboxyethyl)phosphine (TCEP).

4.4.2 CD measurements

A CD spectrum of the purified cleaved protein was measured from 260 to 185 nm at 20 °C using an Applied Photophysics Chirascan Plus spectropolarimeter equipped with a TC125 thermal control unit, a direct temperature probe and a 1 mm path-length quartz cuvette.

4.4.3 Analysis of CD spectra

The spectra were averaged and the spectrum measured from the corresponding buffer was substracted. The CD units (mdeg) were converted to $\Delta\varepsilon$ (M^{-1} cm^{-1}). The DichroWeb (Lobley *et al.*, 2002) server was used for secondary-structure determination using the *CDSSTR* algorithm (Compton and Johnson, 1986) and set3 optimized for 185-240 nm as a reference data set.

4.5 Thermal shift assay for optimizing protein buffer conditions

The thermal shift assay is a fast, cheap technique that requires relatively little protein. It is also called Thermofluor® or differential scanning fluorometry and monitors the effects of buffer conditions on thermally-induced protein unfolding (Ericsson *et al.*, 2006; Pantoliano *et al.*, 2001). The method involves the binding of a hydrophobic fluoroprobe to the exposed hydrophobic core of an unfolding protein resulting in an increase in the fluorescence emission. The increase in fluorescence is measured as a function of temperature. In this study, the thermal shift assay was performed to screen several buffers with varying NaCl concentrations to find an optimized protein buffer for

crystallization trials. A correct buffer choice increases the protein homogeneity, stability and solubility, crucial parameters, which are highly correlated to the protein's probability to crystallize.

4.5.1 Preparation of samples

Protein samples for the thermal shift assay were purified by size exclusion chromatography and prepared to a concentration of 1 mg/ml. A series of different buffer conditions (see 9.3) were chosen and prepared in a 96-deep well plate. Each well in a 96-well thin-wall PCR plate was filled with 20 µl of a buffer solution. The working solution of the fluoroprobe, SYPRO Orange, was prepared by adding 5 µl of the 5000X gel stain into 1000 µl of ddH_2O and by vigorous shaking on a vortex. Based on the number of wells to be used, the required amount of protein and dye (2.5 µl each per well) were estimated and used to prepare the [protein+dye] mixture. 5 µl of the [protein+dye] mixture was added to each well, and the solution was mixed by gently pipetting it up and down.

4.5.2 Measurements

The plate was covered with optical-quality adhesive film (Bio-Rad) and placed inside the Mini Opticon Real-Time PCR system (Biorad). The plate was heated from 25 °C to 99 °C at 0.5 °C increments. The wavelengths for excitation and emission were 490 and 575 nm, respectively.

4.5.3 Analysis of results

The obtained thermograms were smoothened and the shape of the curves analysed. The melting temperatures (T_m) of the protein in the different solutions were compared, the higher the T_m the more stable the protein is in the particular condition.

4.6 Cosedimentation assay

The cosedimentation assay is an *in vitro* assay to determine whether a protein binds to F- or G-actin. The binding of a specific protein or protein domain to actin can be analysed by incubation of the protein of interest with F-actin. Ultracentrifugation will pellet F-actin whereafter the protein cosedimenting with F-actin can be analysed by SDS-PAGE.

Purified α-actin was ultracentrifuged at 186 000 g for 40 min at 4 °C before use. 5 µM ATP-actin, prepared as described above, was induced to polymerize by adding 4 mM $MgCl_2$ and 200 mM KCl in the presence of 0-12 µM *Sj*Pfn and incubated at room temperature for 30 min. The samples were ultracentrifuged at 186 000 g for 3 h at 4 °C. Equal amounts of the pellet and supernatant fractions were analyzed on SDS-PAGE followed by Coomassie staining.

4.7 Fluorescence spectroscopy

Fluorescence spectroscopy is a spectrochemical technique and involves two processes, absorption of energy between electronic energy levels and subsequent emission. When light of an appropriate wavelength interacts with a protein, absorption takes place and the electronic state of the molecule changes from the ground state to one of many vibrational levels in oune of the excited electronic states (van Holde *et al.*, 1998). The radiation causes an increase in energy of the system and in fluorescence spectroscopy, this energy is lost by radiative transition (Lakowicz, 1999). The molecule produces radiation when it relaxes to its ground state, a process called emission. This emission occurs at a longer wavelength compared to the absorbed light because of vibrational energy lost to the environment (van Holde *et al.*, 1998). Proteins are naturally fluorescent and most of the intrinsic fluorescence emissions of a folded protein are due to excitation of its aromatic amino acid residues, mainly tryptophan (Eftink, 1991; Weber, 1960). Fluorescence spectroscopy is a suitable technique to study ligand binding to proteins as it monitors the quenching of the intrinsic tryptophan fluorescence upon binding a ligand. The lifetime of the fluorophore in the excited state is in the nanosecond range but this is sufficiently long to interact with the environment (Möller and Denicola, 2002). Interactions of the fluorophore with the surrounding solvent molecules may affect fluorescence parameters, e.g. the maximum emission wavelength and lifetime of

the fluorophore. Assuming there is a change in the environment of the fluorophore after ligand binding, these effects are of main interest when monitoring ligand binding to proteins (Möller and Denicola, 2002).

In this study, fluorescence spectroscopy was performed to get insight into the role of *Sj*Pfn in actin polymerization and to analyze the binding of PLP stretches to *Sj*Pfn.

4.7.1 Analysis of actin polymerization kinetics

Actin polymerization can be measured *in vitro* by the introduction of a N-(1-pyrenyl)iodoacetamide (further described as pyrene) fluorophore, which allows detection of filament formation by an increase in pyrene fluorescence (J. A. Cooper *et al.*, 1983; Kouyama and Mihashi, 1981). The fluorescent pyrene reagent conjugates to actin at the site of the most reactive sulfhydryl group and the changes in fluorescence intensity for the actin solution can be measured in real-time. Actin and pyrene actin copolymerize forming filaments and the fluorescent signal of polymeric pyrene actin becomes 7 to 10 times higher than its monomeric form.

For measuring the effect of *Sj*Pfn on actin polymerization kinetics, actin was freshly purified as described above. *Sj*Pfn was gel filtered and both actin and *Sj*Pfn were centrifuged to eliminate impurities before use. Pyrene-labeled actin was purchased from Cytoskeleton Inc. and used without further purification. Different reactions were set up where 0-20 µM *Sj*Pfn was added to 5 µM α-actin, of which 5% was labeled with pyrene. As actin polymerizes under high ionic strength, polymerization was induced by adding F-buffer, which is G-buffer supplemented with 50 mM KCl, 4 mM $MgCl_2$ and 0.2 mM ATP. The change in fluorescence intensity upon incorporation of pyrene-labeled actin protomers into growing filaments was recorded on a Tecan Infinite M200 fluorescence plate reader for 1 h using an excitation wavelength of 365 nm and an emission wavelength of 410 nm with a bandwidth of 9 nm for both excitation and emission.

4.7.2 Analysis of PLP binding to *Sj*Pfn

The main goal of this experiment was to determine the dissociation constant (K_d) of the *Sj*Pfn-peptide binding for different PLP peptides derived from formin. Purified *Sj*Pfn was

used at a concentration of 5 µM and mixed with 0 - 1000 µM peptide in a total volume of 200 µl. The binding of different peptides (listed in Table 7) to *Sj*Pfn was analysed by measuring the change in fluorescence intensity upon titration of the protein with the peptide using a Tecan Infinite M200 apparatus.

Peptide	Sequence
P8	PPPPPPPP
1xP5	Ac-GLPPPPPLMK-NH_2
1xP5*	Ac-NIPPPPPFPT-NH_2
2xP5	Ac-VPPPPPMMGLPPPPPLMK-NH_2
3xP5	Ac-IPPPPPLMGVVPPPPPMMGLPPPPPLMK-NH_2

Table 7: Sequence of the peptides analysed during fluorescence spectroscopy.

Protein, peptide and a buffer containing 100 mM Hepes pH 7, 50 mM NaCl and 5 mM DTT were mixed in a black flat-bottom 96-well plate (Greiner). The measurements were performed in triplicate and the sample plate was incubated for 2 h at room temperature. Excitation was done at a wavelength of 295 nm, and emission spectra were collected between 324-400 nm. Averages of the individual measurements were compared, and the data were corrected for the blank fluorescence. For each peptide, the curve showing the fluorescence as a function of the wavelength was integrated for the region with the biggest fluorescence change. The area under the curve was plotted as a function of the peptide concentration in order to calculate the K_d of the peptide binding to *Sj*Pfn.

4.8 Isothermal titration calorimetry

To find out if *Sj*Pfn is a functional profilin, we attempted to analyse whether it binds to monomeric actin and/or PLP peptides using isothermal titration calorimetry (ITC). This technique measures the heat generated or absorbed when molecules interact in solution. The thermodynamics of the interaction are determined by the stoichiometry of the interaction (n), the binding affinity (K_d) and the enthalpy changes (ΔH). From these parameters, the Gibbs free energy (ΔG) and entropy changes (ΔS) can be calculated as follows:

$$\Delta G = - R.T.\ln K = \Delta H - T.\Delta S$$

where R is the gas constant and T the absolute temperature. ITC is the most quantitative way to study the thermodynamic characteristics of a macromolecule-ligand interaction by defining the heat evolved or absorbed during the binding of the two compounds.

The titration calorimeter consists of two identical cells composed of a highly efficient thermal conducting and chemically inert material surrounded by an adiabatic jacket in order to prevent heat to enter or leave the system. Temperature differences between the cells and the jacket are sensitively detected. To maintain identical temperatures between all components, heaters are located on both cells and the jacket and can be activated when necessary. A baseline signal is detected by the constant power applied to the reference cell to direct the feedback circuit in order to activate the sample cell heater. The reference cell is filled with water and the macromolecule is located in the sample cell. Injection of precise aliquots of the ligand in the sample cell causes heat that is taken up or evolved, depending on the nature of the reaction (endothermic versus exothermic). The raw data of an ITC experiment consist of the amount of heat (µcal/sec) that is imported in order to maintain equal temperatures in sample and reference cell in function of time (min). The heat absorbed or evolved during a calorimetric titration is proportional to the fraction of bound ligand. Each injection of the ligand causes a heat change, which is visible as a power spike in the raw data. As the injections continue, the macromolecule becomes saturated with the ligand and less binding will occur. This results in a decrease in the heat change until the macromolecule is completely saturated. At this point, no binding occurs anymore and only the heat of dilution is observed. Integration of the heat flow spikes with respect to time gives the total heat exchanged per injection. The heat effects in function of the molar ration of ligand to macromolecule can be analysed from where the thermodynamic parameters can be calculated.

4.8.1 Sample preparation

Purified actin and *Sj*Pfn were dialysed overnight against 2 mM Tris (pH 8), 0.2 mM ATP, 0.2 mM $CaCl_2$, 1 mM TCEP and 50 mM NaCl. Before loading, the samples were centrifuged and degassed in order to remove any precipitated material and air bubbles, which could have a negative impact on the measurements. Actin (16-27 µM) was pipetted into the sample cell and titrated with 180-250 µM *Sj*Pfn at 30 °C using a Microcal VP-ITC instrument. Each injection, 30 µl of *Sj*Pfn was

added to 1.6 ml actin in the sample cell. The number of injections was set to 30 in order to reach full saturation.

4.8.2 Data analysis

The data were analysed using the ORIGIN software (Microcal). After baseline correction, the area under the peaks was integrated to calculate ΔH.

4.9 Crystallization

Proteins are soluble in physiological conditions and will undergo phase transition when they are brought into supersaturation conditions. In these conditions, crystallization nuclei are formed from which protein crystals can grow. Proteins show a high variability in physicochemical characteristics and this makes crystallization a rarely predictable process. Empirical testing of many conditions is often needed to overcome the molecular variations between individual proteins since the optimal conditions for the protein must be obtained for a successful crystallization. Physical, chemical and biochemical factors affect the outcome of a crystallization experiment. Beside the temperature, pH and ionic strength, crystallization is also influenced by the purity and concentration of the protein itself, together with the type and concentration of the precipitants.

The goal of crystallization is to grow a pure, well-ordered crystal that is able to provide a diffraction pattern when exposed to X-rays. There are different ways to bring a protein solution to its supersaturation state, where nucleation and crystal growth can occur. The most commonly used method is vapour diffusion where a droplet containing a mixture of purified protein, buffer and precipitant is allowed to equilibrate with a larger reservoir containing similar buffers and precipitant in a higher concentration. Initially, the protein and precipitant concentration is low in the droplet but will increase as the drop and reservoir equilibrate. Water from the drop will evaporate in the reservoir and this will cause a slow increase of the protein and precipitant concentration in the drop. These gentle and gradual changes in the concentration of protein and precipitant aid in the growth of large, well-ordered crystals which will grow if appropriate crystallisation solutions are used.

In the sitting drop vapour diffusion method, the drop is placed on a pedestral that is separated from the reservoir. Controlled evaporation of a concentrated protein solution is maintained by sealing the environment to reach an equilibration between drop and reservoir.

4.9.1 Crystallization trials

4.9.1.1 SjPfn

Crystallization conditions for *Sj*Pfn were screened using the sitting-drop vapour-diffusion method in Swissci MRC 2 96-well plates. Gel-filtered *Sj*Pfn was concentrated to 8 mg/ml. Crystallization experiments were set up manually by mixing 0.3 µl reservoir solution and 0.3 µl protein solution. The plates were sealed from the environment and incubated at 4 °C and 20 °C. Commercially available screens were used for initial screening. Data-collection quality crystals grew in 150 mM ammonium iodide, 25% (w/v) PEG 8000, 50 mM MES pH 5.5 at room temperature (22 °C).

4.9.1.2 SjPfn complexed with actin

Actin and *Sj*Pfn were prepared for an ITC experiment and dialysed overnight against 2 mM Tris (pH 8), 0.2 mM ATP, 0.2 mM $CaCl_2$, 1 mM TCEP and 50 mM NaCl. After the ITC run, the sample was concentrated and the *Sj*Pfn-actin complex purified by size exclusion chromtatography using a Superdex S200 10/300 column equilibrated with 2 mM Tris (pH 8), 0.2 mM ATP, 0.2 mM $CaCl_2$, 1 mM TCEP, and 50 mM NaCl. Finally, the complex was concentrated to 4.5 mg/ml for crystallization. The concentration of the complex was measured at 290 nm with an estimated extinction coefficient of 0.587. The complex crystals grew in sitting drops containing 0.5 µl protein and 0.5 µl well solution, equilibrated against the well solution (150-200 mM ammonium acetate, 0.10-0.15 M bis-Tris (pH 5.3-5.5) and 20-25% PEG 3350) at 8 °C and 20 °C.

4.9.2 Data collection and processing

4.9.2.1 ***Sj*Pfn**

Cystals of *Sj*Pfn were flash-cooled in liquid nitrogen after soaking them in a cryoprotectant solution consisting of 20% (v/v) glycerol in the reservoir solution. Preliminary X-ray diffraction tests and native data-set collection to 1.91 Å resolution were performed on the EMBL beamline P14 at PETRA III/DESY, Hamburg, Germany. Because *Sj*Pfn contains seven cysteines and five methionines and the crystallization condition contained iodide, the SAD method was also attempted using this data set. However, as the data collection wavelength was not optimal, the phasing power was not sufficient to obtain a solution, although some heavy-atom sites could be found. Therefore, a second data set was collected to 2.2 Å resolution at a wavelength of 2 Å in order to obtain anomalous signal from iodide and/or sulfur.

The final data set used for refinement was measured from a crystal that was obtained from a co-crystallization experiment with an octa-proline peptide mixed in 1:1 ratio with the protein prior to setting up the crystallization drop in identical conditions as reported. Diffraction data to 1.45 Å were collected on the EMBL beamline P13 at DESY at a wavelength of 0.97 Å (Table 8).

The crystal used for the latter data set also belonged to space group $P2_12_12_1$, with unit-cell parameters a = 35.34, b = 52.02, c = 59.55 Å. Data processing showed a strong anomalous signal. The Matthews coefficients were calculated as 1.72 and 1.91 $Å^3.Da^{-1}$ with solvent contents of 28.7 and 35.7% (Matthews, 1968) for the two data sets, respectively, suggesting that the asymmetric unit could accommodate only one *Sj*Pfn molecule. Data-collection and processing statistics are given in Table 8. The data quality was evaluated using *phenix.xtriage* (Adams *et al.*, 2010) and no indications of twinning or pseudotranslational symmetry were detected. A self-rotation function calculated using *MOLREP* (Vagin and Teplyakov, 2010) was also consistent with the presence of one molecule in the asymmetric unit.

	Phasing data		**Final high resolution data**
Diffraction source	EMBL beamline P14 at PETRA III/DESY	EMBL beamline P13 at PETRA III/DESY	EMBL beamline P13 at PETRA III/DESY
Wavelength (Å)	1.24	2.00	0.97
Temperature (K)	100	100	100
Detector	PILATUS 6M	PILATUS 6M	PILATUS 6M
Crystal-to-detector distance (mm)	292	141	281.8
Rotation range per image (°)	0.1	0.5	0.25
No. of frames	1800	1500	600
Space group	$P2_12_12_1$	$P2_12_12_1$	$P2_12_12_1$
Unit-cell parameters (Å, °)	a=31.82, b=52.17, c=59.79, α=β=γ=90	a= 35.29, b=52.15, c=59.82, α=β=γ=90	a=35.34, b=52.02, c=59.55, α=β=γ=90
Resolution range (Å)	50-1.91 (1.96-1.91)	39.3-2.20 (2.26-2.20)	39.12-1.45 (1.49-1.45)
Reflections: total unique	47684 (1451) 14494 (729)	138834 (9560) 10071 (696)	100094 (3518) 19830 (1280)
Completeness (%)	96.6 (66.2)	93.1 (86.4)	98.6 (86.5)
Multiplicity	3.3 (1.9)	13.7 (13.7)	5.0 (2.7)
Average I/σ (I)	6.0 (1.3)	24.3 (10.8)	14 (1.4)
R_{meas} (%)	14.3 (75.5)	23.8 (8.0)	6.8 (82.3)
$CC_{1/2}$ (%)	99.4 (72.2)	99.9 (99.5)	99.9 (77.2)
Wilson B factor (Å^2)	34.9	32.3	15.3
SigAno	0.86 (0.77)	3.3 (1.7)	0.87 (0.72)
R_{work}/R_{free}	n/a	n/a	17.7/19.2
No. of atoms (total) macromolecules …ligand …water	n/a n/a n/a n/a	n/a n/a n/a n/a	1081 1010 3 68
Root mean square deviations bond lengths (Å) …bond angles (°)	 n/a n/a	 n/a n/a	 0.01 1.33
Ramachandran plot (%) favoured disallowed	 n/a n/a	 n/a n/a	 95 1.6
B factors (average) …macromolecules …ligand …water	n/a n/a n/a n/a	n/a n/a n/a n/a	24.0 23.9 28.8 25.2

Table 8: Data collection and refinement statistics for the SjPfn structure. The phasing data was not further refined and therefore contains *not applicable* (n/a) parameters.

4.9.2.2 SjPfn complexed with actin

Diffraction data to 1.3-Å resolution were collected on the ID29 beamline at the ESRF, Grenoble, and to 2-Å resolution on the I23-29 beamline (ESRF, Grenoble). The data were integrated and scaled using the XDS program package (Kabsch, 2010) (Table 9). The crystal used for the high resolution data set belonged to space group $P2_1$, with unit-cell parameters a = 53.38, b = 68.22, c = 69.50 Å.

Parameters	***Sj*Pfn-Actin complex**	***Sj*Pfn-Actin complex**
Diffraction source, detector	ID29, PILATUS 6M-F	ID23-2, PILATUS 2M
Wave length (Å)	0.98	0.87
Tempereture K	100	100
Crystal-to-detector distance (mm)	199.6	283.4
Rotation range per image (°)	0.1	0.2
No. of frames	1800	1200
Space group	$P2_1$	$P2_1$
Unit cell parameters (Å,°)	a=53.38, b=68.22, c=69.50; β=106.8	a=53.24, b=65.14, c=59.34; β=106.8
Resolution range (Å)	47.7-1.3 (1.35 -1.3)	47.6-2 (2.07-2)
Reflections: total unique	389536 (27489) 115612 (8394)	139948 (13068) 30744 (3003)
Multiplicity	3.4 (3.3)	4.6 (4.4)
Completeness (%)	98.7 (96.6)	99.6 (98.3)
Average I/σ (I)	7.8 (1.2)	8.2 (1.3)
R_{meas} (%)	9.9 (100.9)	16.1 (117.9)
Wilson B-factor (Å^2)	12.8	28.9
R_{work}/R_{free}	13.5/16.9	19.9/23.1
Root mean square deviations bond lengths (Å) bond angles (°)	 0.009 1.38	 0.009 1.37
Ramachandran plot (%) favored disallowed	 98.4 0	 98 0.2
B factors (average) macromolecules ligand water	21.50 19.70 21.00 34.80	37.9 38 28.4 37.7

Table 9: Data collection and refinement statistics for the actin-*Sj*Pfn structure.

4.10 Structure determination

4.10.1 *Sj*Pfn

The diffraction images were indexed, integrated and scaled using XDS (Kabsch, 2010) and XDSi (Kursula, 2004). Phases for the structure determination were obtained using the SAD method with phenix.autosol (Terwilliger *et al.*, 2009), which found one iodine and two sulphur atoms. Experimental phasing was followed by building of the structure using phenix.autobuild (Terwilliger *et al.*, 2008), and subsequent alternating cycles of manual model building in COOT (Emsley *et al.*, 2010) and refinement using phenix.refine (Afonine *et al.*, 2012). The final model has optimal geometry and R/R_{free} factors of 17.7/19.2.

4.10.2 Actin-*Sj*Pfn complex

The structure was determined by molecular replacement using the program PHASER (McCoy *et al.*, 2007) within the PHENIX package, and the crystal structures of *Sj*Pfn (reported here) and rabbit muscle α-actin (McLaughlin, 1993) as search models. Molecular replacement was followed by rebuilding and cycles of manual model building in COOT and refinement using phenix.refine. The R/R_{free} factors of the final, refined models for the 1.3- and 2-Å structures were 13.5/16.9 and 19.9/23.1, respectively. Both structures display optimal geometry, as validated using MolProbity in PHENIX (Table 9).

4.11 Structure-based sequence alignment

To analyse the homology between profilins, a structure-based sequence alignment was set up. The three dimensional conformation of *Sj*Pfn was compared with other profilins from different families. A structural sequence alignment compares different protein tertiary structures and relies on the information of the 3D conformation of the query sequences. The secondary-structure matching (SSM) approach was used and matches graphs built on the protein's secondary structure elements, followed by an iterative 3D-alignment of protein backbone C_α-atoms. A high sequence similarity leads almost always to structural similarity, but the opposite is not always true. Therefore, an alignment

based on the comparison of geometrical positions of amino acids will provide more significant clues than a sequence alignment alone.

A structure-based sequence alignment was performed for known profilins based on a SSM approach in COOT (Emsley *et al.*, 2010). A sequence alignment was manually modified to correspond to the structural alignment. To compare *Sj*Pfn with profilins from other phyla, the following structures were used: *Acanthamoeba* profilin I, (2PRF; Vinson et al., 1993), *Arabidopsis thaliana* profilin I (1A0K; Thorn et al., 1997), *Saccharomyces cerevisiae* profilin (1YPR; Eads et al., 1998), human profilins I (1PFL; Metzler et al., 1995), and II (1D1J; Nodelman et al., 1999), birch pollen profilin (1CQA; Fedorov et al., 1997), *Arachis hypogaea* profilin (4ESP; Wang et al., 2013), and *P. falciparum* profilin (2JKF; Kursula et al., 2008b).

4.12 PISA analysis of the actin-*Sj*Pfn complex

For the profilin actin complex, a Proteins, Interfaces, Structures and Assemblies (PISA) – analysis was performed with the PDBePISA server (Krissinel and Henrick, 2007) in order to see if there are differences between actin binding interfaces in different profilins. The PISA analysis tool is an interactive tool for the exploration of macromolecular interfaces. The program analyses crystal structures to identify the component chemical monomers and the interfaces between the monomers. PISA will also evaluate the strength of interaction between the neighbouring monomers in a crystal and predict what would be the most stable multimer and therefore the most likely biological form of the structure (Krissinel and Henrick, 2007).

5 Results

5.1 *Sj*Pfn is a stable monomeric protein

GST-*Sj*Pfn could be purified to near homogeneity using glutathione affinity chromatography. The molecular weight of the fusion protein was estimated to be ~40 kDa, based on the protein molecular weight standards. Most other proteins present in the cell lysate could be washed away during the washing steps of the purification. Analysis of the fractions using SDS-PAGE showed a high purity of the final eluted fusion protein (figure 9).

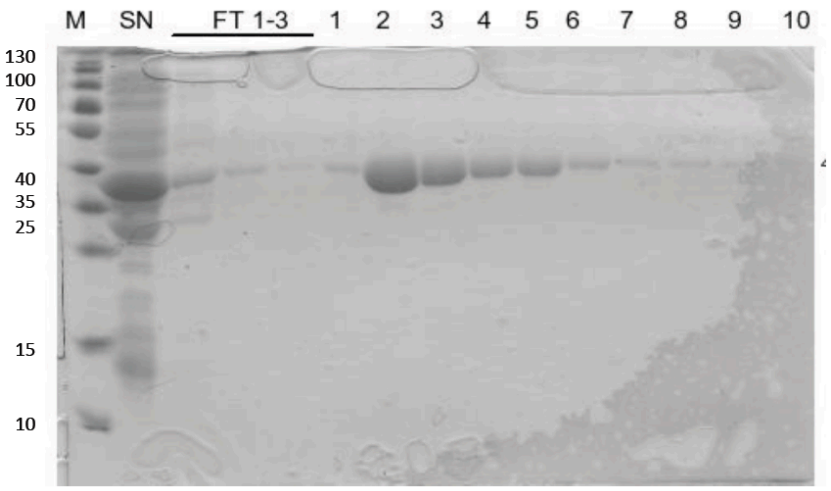

Figure 9: Affinity purification of GST-*Sj*Pfn. M: molecular weight standards, FT1-3: flow-through samples of the washing steps, 1-10: fractions eluted with 30 mM reduced glutathione. The apparent size of the fusion protein is ~40 kDa.

After cleavage of the GST tag, the protein was further purified using size exclusion chromatography (SEC). GST and SjPfn eluted as two peaks at volumes of 59 and 77 ml, respectively (figure 10a). SDS-PAGE analysis of the purified *Sj*Pfn corresponding to a peak at 77 ml in SEC showed a single band at an apparent molecular weight of 14 kDa, showing high purity. GST was found in the first peak with an apparent molecular weight of 27 kDa (figure 10b).

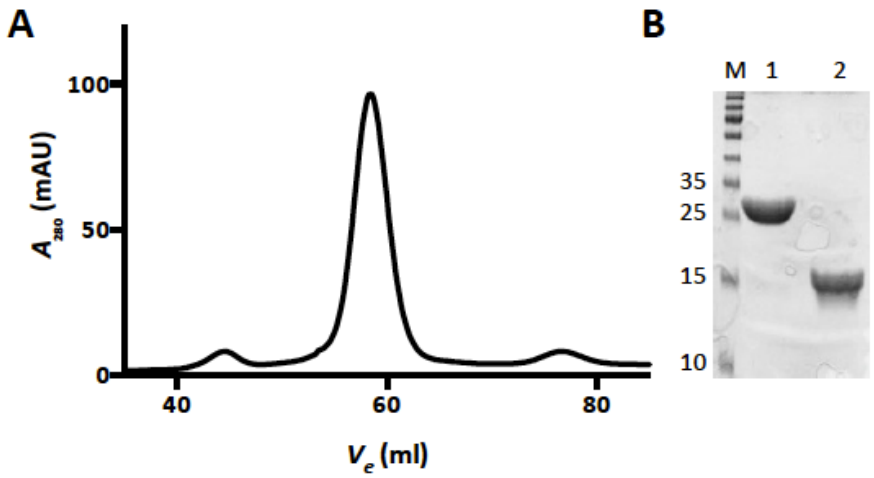

Figure 10: SEC profile of *Sj*Pfn. *A*) GST and *Sj*Pfn elute from a Superdex 75 10/300 GL column (GE Healthcare) at 59 ml and 77 ml, respectively. *B*) Coomassie-stained denaturing gel of the peak fractions containing GST and *Sj*Pfn. The position of molecular mass markers are shown at the side of the gel and are labelled in kDa. M: marker; Lane 1: GST; lane 2: *Sj*Pfn

Comparing the peak sizes of the eluted GST and *Sj*Pfn, it was apparent that a considerable amount of pure *Sj*Pfn was lost during purification. This, together with unefficient cleavage of the GST tag by thrombin, was the major reason to change to another construct, where *Sj*Pfn was fused to an N-terminal 6xHis-SUMO3 tag.

Recombinant His-SUMO-tagged *Sj*Pfn was purified using a two-step protocol similarly to the purification of the GST-tagged protein. The fusion protein in the different elution fractions analyzed by SDS-PAGE was already quite pure with an apparent size of 26 kDa (figure 11). After cleavage of the His-SUMO tag, final purification was carried out using size exclusion chromatography. The chromatogram contained two peaks, which both contained *Sj*Pfn, as analysed by SDS-PAGE (data not shown). This is likely due to formation of disulfide-mediated *Sj*Pfn dimers due to the large number of cysteine residues in *Sj*Pfn. Only the fractions of the second, presumable monomeric peak, eluting at a volume of 14 ml, were used for further experiments (figure 12).

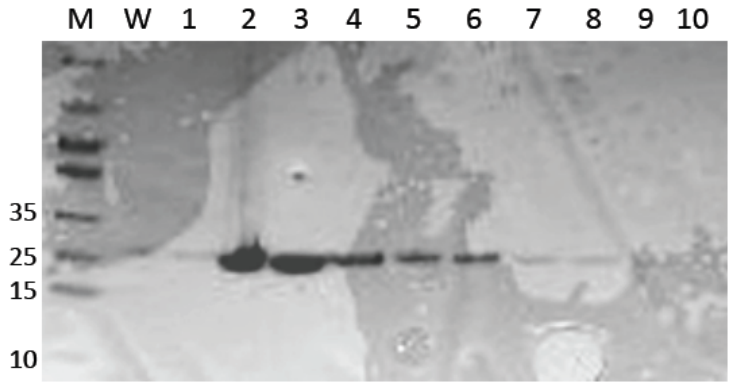

Figure 11: Affinity purification of his-SUMO3-*Sj*Pfn. The molecular weights of the protein standards in kDa are shown at the side of the gel. The apparent size of the fusion protein is 26 kDa, as expected. M: marker; W: fraction collected from washing the column; 1-10: elution fractions 1 to 10.

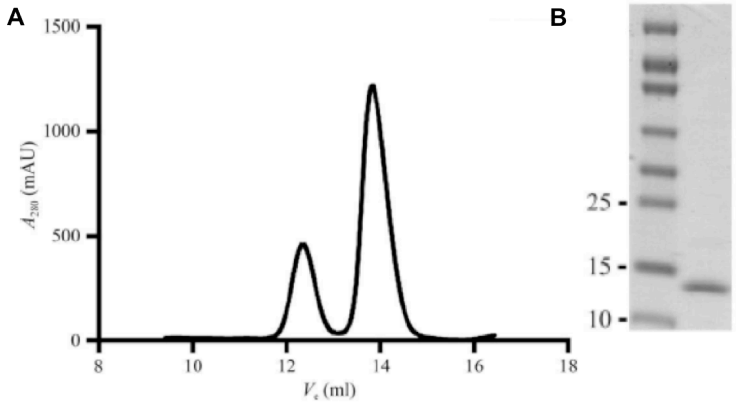

Figure 12: SEC profile of *Sj*Pfn. *A)* Size-exclusion chromatogram of *Sj*Pfn eluting as two peaks at 12.5 and 14 ml. *B*) Coomassie-stained denaturing gel of the second peak fraction containing monomeric *Sj*Pfn. The molecular weights of the protein standards in kDa are shown at the side of the gel.

The identity of the purified protein was verified by peptide mass fingerprinting using mass spectrometry at the Biocenter Oulu Proteomics Core Facility.

The stability of *Sj*Pfn in buffers with varying salt concentrations and pH was analyzed by a thermal shift assay, in order to identify conditions optimal to stabilise the protein. The thermally induced melting points (T_m) were measured for all 28 conditions over a temperature range of 25 °C to 99 °C. The melting curve and corresponding T_m indicate that *Sj*Pfn is most stable around a pH of 7 (Table 10). Observed from the graphs (figure 13) and corresponding melting temperatures, an improved stability of *Sj*Pfn was found in a buffer with 100 mM Hepes pH 7.0 and 50 mM NaCl. This buffer was identified as an optimal stabilizing buffer and was used during the SEC purification step.

pH	Buffer	NaCl concentration	T_m (°C)
pH 4.5	100 mM Ammonium acetate	50 mM	44.5
		150 mM	42.0
pH 5.0	100 mM citric acid	50 mM	55.5
		150 mM	54.75
pH 5.5	100 mM citric acid	50 mM	56.25
		150 mM	54.5
pH 6.0	100 mM MES	50 mM	56.6
		150 mM	48.5
	100 mM Sodium acetate	50 mM	61.0
		150 mM	60.75
pH 6.5	100 mM MES	50 mM	61.5
		150 mM	61.5
pH 7.0	100 mM HEPES	50 mM	61.5
		150 mM	61.5
pH 7.5	100 mM HEPES	50 mM	61.5
		150 mM	61.25
pH 8.0	100 mM Imidazole	50 mM	60.5
		150 mM	60.0
pH 8.5	100 mM Na-K phosphate	50 mM	58.0
		150 mM	58.25
pH 9.0	100 mM Bicine	50 mM	51.0
		150 mM	47.5

Table 10: Comparison of T_m values obtained for *Sj*Pfn under different conditions. The buffers differ in pH and salt concentration.

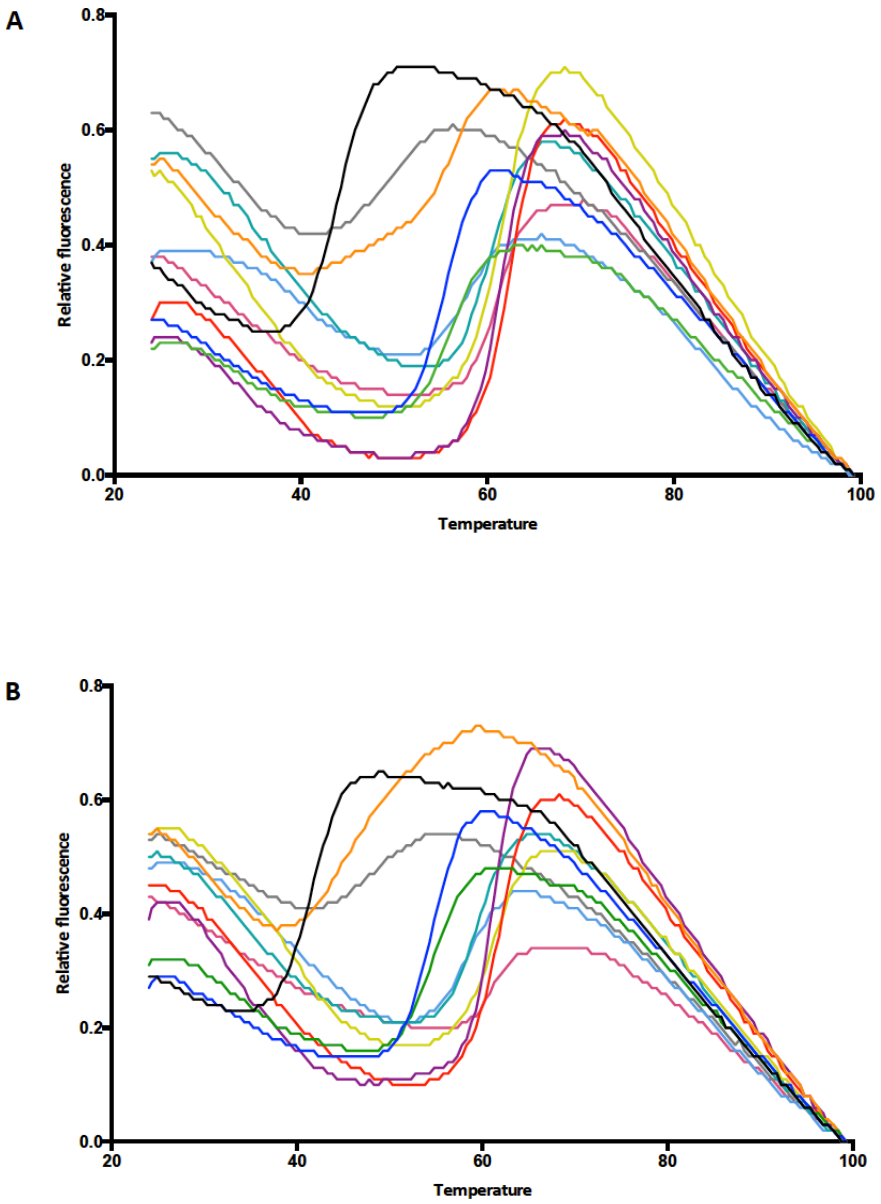

Figure 13: Thermal stability analysis of *Sj*Pfn. Melting curves for *Sj*Pfn in different buffers with *A*) 50 mM and *B*) 150 mM NaCl with varying pH. Color code: Black – 100 mM ammonium acetate, pH 4.5; Blue – 100 mM citric acid, pH 5.0; Green – 100 mM citric acid, pH 5.5; Orange – 100 mM MES, pH 6.0; Pink – 100 mM sodium acetate, pH 6.0; Violet – 100 mM MES, pH 6.5; Red – 100 mM HEPES, pH 7.0; Yellow – 100 mM HEPES, pH 7.5; Cyan – 100 mM imidazole, pH 8.0; Light blue – 100 mM sodium potassium phosphate, pH 8.5; Grey – 100 mM bicine, pH 9.0

5.2 Analysis of the *Sj*Pfn secondary structure

Profilins share a highly conserved tertiary structure (Fedorov *et al.*, 1997; Schutt *et al.*, 1993; V K Vinson *et al.*, 1993). The profilin polypeptide is folded into a central ß-pleated sheet composed of 5-7 antiparallel ß-strands flanked by α-helices. The folding and secondary-structure content of the purified *Sj*Pfn was analyzed using CD spectroscopy.

The CD spectrum clearly indicates that the protein is folded and contains both α-helices and β-strands (figure 14). Examination of the spectra shows characteristic negative peaks at 208 and 220 nm and a positive peak around 190 nm corresponding to an α-helical peptide and a broad negative peak around 218 nm for a β-stranded peptide. The percentages of secondary structure elements were calculated using Dichroweb. *Sj*Pfn was estimated to contain 18% α-helices and 31% β-strands which is comparable to the crystal structure of *Acanthamoeba* profilin which has 28% α-helices and 29% β-strands (Reichstein and Korn, 1979).

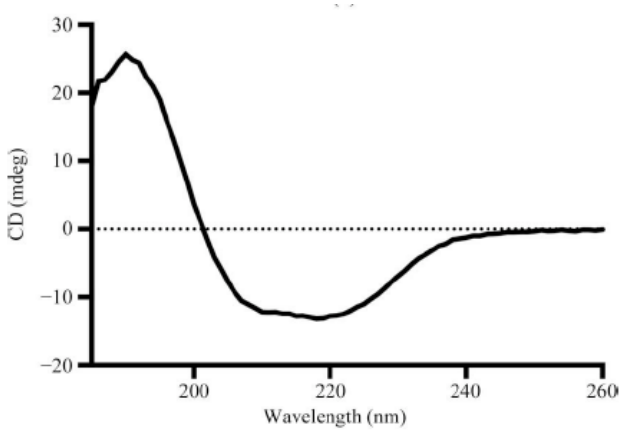

Figure 14: CD analysis of *Sj*Pfn. CD spectrum of *Sj*Pfn from 260 to 185 nm measured at 20°C (Vervaet *et al.*, 2013).

5.3 Structure of *Sj*Pfn

The initial crystallization hit for *Sj*Pfn was obtained from the PEG/Ion screen (Hampton) and consisted of 200 mM ammonium iodide, 20% (w/v) polyethylene glycol (PEG) 2250, pH 6.2. After optimization by screening different PEGs at different concentrations, combined with altering the ammonium iodide concentration and the pH, single crystals with a longest dimension of approximately 100 µm were obtained from the optimized condition (Table 11) in 5 to 7 days (figure 15).

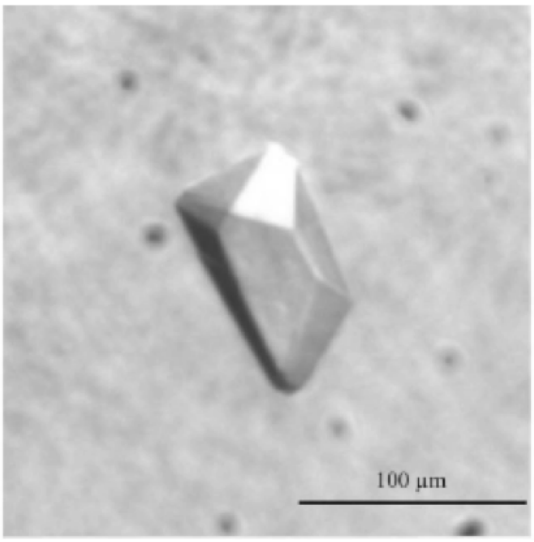

Figure 15: *Sj*Pfn crystal. A single crystal of *Sj*Pfn grown in 150 mM ammonium iodide, 25% (w/v) PEG 8000, 50 mM MES pH 5.5 at 22°C (Vervaet *et al.*, 2013).

Method	Sitting-drop vapour diffusion
Plate type	Swissci MRC 2 96-well plates
Temperature (°C)	22
Protein concentration (mg.ml-1)	8
Buffer composition of protein solution	100 mM Hepes pH 7, 150 mM NaCl, 5 mM BME
Composition of reservoir solution	150 mM ammonium iodide, 25% (w/v) PEG 8000, 50 mM MES pH 5.5
Volume and ratio of drop	0.3 µl protein + 0.3 µl reservoir
Volume of reservoir (µl)	70

Table 11: Crystallization details for *Sj*Pfn

The diffraction power of the crystals varied greatly from no diffraction to diffraction beyond 2 Å resolution, and it was not possible to predict the diffraction properties from the crystal morphology. After screening many crystals from slightly different conditions, a native data set to 1.91 Å resolution could be recorded (Table 8 in methods). The crystal belonged to space group $P2_12_12_1$, with unit-cell parameters a = 31.82, b = 52.17, c = 59.79 Å. This data set was initially used in phasing attempts using molecular replacement. Probably because of the small size and the rather featureless shape of the profilin monomer and its low sequence identity to the closest homologues (~20%), the molecular replacement trials were not successful. Both Matthews coefficient and

calculation of a self-rotation function indicated the presence of only one molecule in the asymmetric unit.

The structure of *Sj*Pfn was finally determined to a resolution of 1.45 Å using the SAD method based on anomalous signal from one iodine and two sulphur atoms and refined to a crystallographic R/R_{free} factors of 17.7/19.2. The crystal also belonged to space group $P2_12_12_1$, with unit-cell parameters a=35.34, b=52.02,
c=59.55 Å. The refined model contains 124 amino acids. All residues are located in the 'most favored' or 'allowed' regions of the Ramachandran (ϕ,ψ) plot.

*Sj*Pfn is composed of three α-helices, seven β-strands and nine turns. The central 7-stranded β-sheet appears as two orthogonal β-sheets, with the first sheet formed by strands β1, β2, β5, β6 and β7, and the smaller second sheet formed by two additional small strands β3 and β4. On one side, this core is flanked by the N- and C-terminal helices while α-helix 2 is positioned at the other side, next to β3 and β4 (figure 16). *Sj*Pfn adopts the canonical profilin fold with rather short loops between the secondary structure elements. Between β strand 7 and the C-terminal α-helix, *Sj*Pfn contains an elongated loop ($_{103}$VDDDQN$_{108}$). This acidic loop is located at the edge of the canonical actin-binding site and may, therefore, function in the recognition and binding of monomeric actin. Another putative function for the acidic loop is to raise an immune response as was reported for *Toxoplasma gondii* profilin for an acidic loop between β2 and α2 (Kucera et al., 2010).

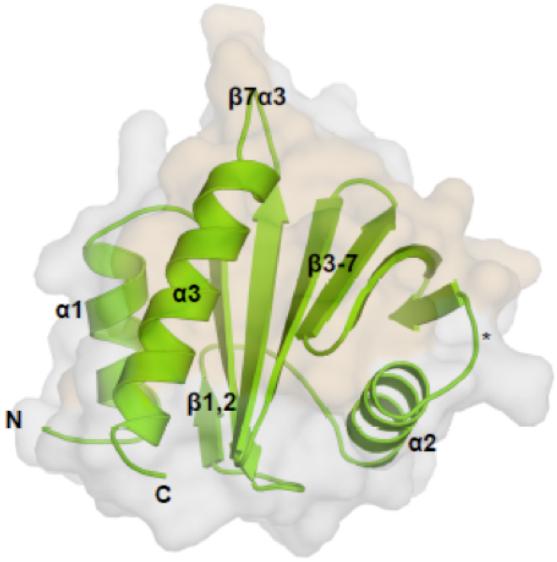

Figure 16: Crystal structure of *Sj*Pfn. The secondary structure elements of *Sj*Pfn are presented in a cartoon representation surrounded by the protein's surface. The actin-binding surface is indicated in orange in the surface model.

5.3 Comparison of *Sj*Pfn with other profilins

Plathyhelmintic genomes contain sequences that are recognized as profilin orthologs. The structure-based sequence alignment of *Sj*Pfn with homologous profilins from other parasites, plants, *Protozoa*, yeast and human was built using the Espript program and shows the location of conserved residues, ligand binding sites and the presence of different secondary structure elements (figure 18). The different profilin structures were compared pairwise by an iterative 3D-alignment of protein backbone C_α atoms. Because of the low degree of homology across the profilin family and the availability of extensive structural data on profilins, a structure-based sequence alignment was preferred rather than an alignment based on sequence information only.

Based on sequence conservation, *Sj*Pfn is closest related to plant profilins. The amino acid sequence of *Arabidopsis* profilin is 23 % identical to that of *S. japonicum*, and profilins from birch (*Betula pendula*) pollen and peanut (*Arachis hypogaea*) both share a sequence identity of 21 % with *Sj*Pfn. *Sj*Pfn is more related to *Acanthamoeba castellani* profilin compared to human or yeast profilin, showing sequence identities of 21, 12 and 14%, respectively. The percentage identities were determined by comparison of the amino acid sequences after multiple sequence alignment. Typically for profilins, the sequence identities are very low, around 20-22%, even to the closest homologs. Despite the low sequence conservation between profilins in general, 18 residues are identical in

80% of sequenced profilins. These residues are integral for the profilin fold or play important roles in binding to proline-rich sequences or G-actin. Sequence comparison between *Sj*Pfn and the other profilins reveal that *Sj*Pfn contains only a minority of these conserved amino acids.

Inspection of the residues in the inferred actin- and polyproline binding sites shows that none of these sites are particularly well conserved in *Sj*Pfn, nonconserved substitutions are present in all of them. Derived from the sequence alignment, it is not obvious that the profilin-like protein of *S. japonicum* functions as canonical profilins. The conserved residues Ala19, Ala20, Glu46, Gly62, Gly67 and Thr105 (human Pfn numbering) are essential for the stability of the profilin fold. Although the profilin tertiary structure is conserved in *Sj*Pfn, only Gly62 and Thr105 are found in *Sj*Pfn and align respectively to Gly66 and Thr93 (*Schistosoma* numbering). The remaining conserved residues play important roles in maintaining the PLP and actin-binding surfaces of profilin.

PLP stretches bind to a patch of aromatic residues in profilins. In birch pollen profilin, the PLP binding site consists of the conserved residues Trp3, Tyr6, Ile27, Trp35, Ala36, Tyr128, Leu129. *Sj*Pfn shares only Trp6 in this patch of conserved residues (figure 17).

Unlike the parasitic *Plasmodium* species, *Sj*Pfn does not contain insertions before α-helix 2 and after β-strand 2. These insertions are conserved in *Plasmodium* but less in other apicomplexan species (figure 18).

*Sj*Pfn has an elongated acidic loop ($_{103}$VDDDQN$_{108}$) between β strand 7 and the C-terminal α helix. The presence of this extension is also described in apicomplexan parasites like *Plasmodium* and *T. gondii* profilins but is not observed in mammalian and plant profilins.

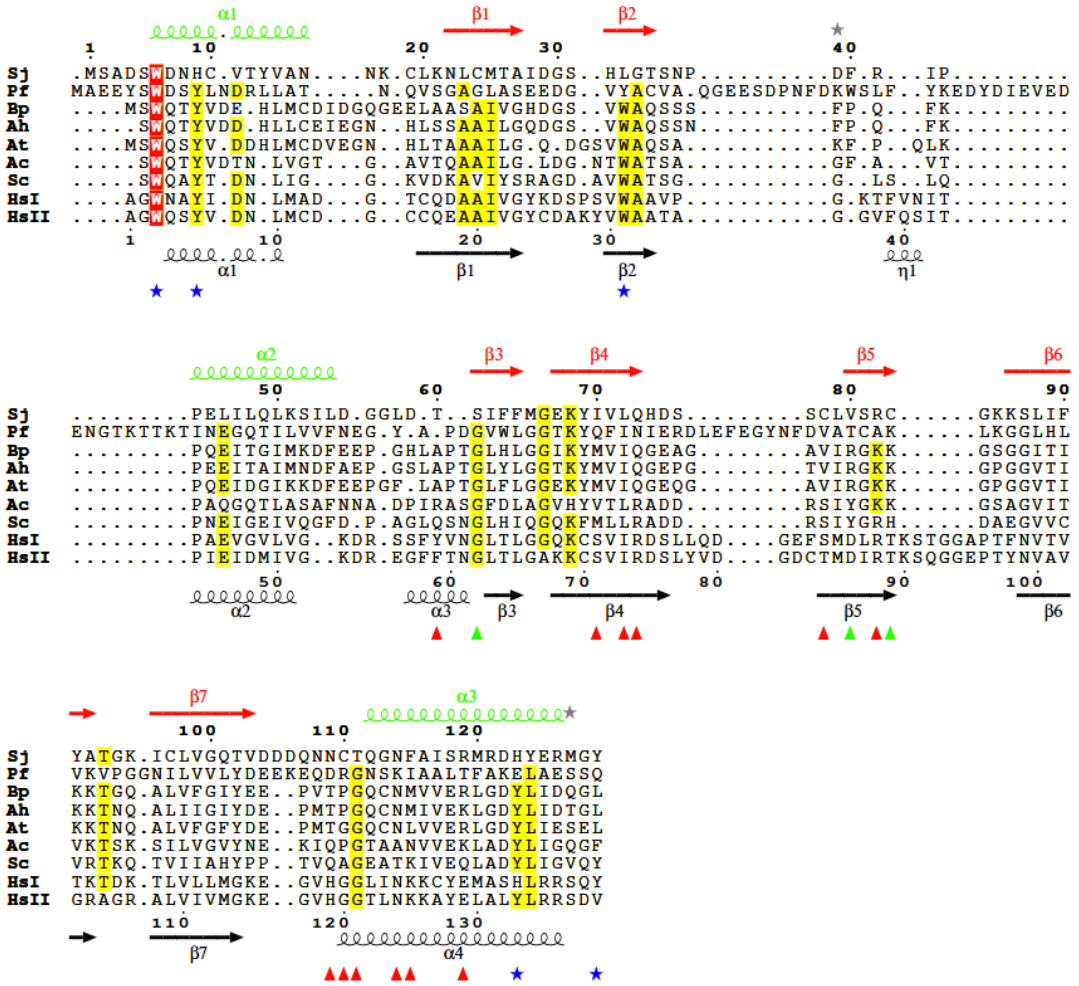

Figure 17: Structure-based sequence alignment of profilins from different species. The sequence alignment represents profilins with a known 3-dimensional structure from the four kingdoms of *Eukarya*. Crystal structures of the profilins were superimposed, performing secondary-structure matching (SSM), in coot. The structurally homologous residues were then used to align the *S. mansoni* profilin based on sequence. The residue numbering of *Sj*Pfn is used in the figure. Secondary structure elements are indicated for *Sj*Pfn and *H. sapiens* profilin above and below the respective sequences. The α-helix 3 is missing in *Schistosoma*. Amino acids, which are conserved in more than 80% of profilin sequences are boxed in yellow. The residue boxed in red is the only amino acid conserved among all sequences in the alignment. Profilin residues involved in polyproline binding are marked with blue asterisks; residues performing a functional role in actin binding are marked with red (for *Sj*Pfn) and green (for other profilins) arrowheads. Shown are the sequences of the profilins of *S. japonicum* (AY223457), *S. mansoni* (GeneDB Smp_080920.1), *P. falciparum* (gi:23613835), *B. pendula* (P25816), *A. hypogaea* (D3K177), *A. thaliana* (Q42449), *A. castellani* isoform 1a (P68696), *S. cerevisiae* (P07274), *H. sapiens* isoforms I (P07737) and II (P35080).

An additional α-helix named α3 is located between α-helix 2 and β-strand 3 in human profilin, deriving from the sequence alignment and the superpositioned structures (figure 17 and 18). This extra short helix is present in many canonical profilins, including *Saccharomyces* and *Acanthamoeba* proteins but is not seen in *S. japonicum*.

Additionally, human profilin contains an extended loop between β strand 5 and 6 which subsequently shorter in *Sj*Pfn.

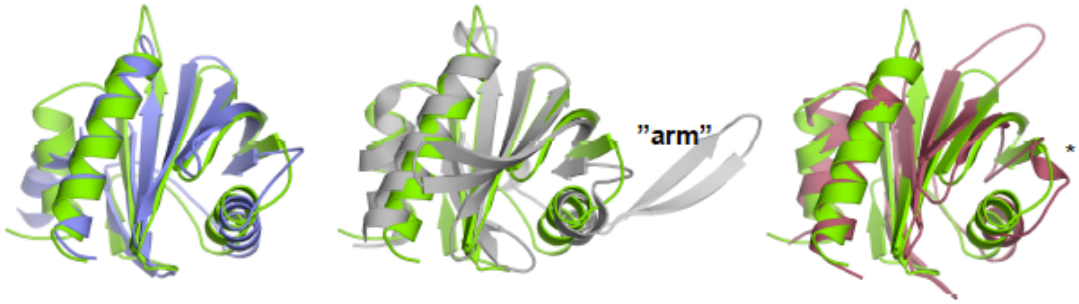

Figure 18: Superposition of the *Sj*Pfn crystal structure with other profilins. The *Sj*Pfn crystal structure is presented as a cartoon (green) and is superimposed with profilins from Birch (blue), Plasmodium (gray) and Human (profilin 1, red). Helix 3 in human profilin is marked with an asterisk.

Regarding the sequence, *Sj*Pfn is closest related to birch pollen profilin. Superposition of the crystal structures of these organisms shows that the secondary structure elements are similar with varying positions of the termini. Plant profilins contain a specific pocket that is composed of the loops between β-strands 4 and 5, and β-strands 5 and 6 and has a function in actin binding. Rather than these characteristic loops, *Sj*Pfn contains an acidic loop between β-strand 7 and α-helix 3.

5.4 *Sj*Pfn binds octameric poly-L-proline stretches

Profilins have the capacity of binding PLP (Mahoney et al., 1997). In this study, different experiments were performed in order to analyze the binding of an octaproline peptide and 4 peptides derived from a putative S. japonicum formin-like protein that contains several repeats of 5 consecutive proline residues to *Sj*Pfn.

To assess the binding of polyproline peptides to purified *Sj*Pfn, a tryptophan fluorescence assay was perfomed to investigate the changes in the local environment of these residues upon interaction. Measurements were performed for *Sj*Pfn (5 µM) with increasing concentrations of the different PLP peptides. Different lengths of proline repeats were tested: one peptide containing an octaproline repeat (P8) and four

peptides composed of one (1xP5 and 1xP5*), two (2xP5) or three (3xP5) pentaproline repeats. The sequences of the different peptides are listed in Table 7.

Binding of P8 to *Sj*Pfn enhances the intrinsic tryptophan fluorescence of profilin, showing an increase in the fluorescence intensity when *Sj*Pfn is titrated with aliquots of P8 (figure 19*A*). The fluorescence change upon binding P8 to profilin is saturable, the curve reaches a plateau approximately around 10 µM. Despite the poorly conserved poly-L-proline binding site, *Sj*Pfn binds to octaproline with a relatively high affinity (K_d ~4.3 µM), which is comparable to other profilins with generally a K_d in the µM range. Pentaproline peptides seem to be, irrespectively of the amount of repeats in one peptide, too short to cause a significant increase in tryptophan fluorescence intensity upon binding to *Sj*Pfn (figure 19*B-E*). An other explanation might be that the flanking residues in this particular formin homolog do not allow for binding. The relative fluorescence remains quite low and saturation was not reached even at high peptide concentrations. This is different than in other profilins where a minimum of five prolines counts as the minimum required to bind profilin in the PLP binding site. In addition, these peptides did not co-elute with *Sj*Pfn in size excusion chromatography (data not shown). Also co-crystallization attempts with the peptides repeatedly resulted in crystals with *Sj*Pfn alone.

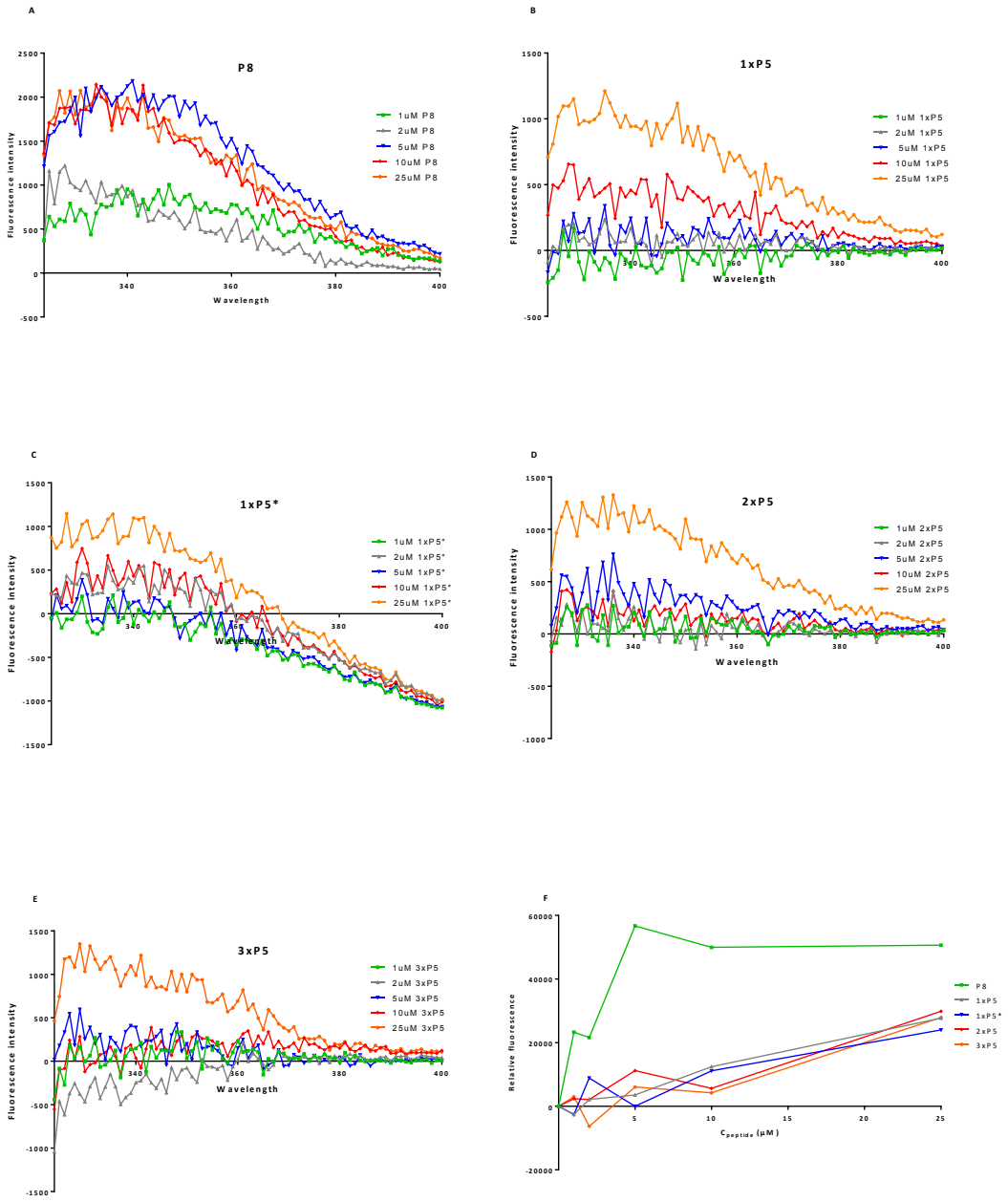

<u>Figure 19:</u> Emission spectra of tryptophan fluorescence of PLP binding to *Sj*Pfn. *A-E)* The fluorescence intensity in function of the wavelength for the different PLP peptides. Different concentrations of each peptide were analyzed (green: 1 µM, grey: 2 µM, blue: 5 µM, red: 10 µM, orange: 25 µM). *F)* The fluorescence intensity shown in function of the peptide concentration. Color code: Grey – 1xP5; Blue – 1xP5*; Red – 2xP5; Orange – 3xP5; Green – P8.

In addition, ITC was performed as an alternative technique to analyze the binding of *Sj*Pfn to PLP (data not shown). Unfortunately, clear results could never be obtained from the titrations.

5.5 *Sj*Pfn is an actin monomer sequestering protein

In order to assess the effect of *Sj*Pfn on actin monomer-to-filament dynamics and its binding to either G- or F-actin, the *Sj*Pfn-actin interaction was investigated. A co-sedimentation assay was performed to test the interaction of *Sj*Pfn with actin. This interaction was further characterized quantitatively by a polymerization assay.

In polymerizing high-salt conditions, a clear concentration-dependent transition of actin from a filamentous to a monomeric form was seen upon increasing *Sj*Pfn concentration (figure 20). *Sj*Pfn was seen exclusively in the supernatant with monomeric actin, indicating no binding to actin filaments, likewise canonical profilins. SDS-PAGE analysis, where supernatant and pellet samples from the different conditions were loaded, showed that increasing concentrations of *Sj*Pfn inhibited actin polymerization (figure 20). When actin is in G-buffer, it stays in the supernatant in its monomeric form, while F-buffer causes the polymerization of actin into filaments and most of the protein will be pelleted down after ultracentrifugation. *Sj*Pfn is fully soluble in both conditions.

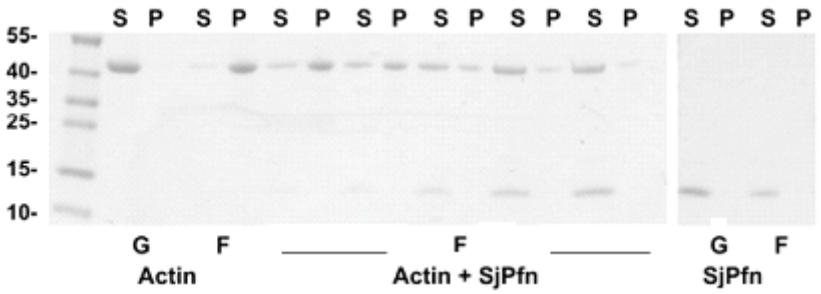

Figure 20: Actin co-sedimentation assay with *Sj*Pfn. 5 µM actin and an increasing concentration of *Sj*Pfn was used and ultracentrifugated at 186000 x g. *Sj*Pfn is severing actin and transferring it to soluble form as concentration increases. Lanes 1-2: actin in G-buffer; 3-4: actin in polymerizing F-buffer; 5-14: actin+*Sj*Pfn (1, 4, 4, 8, 12 µM) in F-buffer; 15-16: *Sj*Pfn in G-buffer; 17-18: *Sj*Pfn in F-buffer.

In a second experiment, the effect of *Sj*Pfn on the kinetics of actin polymerization was tested by a polymerization assay. The incorporation of pyrene-labeled actin into a growing filament was measured using fluorescence spectroscopy in the presence and absence of *Sj*Pfn. Increasing concentrations of *Sj*Pfn inhibited actin polymerization (figure 21). Already a 1:1 ratio of actin:*Sj*Pfn resulted in 65.7 % lower initial rate of polymerization, suggesting that *Sj*Pfn is a monomer sequestering protein (figure 21).

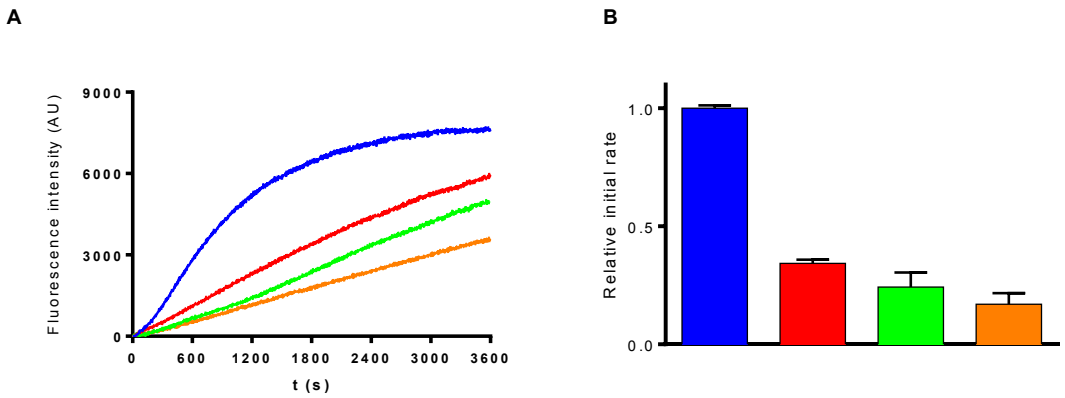

Figure 21: Pyrene-actin polymerization assay. *A)* 5 µM α-actin, containing 5% pyrene-labeled actin, was polymerized in the absence (blue) or presence of *Sj*Pfn (red: 5 µM, green: 10 µM, or orange: 20 µM). Averages of three measurements are shown. *B)* The initial rates (ΔF/s) were calculated as the slope of the linear part of the fluorescence curves. The rate of the actin-only sample was set to the value 1.

The binding of *Sj*Pfn to monomeric actin was also tested using ITC. This experiment rather did not give clear results, probably due to actin polymerization in the beginning of the titration due to the high concentration required for the experiment. However, from the final titrated sample, we could purify a stable complex between *Sj*Pfn and pig skeletal muscle α-actin using SEC (see below).

5.6 *Sj*Pfn binds α-actin in the canonical binding site

The SEC profile of the actin-*Sj*Pfn complex showed a large, symmetric peak eluting at a volume of 14.5 ml. SDS-PAGE analysis confirmed that this peak contains the actin-*Sj*Pfn complex. The actin and *Sj*Pfn bands have an apparent molecular weight of 45 kDa and 14 kDa, respectively (figure 22).

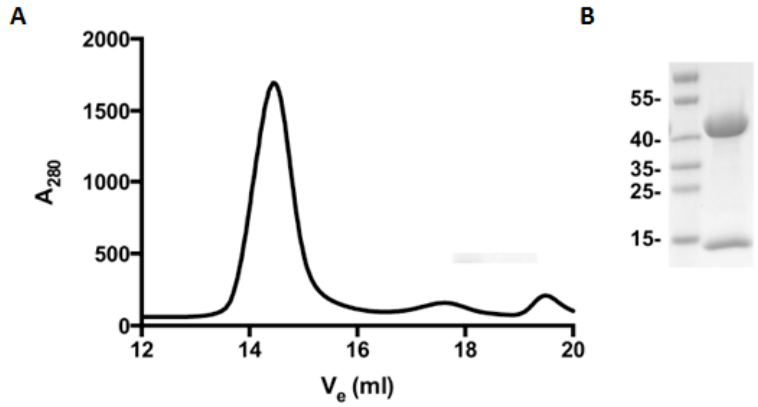

Figure 22: SEC profile of the actin-*Sj*Pfn complex. *A*) Elution volume of S200 10/300 size exclusion column indicates a 1:1 complex between actin and profilin. *B*) The result was confirmed by analysis of the peak fractions by SDS-PAGE.

After purification of the actin-*Sj*Pfn complex by SEC, the complex was concentrated to 3-4 mg/ml for crystallization. The complex crystals grew in sitting drops equilibrated against 150-200 mM ammonium acetate, 0.10-0.15 M bis-Tris (pH 5.3-5.5) and 20-25 % PEG 3350 at 8 °C and 20 °C. Single crystals with a longest dimension of approximately 200 µm were obtained from the optimized condition (table 12) in ca. 10 days (figure 23).

Figure 23: Actin-*Sj*Pfn crystal. A single crystal of *Sj*Pfn grown using 0.2 mM ammonium acetate, 0.1 M bis-Tris (pH 5.5) and 25% PEG 3350 at 22 °C.

Method	Sitting-drop vapour diffusion
Plate type	Swissci MRC 2 96-well plates
Temperature (°C)	8°C (2 Å data) and RT 1.5Å data
Protein concentration (mg.ml-1)	2Å: 4.5 mg/ml & 1.3Å: 3.1 mg/ml
Buffer composition of protein solution	2 mM Tris (pH 8), 0.2 mM $CaCl_2$, 1 mM TCEP, 50 mM NaCl
Composition of reservoir solution	2 Å: 0.15 M NH4Ac, 0.1 M bis tris ph 5.5, 20% PEG 3350 1.3 Å: 0.2 mM ammonium acetate, 0.1 M bis-tris (pH 5.5) and 25 % PEG 3350
Volume and ratio of drop	0.5 µl protein + 0.5 µl reservoir
Volume of reservoir (µl)	50

Table 12: Crystallization details for the actin-*Sj*Pfn complex

The actin-*Sj*Pfn crystal structure was refined to 1.3 Å with a final R/R_{free} of 13.5%/16.9% and allows for a detailed analysis of the binding mode of *Sj*Pfn to actin as well as the interactions of actin with the bound nucleotide. Ramachandran analysis indicates that 98.4% of the residues lie within the most favoured regions, with no residues existing as outliers. *Sj*Pfn forms a 1:1 stoichiometric complex with skeletal muscle α-actin, the interface comprises a region of profilin defined by β-strands 3-6 and α-helix 3 including the loops connecting them. This hydrophobic groove between subdomains 1 and 3 is considered as the canonical actin-binding site for profilin and other G-actin binding proteins. Twenty-nine residues each from actin and profilin contribute to this contact, forming a solvent accessible area of the profilin interface of 997 $Å^2$, which is comparable to 1054 $Å^2$ as observed in the human profilin 1-actin complex.

When comparing the overall fold of the complex, the structures of actin-*Sj*Pfn and human profilin with α-actin from *Dictyostelium* are similar to one another and to the original structure of bovine profilin and β-actin, but are different from the wide-open structure of β–actin and profilin. The original structure of β–actin-profilin revealed a moderately open nucleotide cleft in actin and also for *Sj*Pfn, profilin binding causes a moderate opening of the nucleotide cleft. The wide-open state of the actin-profilin complex is characterized by a 2.7 Å increased separation of the tips (residues G15 and D157) of two hairpin loops clamping the nucleotide (figure 24). In the original closed

structure of the complex, the tips are separated by 5.3 Å, which is a bit closer compared to the distance observed in the actin-*Sj*Pfn complex (5.5 Å).

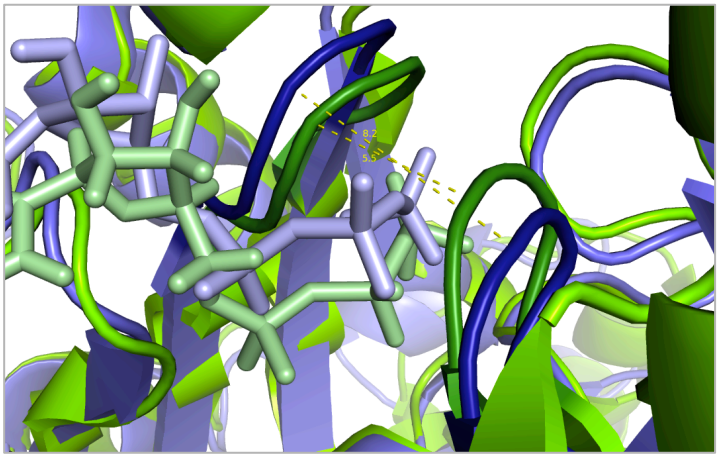

Figure 24: Superimposed structures of the actin-*Sj*Pfn complex with the wide open structure of bovine β-actin-profilin. The actin-*Sj*Pfn complex is shown in green, bovine β-actin-profilin in blue. ATP bound in both structures is presented in sticks.

Although actin is a highly conserved protein, the side chains contributed to the actin-binding interface in profilins are only partially conserved. The most important interactions for *Sj*Pfn binding to actin are described in detail in figure 25. The binding face formed by β-strands 3-6 can be divided in two interacting regions. Thr60, Ser61 and Lys68 point towards actin subdomain 3 and interact with residues Asp288 and Asp290. Additionally, hydrogen bonds and salt bridges connect residues Gln73, Asp75, Arg82, Lys85 from *Sj*Pfn to actin residues Glu167, which is located at the end of the W-loop, and Tyr168. Helix 3 is an important part of the actin-profilin 'hotspot', the side chains of Arg119 and Asn114 are involved in the formation of hydrogen bonds and ionic interactions with actin residues Tyr171, Glu366 and Arg374.

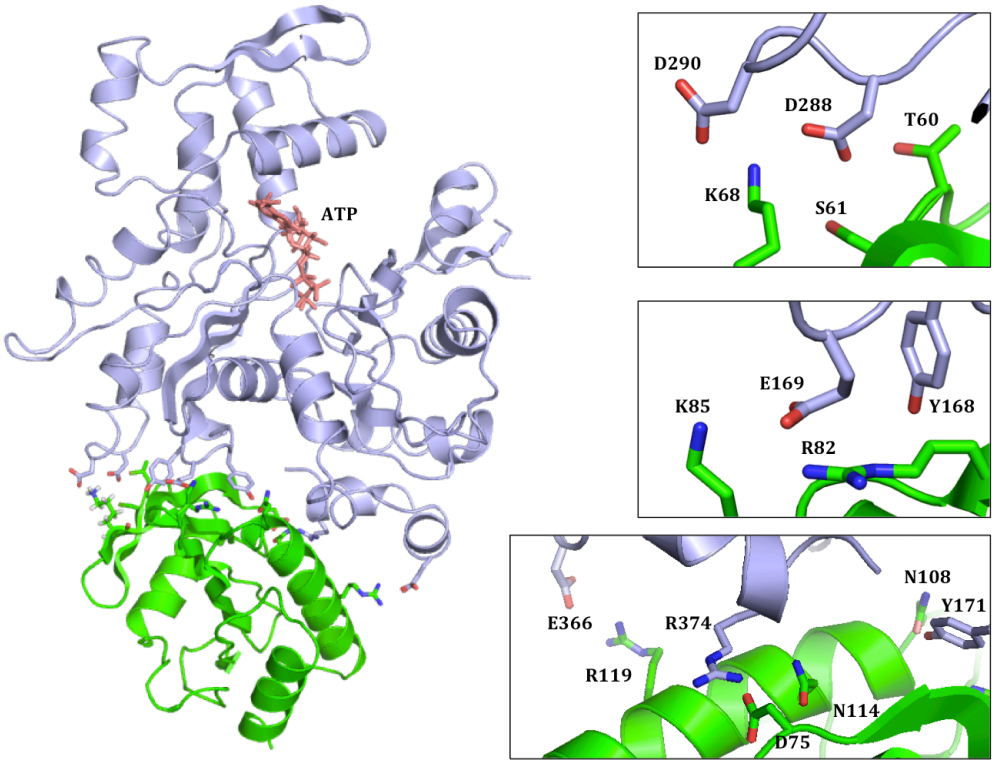

Figure 25: *Sj*Pfn complexed with pig skeletal muscle actin. *Sj*Pfn is represented in green, actin in blue. Residues forming hydrogen bonds and salt bridges are indicated in the close up-panels.

Upon binding to actin, differences in side chain conformations of the interfacial residues are observed in *Sj*Pfn (figure 26). Different residues of α-helix 3 (Gln112, Phe115, Ser118, Arg119) are moving towards actin. The residue Lys85 also moved upon actin binding and makes a salt bridge with Asp288 and Asp290.

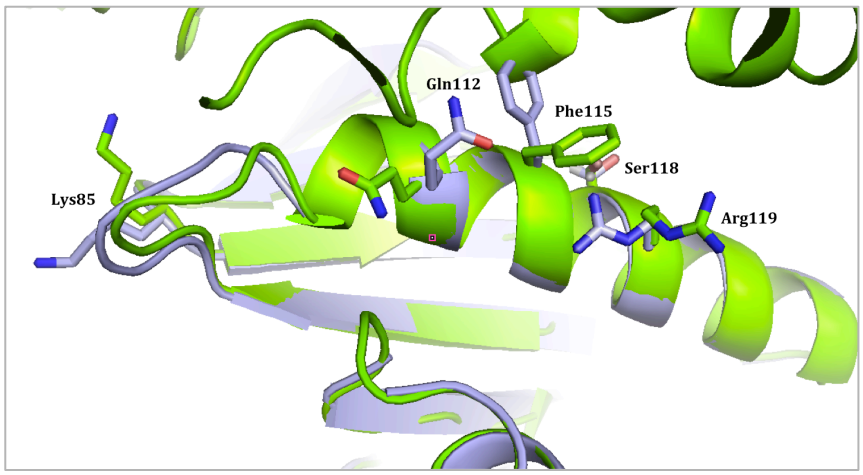

Figure 26: Monomeric *Sj*Pfn superimposed to *Sj*Pfn from the actin-*Sj*Pfn complex. *Sj*Pfn is represented in green, the actin-*Sj*Pfn complex in blue. Residues changing their conformation upon binding to actin are represented in sticks.

ATP tightly binds Mg^{2+} in physiological conditions while this is replaced by Ca^{2+} in the actin-*Sj*Pfn complex. Ca^{2+} is coordinated by the ß- and γ-phosphate groups of the nucleotide. ATP is positioned deep inside a cleft between subdomains 2 and 4. The adenine base rests in a hydrophobic pocket formed between subdomains 3 and 4 , the polyphosphate tail is clamped between two phosphate binding loops. The first loop, P1 or S, is formed by residues Gly13 to Leu16, the second P2 or G-loop comprises residues Ser155-to Thr160. Both the ß- and γ-phosphate groups bridge the two loops with the ß-phospate group interacting with Gly15, Leu16, Lys18 and Asp157. The γ-phosphate group is bound to Ser14, Gly158, Asp157 and Val159. Subdomains 2 and 4 are linked via side chain interactions between Ser14 and Gly 74, and Asp157 and Arg183, respectively.

6 Discussion

Profilins are among the most abundant proteins in the cell and are differentially expressed during the different growth stages. Profilins are actively involved in the regulation of actin dynamics. Their affinity towards actin and poly-L-proline stretches give them a considerable role in the maintainance of the cell architecture, the interaction with phosphoinositides makes them crucial hubs in signal transduction. Although profilins have a critical role in the cell, their *in vivo* functions vary, depending on the studied cell type and organism.

In *S. japonicum,* profilin is located in the tegument and the underlying tissues of adult worms. *Sj*Pfn has a fairly low sequence identity to canonical profilins, and from the sequence it was not clear whether it possesses the characteristic functional properties of profilins. Our research presents more insight in the structural and functional characterization of profilin from *S. japonicum*.

The tertiary structure of *Sj*Pfn is conserved with other profilin classes

Despite a slightly lower helical content, *Sj*Pfn has secondary structure contents roughly similar to homologous profilin folds, which generally consist of 30-32% α-helices and 31-33% β-strands (Fedorov *et al.*, 1997; Thorn *et al.*, 1997; Wang *et al.*, 2013). The crystal structure of *Sj*Pfn was solved to a resolution of 1.45 Å. *Sj*Pfn is composed of three α-helices, seven β-strands and nine turns and contains the core profilin fold with a central 7-stranded antiparallel β-sheet flanked with the N- and C-terminal α-helices on one side, and a short α-helix on the other. The overall tertiary structure of profilins is conserved, and the *Sj*Pfn crystal structure shares a similar fold as *e.g.* the birch, *Plasmodium* and human structures and aligns to these structures with a root mean square deviation of 1.77, 2.19 and 2.33 Å, respectively. Despite having a low sequence identity, these distant profilins share a high level of structural similarity, indicating they belong to the same structural family.

Species-specific characteristics refine the functions of profilin.

*Sj*Pfn contains an elongated acidic loop ($_{103}$VDDDQN$_{108}$) between β-strand 7 and α-helix 3. Such an extension, although differently located in the structure, is also described in the apicomplexan parasites *Plasmodium* and *Toxoplasma gondii* but cannot be observed in the mammalian and plant homologs. Located at the edge of the canonical actin

binding site, this acidic loop might have a role in actin binding. Another putative function may be to evoke an immune response, as has been reported for *T. gondii* profilin for an acidic loop between β-strand 2 and α-helix 2 (Kucera *et al.*, 2010).

Plant profilins contain three characteristic loops, forming a specific binding pocket and distinguishing their structure from other profilins. The plant specific binding pocket is the major immunogenic region of plant profilins. In patients with type I allergies, the IgE epitope probably encompasses the adjacent actin-binding site, causing cross-reactivity with human profilins (Thorn *et al.*, 1997). The loops are located between the N-terminal helix and β-strand 1, between β4 and β5, and between β5 and β6. *Sj*Pfn does not align with the residues forming a loop between the N-terminal α-helix and β-strand 1 in plants and shows different conformations in the other plant-specific regions.

In many canonical profilins, including the human, yeast, and *Acanthamoeba* proteins, α-helix 3 is located between α-helix 2 and β-strand 3 and is important for actin binding (Metzler *et al.*, 1995; Nodelman *et al.*, 1999; Eads *et al.*, 1998; Vinson *et al.*, 1993). In *Sj*Pfn, as in apicomplexan profilins, residues corresponding to α-helix 3 are non-helical and form a loop that is a few amino acids shorter than in the higher eukaryotic profilins (Kursula *et al.*, 2008). This might cause a different binding mode and affinity to actin.

***Sj*Pfn binds the octaproline motif with a micromolar affinity**.

Profilins are targeted to sites requiring filament assembly through interactions with proline-rich motifs present within its binding partners (Boukhelifa *et al.*, 2006; Kursula *et al.*, 2008; Manseau *et al.*, 1996; Reinhard *et al.*, 1995; Witke *et al.*, 1998). In *Acanthamoeba* and mammalian profilins, residues of the N- and C-terminal helix, β1, β2 and β7 strands are involved in binding of polyproline stretches. The peptide binding site is formed by a conserved hydrophobic patch of five aromatic residues (Trp3, Tyr6, Trp31, His133, Tyr139 following the human profilin 1 numbering). Comparison of the crystal structures shows that residues Trp6, His123, Tyr129 in *Sj*Pfn are present at the surface and align with the peptide binding site in other profilins although they cover a much smaller hydrophobic region. The affinity for proline-rich repeats is regulated by phosphorylation of tyrosine and threonine residues and differs in profilins from different organisms. It has been shown that profilin tyrosine phosphorylation may be involved in inhibiting the interactions between profilin and some of its proline-rich ligands in *Phaseolus vulgaris* (Aparicio-Fabre *et al.*, 2006). In this plant profilin, the role of Tyr72 was described to be involved in the regulation of ligand binding. This residue

aligns to Tyr69 in *Sj*Pfn, which is also exposed to the solvent. Modeling of the octaproline peptide to *Sj*Pfn shows that the protein requires a different conformation of the peptide main chain in order to fit into the hydrophobic binding site. Despite the poorly conserved binding site, *Sj*Pfn binds to octaproline with a relatively high affinity (K_d ~4.3 μM). Profilins generally bind to at least 5 consecutive proline repeats flanked with hydrophobic residues. However, no specific binding was observed for peptides from the *S. japonicum* formin-like protein, containing 1, 2, or 3 pentaproline repeats although each of which should be able to bind one profilin monomer, inducing peptide-mediated oligomerization, as seen for *e.g.* mammalian profilin 2a (Kursula *et al.*, 2008). No complex formation could be seen for any of these peptides in size exclusion chromatography. In spite of repeated efforts, attempts to co-crystallize *Sj*Pfn with these peptides resulted only in crystals containing *Sj*Pfn without a bound peptide.

Beside the proline repeats, the hydrophobic residues flanking these motifs are important in profilin binding. In our group, the structure of mouse profilin 2a with an mDia1 peptide was solved and elucidated the binding determinants of an IPPPPPL motif (Kursula et al., 2008). Here, it was shown that both of the flanking hydrophobic residues act as "anchors", both lying against an aromatic residue and forming CH···π hydrogen bonds. In *Sj*Pfn, none of these aromatic residues were conserved when comparing with mouse profilin 2a. This observation explains the lack of binding of the formin peptides to *Sj*Pfn, as well as highlights the crucial role of these hydrophobic anchors in the binding of mammalian formin FH1 repeats to mammalian profilin. Apart from a central tryptophan residue, Trp6, the residues interacting with the proline residues are also not conserved in *S. japonicum*. Two profilin 2a tyrosine residues (Tyr6 and Tyr133) are replaced by histidines. On the other hand, *Sj*Pfn has two extra aromatic residues that could interact with proline-rich peptides: Asn9 and Leu134 of profilin 2a are both replaced by tyrosines (Tyr13 and Tyr124) in *Sj*Pfn. These observations indicate that a similar binding mode of a formin pentaproline repeat as seen for mammalian profilins, is highly unlikely for *Sj*Pfn. The binding site does contain, though, approximately the same amount of aromatic residues, and a slightly different binding mode could accommodate a proline-rich peptide.

Although it is a major characteristic of the protein family, there are profilins described without affinity for polyproline peptides. *Vaccinia* virus profilin does not bind poly-L-proline and has a very low affinity for actin (Machesky et al., 1994) while mammalian profilin 4, the testis-specific isoform, does not interact with proline-rich peptides or actin (Behnen et al., 2009). Other parasites, such as the *Apicomplexa*, also possess highly

divergent profilins, which still bind to actin, proline-rich sequence motifs and phosphoinositides (Kursula et al., 2008; Kucera et al., 2010).

Profilin is an important regulator of the G-actin pool.

A clear concentration-dependent transition of actin from the filamentous to monomeric form was seen upon increasing *Sj*Pfn concentration in polymerizing high-salt conditions. Using fluorescence spectroscopy, the incorporation of pyrene-labeled actin into a growing filament was measured in the presence and absence of *Sj*Pfn. *Sj*Pfn was seen exclusively in the supernatant with monomeric actin, indicating no significant binding to actin filaments. In the actin polymerization assay, increasing concentrations of *Sj*Pfn inhibited actin polymerization, which is in line with the results of the co-sedimentation assay. A 1:1 ratio of actin:*Sj*Pfn resulted already in a 66% lower initial rate of polymerization. These data show that *Sj*Pfn negatively regulates the polymerization of monomeric actin into filaments.

***Sj*Pfn binds actin at the canonical face through unconserved interactions.**

Several structures of profilins interacting with actin have been described. Both structures of profilins interacting with α-actin (*e.g.* human profilin 1) and β-actin (*Bos taurus* profilin) have been published. Although the binding face is comparable to other actin-profilin complexes, the binding interactions of actin-*Sj*Pfn seem to be remarkably unconserved. Our structure of the complex showed a moderately open nucleotide cleft in actin, *Sj*Pfn is bound to subdomains 1 and 3.

In other actin-profilin complexes, Phe375 is an important anchor for the interaction with profilin, where this residue is bound to a pocket formed by Ile73, Arg74, Asp86, His119, Gly120, Gly121 and Asn124 (figure 27). Comparison of the crystal structures shows that in *Sj*Pfn, this pocket is poorly conserved. In this region, only Asn124 is conserved (Asn114) and Ile73 is conservatively replaced by Leu72. Asp86 has been replaced to a hydrophobic residue Val 80. The replacement of both glycine residues in helix 4 to Cys110 and Thr11 cause an altered conformation of the main chain in *Sj*Pfn. Remarkably, profilins from all other phyla have one or two glycines at this site.

His119 is known to be partially responsible for the pH sensitivity of the interaction in mammalian profilins. It is located at the C-terminal helix and is bound by a pocket lined by Tyr169, Met355 and Phe375. In contrast, there is no histidine present in this region in *Sj*Pfn and given the fact that the actin-*Sj*Pfn crystals were grown at a pH of 5.3-5.5, the complex seems to be stable under acidic conditions. This might be explained by the

presence of an acidic loop ($_{103}$VDDDQN$_{108}$) in *Sj*Pfn located at the edge of the actin-binding site, causing structural rearrangements in the C-terminal helix.

In mammalian, yeast and amoeba profilin, Arg74 forms a stacking interaction with Phe375. The side chain of Gln73 found in *S. japonicum* and plants at this position does not interact with the aromatic ring of Phe375 but is at a 3.8 Å distance from the terminal carboxyl group.

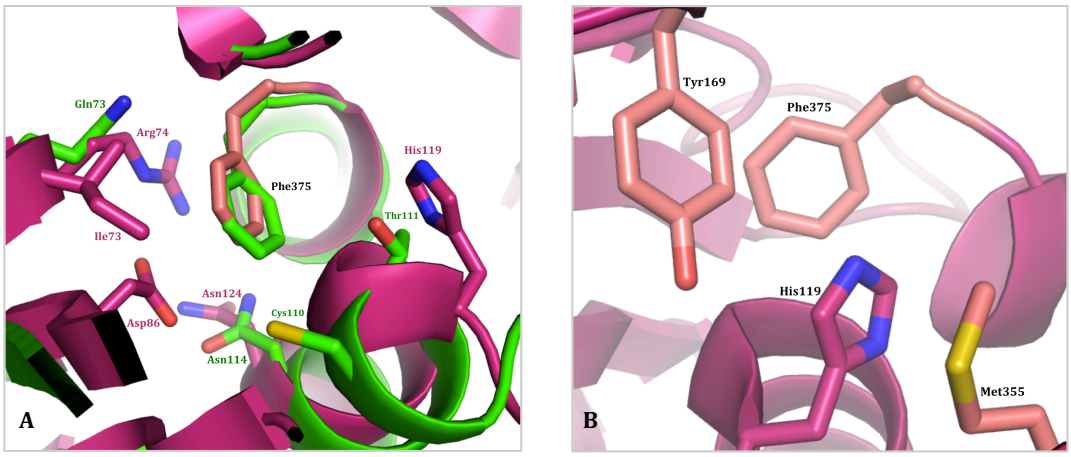

Figure 27: Detailed view of the actin-profilin binding mode. *A)* The pocket interacting with Phe375 is poorly conserved in *Sj*Pfn. Shown are the actin-profilin complex of *S. japonicum* (green) and human Profilin I (pink). *B)* In animal profilins, His119 is coordinated by actin Tyr169, Met355, Phe375.

Analogous to the wide-open structures, the acidic loop $_{103}$VDDDQN$_{108}$ causes an upward movement of the $_{348}$SLSTFQQMW$_{356}$ loop in actin (figure 28). In contrast, Trp356, which is found in different rotamers in the "wide-open" structures compared to all others, occupies the same orientation in *Sj*Pfn as in the other "moderately open" structures (figure 28).

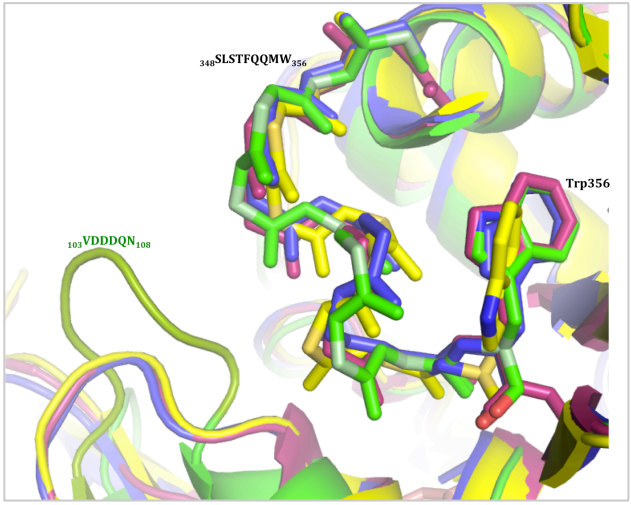

Figure 28: Upward movement of the $_{348}$SLSTFQQMW$_{356}$ loop in actin upon binding to *Sj*Pfn. Detailed view of the superpositioned structures of actin-*Sj*Pfn (green), the closed structure (2BTF; blue), open complex (1HLU; yellow) and moderate open complex (3CHW; pink). The conformation of Trp356 is highlightened in sticks.

Glu82 present in the loop between β-strand 4 and 5 in bovine profilin, interacts with actin Lys113. Like in *Arabidopsis*, this interaction is not observed in *S. japonicum.*

In summary, our work shows that *Sj*Pfn is both structurally and functionally a profilin that efficiently binds to and sequesters actin monomers. Although having a low sequence identity, *Sj*Pfn shares the canonical profilin fold. *Sj*Pfn contains an elongated acidic loop, which is unique within the profilin family. The presence of an additional helix between α2 and β3 is not observed in *Sj*Pfn. In contrast, these residues are unfolded and form a loop. All of these features may affect the interaction of *Sj*Pfn with actin, which takes place by unconserved interactions to subdomains 1 and 3.

7 Conclusions and Future Perspectives

Schistosomiasis is prevalent in tropical and subtropical countries and causes severe health and social problems despite a rather low mortality rate. Intervention strategies against parasitic infections include, in general, the identification of novel drug targets, development of target-based therapy and development of vaccines. In this context, a better insight in the parasite biology will guide the design of new strategies to search for potent vaccines or therapeutic targets. Parasite tegument proteins represent interesting candidates to be used in vaccine formulations and in the diagnosis of early infections, since the tegument represents the interface between host and parasite and is largely responsible for vital functions of the parasite, such as host recognition and immune evasion. Up to date, profilins have not been described in *Trematoda.* In this work, structure-function relationships in the profilin-mediated regulation of actin polymerization in *S. japonicum* were investigated by the characterization of the ligand binding properties using biochemical and biophysical methods.

Several residues from the amino acid sequence, known to be conserved among the profilin family, are divergent in *Sj*Pfn. Our structure of the profilin monomer shows that *Sj*Pfn shares the profilin topology with a canonical central β-sheet sandwiched between α-helices. The presence of an extended loop between β7 and α3 gives a unique touch to the parasitic profilin.

We show here that *Sj*Pfn is a true profilin sequestering actin monomers. In the presence of *Sj*Pfn, the initial actin polymerization rate was decreased, showing that *Sj*Pfn inhibits the formation of actin filaments. From the actin-*Sj*Pfn crystal structure, we can conclude that *Sj*Pfn binds actin in the canonical binding face, although the binding site contains unconserved interactions.

Additionally, we found preliminary evidence that *Sj*Pfn has the capacity of binding octaproline peptides. Although the results show that *Sj*Pfn binds the octaproline peptide with micromolar affinity, detailed mapping of the molecular interaction to completely understand the importance of the peptide composition is required.

The capability of *Sj*Pfn to bind polyphosphoinositides remains to be investigated in order to make the characterization of *Sj*Pfn more complete. We noted that *Sj*Pfn is an important regulator of actin dynamics, while the interaction with polyphosphoinositides will shed light of a possible function of *Sj*Pfn in cell signaling.

8 Bibliography

Adams, P. D., Afonine, P. V, Bunkóczi, G., Chen, V. B., Davis, I. W., Echols, N., *et al.* (2010), "PHENIX: a comprehensive Python-based system for macromolecular structure solution.," *Acta crystallographica. Section D, Biological crystallography*, **66**(Pt 2): 213–21.

Adler, A. J., Greenfield, N. J. and Fasman, G. D. (1973), "Circular dichroism and optical rotatory dispersion of proteins and polypeptides.," *Methods in enzymology*, **27**: 675–735.

Afonine, P. V, Grosse-Kunstleve, R. W., Echols, N., Headd, J. J., Moriarty, N. W., Mustyakimov, M., *et al.* (2012), "Towards automated crystallographic structure refinement with phenix.refine.," *Acta crystallographica. Section D, Biological crystallography*, **68**(Pt 4): 352–67.

Amann, K. J. and Pollard, T. D. (2001), "The Arp2/3 complex nucleates actin filament branches from the sides of pre-existing filaments.," *Nature cell biology*, **3**(3): 306–10.

Ampe, C., Markey, F., Lindberg, U. and Vandekerckhove, J. (1988), "The primary structure of human platelet profilin: reinvestigation of the calf spleen profilin sequence.," *FEBS letters*, **228**(1): 17–21.

Aparicio-Fabre, R., Guillén, G., Estrada, G., Olivares-Grajales, J., Gurrola, G. and Sánchez, F. (2006), "Profilin tyrosine phosphorylation in poly-L-proline-binding regions inhibits binding to phosphoinositide 3-kinase in Phaseolus vulgaris.," *The Plant journal : for cell and molecular biology*, **47**(4): 491–500.

Arasada, R., Gloss, A., Tunggal, B., Joseph, J. M., Rieger, D., Mondal, S., Faix, J., Schleicher, M. and Noegel, A. A. (2007), "Profilin isoforms in Dictyostelium discoideum.," *Biochimica et biophysica acta*, **1773**(5): 631–41.

Artimo, P., Jonnalagedda, M., Arnold, K., Baratin, D., Csardi, G., de Castro, E., *et al.* (2012), "ExPASy: SIB bioinformatics resource portal.," *Nucleic acids research*, **40**(Web Server issue): W597–603.

Bamburg, J. R. (1999), "Proteins of the ADF/cofilin family: essential regulators of actin dynamics.," *Annual review of cell and developmental biology*, **15**: 185–230.

Basch, P. F. (1991), *Schistosomes: development, reproduction, and host relations.* Oxford University Press, New York.

Beer (1852), "Determination of the absorption of red light in colored liquids A," *Annalen der Physik und Chemie*, **86**: 78–88.

Bergquist, R., Utzinger, J. and McManus, D. P. (2008), "Trick or treat: the role of vaccines in integrated schistosomiasis control.," *PLoS neglected tropical diseases*, **2**(6): e244.

Berriman, M., Haas, B. J., LoVerde, P. T., Wilson, R. A., Dillon, G. P., Cerqueira, G. C., *et al.* (2009), "The genome of the blood fluke Schistosoma mansoni.," *Nature*, **460**(7253): 352–8.

Bertani, G. (1951), "Studies on lysogenesis. I. The mode of phage liberation by lysogenic Escherichia coli.," *Journal of bacteriology*, **62**(3): 293–300.

Beychok, S. (1966), "Circular dichroism of biological macromolecules.," *Science (New York, N.Y.)*, **154**(3754): 1288–99.

Blasco, R., Cole, N. B. and Moss, B. (1991), "Sequence analysis, expression, and deletion of a vaccinia virus gene encoding a homolog of profilin, a eukaryotic actin-binding protein.," *Journal of virology*, **65**(9): 4598–4608.

Boukhelifa, M., Moza, M., Johansson, T., Rachlin, A., Parast, M., Huttelmaier, S., *et al.* (2006), "The proline-rich protein palladin is a binding partner for profilin.," *The FEBS journal*, **273**(1): 26–33.

Brant, S. V, Morgan, J. A. T., Mkoji, G. M., Snyder, S. D., Rajapakse, R. P. V. J. and Loker, E. S. (2006), "An approach to revealing blood fluke life cycles, taxonomy, and diversity: provision of key reference data including DNA sequence from single life cycle stages.," *The Journal of parasitology*, **92**(1): 77–88.

Braun, A., Aszódi, A., Hellebrand, H., Berna, A., Fässler, R. and Brandau, O. (2002), "Genomic organization of profilin-III and evidence for a transcript expressed exclusively in testis.," *Gene*, **283**(1-2): 219–25.

Bubb, M. R., Baines, I. C. and Korn, E. D. (1998), "Localization of actobindin, profilin I, profilin II, and phosphatidylinositol-4,5-bisphosphate (PIP2) in Acanthamoeba castellanii.," *Cell motility and the cytoskeleton*, **39**(2): 134–46.

Buss, F., Temm-Grove, C., Henning, S. and Jockusch, B. M. (1992), "Distribution of profilin in fibroblasts correlates with the presence of highly dynamic actin filaments.," *Cell motility and the cytoskeleton*, **22**(1): 51–61.

Caldwell, J. E., Heiss, S. G., Mermall, V. and Cooper, J. A. (1989), "Effects of CapZ, an actin capping protein of muscle, on the polymerization of actin.," *Biochemistry*, **28**(21): 8506–14.

Cardoso, F. C., Macedo, G. C., Gava, E., Kitten, G. T., Mati, V. L., de Melo, A. L., *et al.* (2008), "Schistosoma mansoni tegument protein Sm29 is able to induce a Th1-type of immune response and protection against parasite infection.," *PLoS neglected tropical diseases*, **2**(10): e308.

Carlsson, L., Nystrom, L., Sundkvist, I., Markey, F. and Lindberg, U. (1976), "Profilin, a low-molecular weight protein controlling actin polymerisability.," in S. Perry, A. Marzella and R. Adelstein (eds), *Contractile systems in non muscle tissues*. Amsterdam: North Holland Publishing, 39–49.

Carlsson, L., Nyström, L.-E., Sundkvist, I., Markey, F. and Lindberg, U. (1977), "Actin polymerizability is influenced by profilin, a low molecular weight protein in non-muscle cells," *Journal of Molecular Biology*, **115**(3): 465–483.

Castellano, F., Chavrier, P. and Caron, E. (2001), "Actin dynamics during phagocytosis.," *Seminars in immunology*, **13**(6): 347–55.

Chen, H. and Lin, D. (2004), "The prevalence and control of schistosomiasis in Poyang Lake region, China.," *Parasitology international*, **53**(2): 115–25.

Chik, J. K., Lindberg, U. and Schutt, C. E. (1996), "The structure of an open state of beta-actin at 2.65 A resolution.," *Journal of molecular biology*, **263**: 607–623.

Cohen, C., Reinhardt, B., Castellani, L., Norton, P. and Stirewalt, M. (1982), "Schistosome surface spines are 'crystals' of actin.," *The Journal of cell biology*, **95**(3): 987–8.

Compton, L. A. and Johnson, W. C. (1986), "Analysis of protein circular dichroism spectra for secondary structure using a simple matrix multiplication.," *Analytical biochemistry*, **155**(1): 155–67.

Consortium, S. japonicum G. S. and F. A. (2009), "The Schistosoma japonicum genome reveals features of host-parasite interplay.," *Nature*, **460**(July): 345–351.

Cook, R. M., Carvalho-Queiroz, C., Wilding, G. and LoVerde, P. T. (2004), "Nucleic acid vaccination with Schistosoma mansoni antioxidant enzyme cytosolic superoxide dismutase and the structural protein filamin confers protection against the adult worm stage.," *Infection and immunity*, **72**(10): 6112–24.

Cooper, G. M. (2000), "Structure and Organization of Actin Filaments." Sinauer Associates.

Cooper, J. A., Walker, S. B. and Pollard, T. D. (1983), "Pyrene actin: documentation of the validity of a sensitive assay for actin polymerization.," *Journal of muscle research and cell motility*, **4**(2): 253–62.

Cornford, E. M. and Oldendorf, W. H. (1979), "Transintegumental uptake of metabolic substrates in male and female Schistosoma mansoni.," *The Journal of parasitology*, **65**(3): 357–63.

Cutts, L. and Wilson, R. A. (1997), "The protein antigens secreted in vivo by adult male Schistosoma mansoni.," *Parasitology*, **114 (Pt 3**: 245–55.

Deng, J., Gold, D., LoVerde, P. T. and Fishelson, Z. (2003), "Inhibition of the complement membrane attack complex by Schistosoma mansoni paramyosin.," *Infection and immunity*, **71**(11): 6402–10.

Di Nardo, A., Gareus, R., Kwiatkowski, D. and Witke, W. (2000), "Alternative splicing of the mouse profilin II gene generates functionally different profilin isoforms.," *Journal of cell science*, **113 Pt 21**: 3795–803.

Didry, D., Carlier, M. F. and Pantaloni, D. (1998), "Synergy between actin depolymerizing factor/cofilin and profilin in increasing actin filament turnover.," *The Journal of biological chemistry*, **273**(40): 25602–11.

Dos Remedios, C. G., Chhabra, D., Kekic, M., Dedova, I. V, Tsubakihara, M., Berry, D. a and Nosworthy, N. J. (2003), "Actin binding proteins: regulation of cytoskeletal microfilaments.," *Physiological reviews*, **83**: 433–473.

Eads, J. C., Mahoney, N. M., Vorobiev, S., Bresnick, A. R., Wen, K. K., Rubenstein, P. a., Haarer, B. K. and Almo, S. C. (1998), "Structure determination and characterization of Saccharomyces cerevisiae profilin," *Biochemistry*, **37**(97): 11171–11181.

Eads, J. C., Mahoney, N. M., Vorobiev, S., Bresnick, A. R., Wen, K. K., Rubenstein, P. A., Haarer, B. K. and Almo, S. C. (1998), "Structure determination and characterization of Saccharomyces cerevisiae profilin.," *Biochemistry*, **37**(32): 11171–81.

Eftink, M. R. (1991), "Fluorescence techniques for studying protein structure.," *Methods of biochemical analysis*, **35**: 127–205.

Emsley, P., Lohkamp, B., Scott, W. G. and Cowtan, K. (2010), "Features and development of Coot.," *Acta crystallographica. Section D, Biological crystallography*, **66**(Pt 4): 486–501.

Engels, D., Chitsulo, L., Montresor, A. and Savioli, L. (2002), "The global epidemiological situation of schistosomiasis and new approaches to control and research.," *Acta tropica*, **82**(2): 139–46.

Ericsson, U. B., Hallberg, B. M., Detitta, G. T., Dekker, N. and Nordlund, P. (2006), "Thermofluor-based high-throughput stability optimization of proteins for structural studies.," *Analytical biochemistry*, **357**(2): 289–98.

Eriksson, J. E., Dechat, T., Grin, B., Helfand, B., Mendez, M., Pallari, H.-M. and Goldman, R. D. (2009), "Introducing intermediate filaments: from discovery to disease.," *The Journal of clinical investigation*. American Society for Clinical Investigation, **119**(7): 1763–71.

Fedorov, a a, Ball, T., Mahoney, N. M., Valenta, R. and Almo, S. C. (1997), "The molecular basis for allergen cross-reactivity: crystal structure and IgE-epitope mapping of birch pollen profilin.," *Structure (London, England : 1993)*, **5**: 33–45.

Fenn, J. B., Mann, M., Meng, C. K., Wong, S. F. and Whitehouse, C. M. (1989), "Electrospray ionization for mass spectrometry of large biomolecules.," *Science (New York, N.Y.)*, **246**(4926): 64–71.

Fenwick, A., Savioli, L., Engels, D., Robert Bergquist, N. and Todd, M. H. (2003), "Drugs for the control of parasitic diseases: current status and development in schistosomiasis.," *Trends in parasitology*, **19**(11): 509–15.

Fitzsimmons, C. M., Jones, F. M., Stearn, A., Chalmers, I. W., Hoffmann, K. F., Wawrzyniak, J., Wilson, S., Kabatereine, N. B. and Dunne, D. W. (2012), "The Schistosoma mansoni tegumental-allergen-like (TAL) protein family: influence of developmental expression on human IgE responses.," *PLoS neglected tropical diseases*, **6**(4): e1593.

Fitzsimmons, C. M., Stewart, T. J., Hoffmann, K. F., Grogan, J. L., Yazdanbakhsh, M. and Dunne, D. W. (2004), "Human IgE response to the Schistosoma haematobium 22.6 kDa antigen.," *Parasite immunology*, **26**(8-9): 371–6.

Gadermaier, E., Flicker, S., Lupinek, C., Steinberger, P. and Valenta, R. (2013), "Determination of allergen specificity by heavy chains in grass pollen allergen-specific IgE antibodies.," *The Journal of allergy and clinical immunology*, **131**(4): 1185–93, 1193.e1–6.

Giehl, K., Valenta, R., Rothkegel, M., Ronsiek, M., Mannherz, H. G. and Jockusch, B. M. (1994), "Interaction of plant profilin with mammalian actin.," *European journal of biochemistry / FEBS*, **226**(2): 681–9.

Gieselmann, R., Kwiatkowski, D., Janmey, P. and Witke, W. (1995), "Distinct biochemical characteristics of the two human profilin isoforms.," *European journal of biochemistry*, **229**(3): 621–8.

Gobert, G. N., Stenzel, D. J., Jones, M. K., Allen, D. E. and McManusk, D. P. (1997), "Schistosoma japonicum: immunolocalization of paramyosin during development," *Parasitology*. Cambridge University Press, **114**(01): 45–52.

Gobert, G. N., Stenzel, D. J., McManus, D. P. and Jones, M. K. (2003), "The ultrastructural architecture of the adult Schistosoma japonicum tegument.," *International journal for parasitology*, **33**(14): 1561–75.

Goldschmidt-Clermont, P. J., Machesky, L. M., Baldassare, J. J. and Pollard, T. D. (1990), "The actin-binding protein profilin binds to PIP2 and inhibits its hydrolysis by phospholipase C.," *Science (New York, N.Y.)*, **247**(4950): 1575–8.

Gonzalez, V., Combe, A., David, V., Malmquist, N. A., Delorme, V., Leroy, C., Blazquez, S., Ménard, R. and Tardieux, I. (2009), "Host cell entry by apicomplexa parasites requires actin polymerization in the host cell.," *Cell host & microbe*, **5**(3): 259–72.

Goode, B. L. and Eck, M. J. (2007), "Mechanism and function of formins in the control of actin assembly.," *Annual review of biochemistry*, **76**: 593–627.

Gordy, C., Mishra, S. and Rodgers, W. (2004), "Visualization of antigen presentation by actin-mediated targeting of glycolipid-enriched membrane domains to the immune synapse of B cell APCs.," *Journal of immunology (Baltimore, Md. : 1950)*, **172**(4): 2030–8.

Greenberg, R. M. (2005), "Are Ca2+ channels targets of praziquantel action?," *International journal for parasitology*, **35**(1): 1–9.

Greenfield, N. and Fasman, G. D. (1969), "Computed circular dichroism spectra for the evaluation of protein conformation.," *Biochemistry*, **8**(10): 4108–16.

Greenfield, N. J. (2006), "Using circular dichroism spectra to estimate protein secondary structure.," *Nature protocols*, **1**(6): 2876–90.

Gryseels, B., Polman, K., Clerinx, J. and Kestens, L. (2006), "Human schistosomiasis.," *Lancet*, **368**(9541): 1106–18.

Gupta, B. C. and Basch, P. F. (1987), "The role of Schistosoma mansoni males in feeding and development of female worms.," *The Journal of parasitology*, **73**(3): 481–6.

Harper, S. and Speicher, D. W. (2011), "Purification of proteins fused to glutathione S-transferase.," *Methods in molecular biology (Clifton, N.J.)*, **681**: 259–80.

Haugwitz, M., Noegel, A. A., Rieger, D., Lottspeich, F. and Schleicher, M. (1991), "Dictyostelium discoideum contains two profilin isoforms that differ in structure and function.," *Journal of cell science*, **100 (Pt 3**: 481–9.

He, Y. (1993), "He Y.X. (1993). Biology of Schistosoma japonicum from cercaria penetration into host skin to producing egg. Chinese Medical Journal (English) 106, 576–583 - Google zoeken," 576–583.

Herman, I. M. (1993), "Actin isoforms.," *Current opinion in cell biology*, **5**(1): 48–55.

Hertzog, M., van Heijenoort, C., Didry, D., Gaudier, M., Coutant, J., Gigant, B., *et al.* (2004), "The beta-thymosin/WH2 domain; structural basis for the switch from inhibition to promotion of actin assembly.," *Cell*, **117**(5): 611–23.

Higgins, D. G. and Sharp, P. M. (1988), "CLUSTAL: a package for performing multiple sequence alignment on a microcomputer.," *Gene*, **73**(1): 237–44.

Higgs, H. N. and Pollard, T. D. (1999), "Regulation of Actin Polymerization by Arp2/3 Complex and WASp/Scar Proteins," *Journal of Biological Chemistry*, **274**(46): 32531–32534.

Higgs, H. N. and Pollard, T. D. (2001), "Regulation of actin filament network formation through ARP2/3 complex: activation by a diverse array of proteins.," *Annual review of biochemistry*, **70**: 649–76.

Hitchcock, S. E., Carisson, L. and Lindberg, U. (1976), "Depolymerization of F-actin by deoxyribonuclease I.," *Cell*, **7**(4): 531–42.

Hockley, D. J. (1973), "Ultrastructure of the tegument of Schistosoma.," *Advances in parasitology*, **11**: 233–305.

Hockley, D. J. and McLaren, D. J. (1973), "Schistosoma mansoni: changes in the outer membrane of the tegument during development from cercaria to adult worm.," *International journal for parasitology*, **3**(1): 13–25.

Hoffmann, K. F. and Strand, M. (1996), "Molecular identification of a Schistosoma mansoni tegumental protein with similarity to cytoplasmic dynein light chains.," *The Journal of biological chemistry*, **271**(42): 26117–23.

Holmes, K. C., Popp, D., Gebhard, W. and Kabsch, W. (1990), "Atomic model of the actin filament.," *Nature*, **347**(6288): 44–9.

Holzwarth, G. and Doty, P. (1965), "THE ULTRAVIOLET CIRCULAR DICHROISM OF POLYPEPTIDES.," *Journal of the American Chemical Society*, **87**: 218–28.

Honoré, B., Madsen, P., Andersen, A. H. and Leffers, H. (1993), "Cloning and expression of a novel human profilin variant, profilin II.," *FEBS letters*, **330**(2): 151–5.

Hu, E., Chen, Z., Fredrickson, T. and Zhu, Y. (2001), "Molecular cloning and characterization of profilin-3: a novel cytoskeleton-associated gene expressed in rat kidney and testes.," *Experimental nephrology*, **9**(4): 265–74.

Irobi, E., Aguda, A. H., Larsson, M., Guerin, C., Yin, H. L., Burtnick, L. D., Blanchoin, L. and Robinson, R. C. (2004), "Structural basis of actin sequestration by thymosin-beta4: implications for WH2 proteins.," *The EMBO journal*, **23**(18): 3599–608.

Jimenez-Lopez, J. C., Morales, S., Castro, A. J., Volkmann, D., Rodríguez-García, M. I. and de Alché, J. D. (2012), "Characterization of profilin polymorphism in pollen with a focus on multifunctionality," *PLoS ONE*, **7**(2).

Jockusch, B. M., Murk, K. and Rothkegel, M. (2007), "The profile of profilins.," *Reviews of physiology, biochemistry and pharmacology*, **159**: 131–49.

Johnson, M., Zaretskaya, I., Raytselis, Y., Merezhuk, Y., McGinnis, S. and Madden, T. L. (2008), "NCBI BLAST: a better web interface.," *Nucleic acids research*, **36**(Web Server issue): W5–9.

Jones, M. K., Gobert, G. N., Zhang, L., Sunderland, P. and McManus, D. P. (2004), "The cytoskeleton and motor proteins of human schistosomes and their roles in surface maintenance and host-parasite interactions.," *BioEssays : news and reviews in molecular, cellular and developmental biology*, **26**(7): 752–65.

Kabsch, W. (2010), "XDS.," *Acta crystallographica. Section D, Biological crystallography*, **66**(Pt 2): 125–32.

Kabsch, W., Mannherz, H. G., Suck, D., Pai, E. F. and Holmes, K. C. (1990), "Atomic structure of the actin:DNase I complex.," *Nature*, **347**(6288): 37–44.

Kamal, S. M. and El Sayed Khalifa, K. (2006), "Immune modulation by helminthic infections: worms and viral infections.," *Parasite immunology*, **28**(10): 483–96.

Kandasamy, M. K., McKinney, E. C. and Meagher, R. B. (2002), "Plant profilin isovariants are distinctly regulated in vegetative and reproductive tissues.," *Cell motility and the cytoskeleton*, **52**(1): 22–32.

Khalil LF (2002), "Khalil LF. Family Schistosomatidae Stiles & Hassall, 1898. In: Gibson DI, Jones A, Bray RA, editors. Keys to the Trematoda. CABI Publishing; Wallingford, U.K.: 2002. pp. 419–432.

Kohn, A. B., Anderson, P. A., Roberts-Misterly, J. M. and Greenberg, R. M. (2001), "Schistosome calcium channel beta subunits. Unusual modulatory effects and potential role in the action of the antischistosomal drug praziquantel.," *The Journal of biological chemistry*, **276**(40): 36873–6.

Köster, B. and Strand, M. (1994), "Schistosoma mansoni: immunolocalization of two different fucose-containing carbohydrate epitopes.," *Parasitology*, **108 (Pt 4**: 433–46.

Kouyama, T. and Mihashi, K. (1981), "Fluorimetry study of N-(1-pyrenyl)iodoacetamide-labelled F-actin. Local structural change of actin protomer both on polymerization and on binding of heavy meromyosin.," *European journal of biochemistry / FEBS*, **114**(1): 33–8.

Krissinel, E. and Henrick, K. (2007), "Inference of Macromolecular Assemblies from Crystalline State," *Journal of Molecular Biology*, **372**: 774–797.

Kucera, K., Koblansky, A. A., Saunders, L. P., Frederick, K. B., De La Cruz, E. M., Ghosh, S. and Modis, Y. (2010), "Structure-Based Analysis of Toxoplasma gondii Profilin: A Parasite-Specific Motif Is Required for Recognition by Toll-Like Receptor 11," *Journal of Molecular Biology*, **403**: 616–629.

Kursula, I., Kursula, P., Ganter, M., Panjikar, S., Matuschewski, K. and Schüler, H. (2008a), "Structural Basis for Parasite-Specific Functions of the Divergent Profilin of Plasmodium falciparum," *Structure*, **16**: 1638–1648.

Kursula, P. (2004), "XDSi : a graphical interface for the data processing program XDS," *Journal of Applied Crystallography*. International Union of Crystallography, **37**(2): 347–348.

Kursula, P., Kursula, I., Massimi, M., Song, Y.-H., Downer, J., Stanley, W. A., Witke, W. and Wilmanns, M. (2008), "High-resolution structural analysis of mammalian profilin 2a complex formation with two physiological ligands: the formin homology 1 domain of mDia1 and the proline-rich domain of VASP.," *Journal of molecular biology*, **375**(1): 270–90.

Kusel, J. R. and Gordon, J. F. (1989), "Biophysical studies of the schistosome surface and their relevance to its properties under immune and drug attack.," *Parasite immunology*, **11**(5): 431–51.

Kwiatkowski, D., Stossel, T., Orkin, S., Mole, J., Colten, H. and Yin, H. (1986), "Plasma and cytoplasmic gelsolins are encoded by a single gene and contain a duplicated actin-binding domain," *Nature*, 455–458.

Laemmli, U. K. (1970), "Cleavage of Structural Proteins during the Assembly of the Head of Bacteriophage T4," *Nature*, **227**(5259): 680–685.

Lakowicz, J. (1999), *Principles of Fluorescence Spectroscopy*. New York: Plenum Press.

Lambrechts, A., Braun, A., Jonckheere, V., Aszodi, A., Lanier, L. M., Robbens, J., *et al.* (2000), "Profilin II is alternatively spliced, resulting in profilin isoforms that are differentially expressed and have distinct biochemical properties.," *Molecular and cellular biology*, **20**(21): 8209–19.

Lambrechts, A., Van Troys, M. and Ampe, C. (2004), "The actin cytoskeleton in normal and pathological cell motility.," *The international journal of biochemistry & cell biology*, **36**(10): 1890–909.

Lassing, I. and Lindberg, U. (1985), "Specific interaction between phosphatidylinositol 4,5-bisphosphate and profilactin.," *Nature*, **314**(6010): 472–4.

Lazarides, E. and Lindberg, U. (1974), "Actin is the naturally occurring inhibitor of deoxyribonuclease I.," *Proceedings of the National Academy of Sciences of the United States of America*, **71**(12): 4742–6.

Leitch, B., Probert, A. J. and Runham, N. W. (1984), "The ultrastructure of the tegument of adult Schistosoma haematobium.," *Parasitology*, **89 (Pt 1)**: 71–8.

Li, M. Z. and Elledge, S. J. (2012), "SLIC: a method for sequence- and ligation-independent cloning.," *Methods in molecular biology (Clifton, N.J.)*, **852**: 51–9.

Li, Y., Auliff, A., Jones, M. K., Yi, X. and McManus, D. P. (2000), "Immunogenicity and immunolocalization of the 22.6 kDa antigen of Schistosoma japonicum.," *Parasite immunology*, **22**(8): 415–24.

Liu, P., Shi, Y., Yang, Y., Cao, Y., Shi, Y., Li, H., Liu, J., Lin, J. and Jin, Y. (2012), "Schistosoma japonicum UDP-glucose 4-epimerase protein is located on the tegument and induces moderate protection against challenge infection.," *PloS one*, **7**(7): e42050.

Lobley, A., Whitmore, L. and Wallace, B. A. (2002), "DICHROWEB: an interactive website for the analysis of protein secondary structure from circular dichroism spectra.," *Bioinformatics (Oxford, England)*, **18**(1): 211–2.

Lodish, H., Berk, A., Zipursky, S. L., Matsudaira, P., Baltimore, D. and Darnell, J. (2000a), "Molecular Cell Biology." W. H. Freeman.

Lodish, H., Berk, A., Zipursky, S. L., Matsudaira, P., Baltimore, D. and Darnell, J. (2000b), "Myosin: The Actin Motor Protein," *Molecular Cell biology. 4th edition*. New York: W. H. Freeman.

Lu, J. and Pollard, T. D. (2001), "Profilin binding to poly-L-proline and actin monomers along with ability to catalyze actin nucleotide exchange is required for viability of fission yeast.," *Molecular biology of the cell*, **12**(4): 1161–75.

Lu, P.-J., Shieh, W.-R., Rhee, S. G., Yin, H. L. and Chen, C.-S. (1996), "Lipid Products of Phosphoinositide 3-Kinase Bind Human Profilin with High Affinity," *Biochemistry*, **35**(44): 14027–14034.

Machesky, L. M., Atkinson, S. J., Ampe, C., Vandekerckhove, J. and Pollard, T. D. (1994), "Purification of a cortical complex containing two unconventional actins from Acanthamoeba by affinity chromatography on profilin-agarose.," *The Journal of cell biology*, **127**(1): 107–15.

Machesky, L. M. and Poland, T. D. (1993), "Profilin as a potential mediator of membrane-cytoskeleton communication.," *Trends in cell biology*, **3**(11): 381–5.

Maciver, S. K. and Hussey, P. J. (2002), "The ADF/cofilin family: actin-remodeling proteins.," *Genome biology*, **3**(5): reviews3007.

Magdolen, V., Oechsner, U., Müller, G. and Bandlow, W. (1988), "The intron-containing gene for yeast profilin (PFY) encodes a vital function.," *Molecular and cellular biology*, **8**(12): 5108–15.

Mahoney, N. M., Janmey, P. A. and Almo, S. C. (1997), "Structure of the profilin-poly-L-proline complex involved in morphogenesis and cytoskeletal regulation.," *Nature structural biology*, **4**(11): 953–60.

Manseau, L., Calley, J. and Phan, H. (1996), "Profilin is required for posterior patterning of the Drosophila oocyte.," *Development (Cambridge, England)*, **122**(7): 2109–16.

Markus, M. A., Nakayama, T., Matsudaira, P. and Wagner, G. (1994), "1H, 15N, 13C and 13CO resonance assignments and secondary structure of villin 14T, a domain conserved among actin-severing proteins.," *Journal of biomolecular NMR*, **4**(4): 553–74.

Marr, J. J., Nilsen, T. W. and Komuniecki, R. W. (2002), *Molecular Medical Parasitology*. Academic Press.

Matsumoto, Y., Perry, G., Levine, R. J., Blanton, R., Mahmoud, A. A. and Aikawa, M. (1988), "Paramyosin and actin in schistosomal teguments.," *Nature*, **333**(6168): 76–8.

Matthews, B. W. (1968), "Solvent content of protein crystals.," *Journal of molecular biology*, **33**(2): 491–7.

McCoy, A. J., Grosse-Kunstleve, R. W., Adams, P. D., Winn, M. D., Storoni, L. C. and Read, R. J. (2007), "Phaser crystallographic software.," *Journal of applied crystallography*, **40**(Pt 4): 658–674.

McLaughlin, P. J., Gooch, J. T., Mannherz, H. G. and Weeds, A. G. (1993), "Structure of gelsolin segment 1-actin complex and the mechanism of filament severing.," *Nature*, **364**: 685–692.

McLaughlin, P. J. and Weeds, A. G. (1995), "Actin-binding protein complexes at atomic resolution.," *Annual review of biophysics and biomolecular structure*, **24**: 643–75.

McManus, D. P. (2005), "Prospects for development of a transmission blocking vaccine against Schistosoma japonicum.," *Parasite immunology*, **27**(7-8): 297–308.

McManus, D. P. and Dalton, J. P. (2006), "Vaccines against the zoonotic trematodes Schistosoma japonicum, Fasciola hepatica and Fasciola gigantica.," *Parasitology*, **133 Suppl**: S43–61.

McManus, D. P. and Loukas, A. (2008), "Current status of vaccines for schistosomiasis.," *Clinical microbiology reviews*, **21**(1): 225–42.

McWilliam, H. E., Driguez, P., Piedrafita, D., McManus, D. P. and Meeusen, E. N. (2014), "Discovery of novel Schistosoma japonicum antigens using a targeted protein microarray approach," *Parasites & Vectors*, **7**(1): 290.

Metzler, W. J., Farmer, B. T., Constantine, K. L., Friedrichs, M. S., Lavoie, T. and Mueller, L. (1995), "Refined solution structure of human profilin I.," *Protein science : a publication of the Protein Society*, **4**: 450–459.

Milhon, J. L., Thiboldeaux, R. L., Glowac, K. and Tracy, J. W. (1997), "Schistosoma japonicum GSH S-transferase Sj26 is not the molecular target of praziquantel action.," *Experimental parasitology*, **87**(3): 268–74.

Mockrin, S. C. and Korn, E. D. (1980), "Acanthamoeba profilin interacts with G-actin to increase the rate of exchange of actin-bound adenosine 5'-triphosphate.," *Biochemistry*, **19**(23): 5359–62.

Möller, M. and Denicola, A. (2002), "Study of protein-ligand binding by fluorescence," *Biochemistry and Molecular Biology Education*, **30**(5): 309–312.

Mooij, W. T. M., Mitsiki, E. and Perrakis, A. (2009), "ProteinCCD: enabling the design of protein truncation constructs for expression and crystallization experiments.," *Nucleic acids research*, **37**(Web Server issue): W402–5.

Muller, R. (1995), "Human schistosomiasis.," *Journal of Helminthology*. Cambridge University Press, **69**(01): 95.

Mullis, K., Faloona, F., Scharf, S., Saiki, R., Horn, G. and Erlich, H. (1986), "Specific enzymatic amplification of DNA in vitro: the polymerase chain reaction.," *Cold Spring Harbor symposia on quantitative biology*, **51 Pt 1**: 263–73.

Narita, A., Takeda, S., Yamashita, A. and Maéda, Y. (2006), "Structural basis of actin filament capping at the barbed-end: a cryo-electron microscopy study.," *The EMBO journal*, **25**(23): 5626–33.

Nodelman, I. M., Bowman, G. D., Lindberg, U. and Schutt, C. E. (1999), "X-ray structure determination of human profilin II: A comparative structural analysis of human profilins.," *Journal of molecular biology*, **294**: 1271–1285.

Notredame, C., Higgins, D. G. and Heringa, J. (2000), "T-Coffee: A novel method for fast and accurate multiple sequence alignment.," *Journal of molecular biology*, **302**: 205–217.

Nyame, A. K., Kawar, Z. S. and Cummings, R. D. (2004), "Antigenic glycans in parasitic infections: implications for vaccines and diagnostics.," *Archives of biochemistry and biophysics*, **426**(2): 182–200.

Obermann, H., Raabe, I., Balvers, M., Brunswig, B., Schulze, W. and Kirchhoff, C. (2005), "Novel testis-expressed profilin IV associated with acrosome biogenesis and spermatid elongation," *Molecular Human Reproduction*, **11**(1): 53–64.

Pantoliano, M. W., Petrella, E. C., Kwasnoski, J. D., Lobanov, V. S., Myslik, J., Graf, E., *et al.* (2001), "High-density miniaturized thermal shift assays as a general strategy for drug discovery.," *Journal of biomolecular screening*, **6**(6): 429–40.

Pardee, J. D. and Spudich, J. A. (1982), "Purification of muscle actin.," *Methods in enzymology*, **85 Pt B**: 164–81.

Parizade, M., Arnon, R., Lachmann, P. J. and Fishelson, Z. (1994), "Functional and antigenic similarities between a 94-kD protein of Schistosoma mansoni (SCIP-1) and human CD59.," *The Journal of experimental medicine*, **179**(5): 1625–36.

Pearce, E. J. and MacDonald, A. S. (2002), "The immunobiology of schistosomiasis.," *Nature reviews. Immunology*, **2**(7): 499–511.

Peitsch, M. C., Polzar, B., Stephan, H., Crompton, T., MacDonald, H. R., Mannherz, H. G. and Tschopp, J. (1993), "Characterization of the endogenous deoxyribonuclease involved in nuclear DNA degradation during apoptosis (programmed cell death).," *The EMBO journal*, **12**(1): 371–7.

Perelroizen, I., Didry, D., Christensen, H., Chua, N. H. and Carlier, M. F. (1996), "Role of nucleotide exchange and hydrolysis in the function of profilin in action assembly.," *The Journal of biological chemistry*, **271**(21): 12302–9.

Perelroizen, I., Marchand, J. B., Blanchoin, L., Didry, D. and Carlier, M. F. (1994), "Interaction of profilin with G-actin and poly(L-proline).," *Biochemistry*, **33**(28): 8472–8.

Perrin, D., Möller, K., Hanke, K. and Söling, H. D. (1992), "cAMP and Ca(2+)-mediated secretion in parotid acinar cells is associated with reversible changes in the organization of the cytoskeleton.," *The Journal of cell biology*, **116**(1): 127–34.

Plattner, F., Yarovinsky, F., Romero, S., Didry, D., Carlier, M.-F., Sher, A. and Soldati-Favre, D. (2008), "Toxoplasma profilin is essential for host cell invasion and TLR11-dependent induction of an interleukin-12 response.," *Cell host & microbe*, **3**(2): 77–87.

Polet, D., Lambrechts, A., Ono, K., Mah, A., Peelman, F., Vandekerckhove, J., Baillie, D. L., Ampe, C. and Ono, S. (2006), "Caenorhabditis elegans expresses three functional profilins in a tissue-specific manner.," *Cell motility and the cytoskeleton*, **63**(1): 14–28.

Pollitt, A. Y. and Insall, R. H. (2009), "WASP and SCAR/WAVE proteins: the drivers of actin assembly.," *Journal of cell science*, **122**(Pt 15): 2575–8.

Porath, J., Carlsson, J., Olsson, I. and Belfrage, G. (1975), "Metal chelate affinity chromatography, a new approach to protein fractionation.," *Nature*, **258**(5536): 598–9.

Porath, J. and Flodin, P. (1959), "Gel filtration: a method for desalting and group separation.," *Nature*, **183**(4676): 1657–9.

Porta, J. C. and Borgstahl, G. E. O. (2012), "Structural basis for profilin-mediated actin nucleotide exchange.," *Journal of molecular biology*, **418**(1-2): 103–16.

Rajakylä, E. K. and Vartiainen, M. K. (2014), "Rho, nuclear actin, and actin-binding proteins in the regulation of transcription and gene expression.," *Small GTPases*, **5**: e27539.

Rao, J. N., Madasu, Y. and Dominguez, R. (2014), "Mechanism of actin filament pointed-end capping by tropomodulin.," *Science (New York, N.Y.)*, **345**(6195): 463–7.

Reichstein, E. and Korn, E. D. (1979), "Acanthamoeba profilin. A protein of low molecular weight from Acanpthamoeba castellanii that inhibits actin nucleation.," *The Journal of biological chemistry*, **254**(13): 6174–9.

Reinhard, M., Giehl, K., Abel, K., Haffner, C., Jarchau, T., Hoppe, V., Jockusch, B. M. and Walter, U. (1995), "The proline-rich focal adhesion and microfilament protein VASP is a ligand for profilins.," *The EMBO journal*, **14**(8): 1583–9.

Ren, H. and Xiang, Y. (2007), "The function of actin-binding proteins in pollen tube growth.," *Protoplasma*, **230**(3-4): 171–82.

Robert, X. and Gouet, P. (2014), "Deciphering key features in protein structures with the new ENDscript server.," *Nucleic acids research*, **42**(Web Server issue): W320–4.

Rollinson, D. and Simpson, A. J. G. (1987), "The biology of schistosomes. From genes to latrines." Academic Press Ltd.

Ross, A. G. P., Bartley, P. B., Sleigh, A. C., Olds, G. R., Li, Y., Williams, G. M. and McManus, D. P. (2002), "Schistosomiasis.," *The New England journal of medicine*, **346**(16): 1212–20.

Sadava, D., Heller, H. C., Orians, G. H., Purves, W. K. and Hillis, D. M. (2013), *Life: the Science of Biology*. Palgrave Macmillan.

Salvador-Recatalà, V. and Greenberg, R. M. (2012), "Calcium channels of schistosomes: Unresolved questions and unexpected answers," *Wiley Interdisciplinary Reviews: Membrane Transport and Signaling*, **1**: 85–93.

Sanger, J. W. (1977), "Mitosis in beating cardiac myoblasts treated with cytochalasin-B.," *The Journal of experimental zoology*, **201**(3): 463–9.

Santiago, M. L., Hafalla, J. C., Kurtis, J. D., Aligui, G. L., Wiest, P. M., Olveda, R. M., Olds, G. R., Dunne, D. W. and Ramirez, B. L. (1998), "Identification of the Schistosoma japonicum 22.6-kDa antigen as a major target of the human IgE response: similarity of IgE-binding epitopes to allergen peptides.," *International archives of allergy and immunology*, **117**(2): 94–104.

Santos, A. and Van Ree, R. (2011), "Profilins: mimickers of allergy or relevant allergens?," *International archives of allergy and immunology*, **155**(3): 191–204.

Sathish, K. (2004), "Phosphorylation of profilin regulates its interaction with actin and poly (?proline)," *Cellular Signalling*, **16**(5): 589–596.

Schlüter, K., Jockusch, B. M. and Rothkegel, M. (1997), "Profilins as regulators of actin dynamics," *Biochimica et Biophysica Acta (BBA) - Molecular Cell Research*, **1359**(2): 97–109.

Schnuchel, A., Wiltscheck, R., Eichinger, L., Schleicher, M. and Holak, T. A. (1995), "Structure of severin domain 2 in solution.," *Journal of molecular biology*, **247**(1): 21–7.

Schutt, C. E., Myslik, J. C., Rozycki, M. D., Goonesekere, N. C. and Lindberg, U. (1993), "The structure of crystalline profilin-beta-actin.," *Nature*, **365**(6449): 810–6.

Schutt, C. E., Rozycki, M. D., Myslik, J. C. and Lindberg, U. "A discourse on modeling F-actin.," *Journal of structural biology*, **115**(2): 186–98.

Secor, W. E. (2005), "Immunology of human schistosomiasis: off the beaten path.," *Parasite immunology*, **27**(7-8): 309–16.

Selden, L. A., Kinosian, H. J., Newman, J., Lincoln, B., Hurwitz, C., Gershman, L. C. and Estes, J. E. (1998), "Severing of F-actin by the amino-terminal half of gelsolin suggests internal cooperativity in gelsolin.," *Biophysical journal*, **75**(6): 3092–100.

Sept, D. and McCammon, J. A. (2001), "Thermodynamics and kinetics of actin filament nucleation.," *Biophysical journal*, **81**(2): 667–74.

Sharma, A., Lambrechts, A., Hao, L. T., Le, T. T., Sewry, C. A., Ampe, C., Burghes, A. H. M. and Morris, G. E. (2005), "A role for complexes of survival of motor neurons (SMN) protein with gemins and profilin in neurite-like cytoplasmic extensions of cultured nerve cells.," *Experimental cell research*, **309**(1): 185–97.

Simons, P. C. and Vander Jagt, D. L. (1977), "Purification of glutathione S-transferases from human liver by glutathione-affinity chromatography.," *Analytical biochemistry*, **82**(2): 334–41.

Skare, P., Kreivi, J.-P., Bergström, A. and Karlsson, R. (2003), "Profilin I colocalizes with speckles and Cajal bodies: a possible role in pre-mRNA splicing.," *Experimental cell research*, **286**(1): 12–21.

Skelly, P. J. and Alan Wilson, R. (2006), "Making Sense of the Schistosome Surface," *Advances in Parasitology*, **63**(06): 185–284.

Skelly, P. J. and Shoemaker, C. B. (1996), "Rapid appearance and asymmetric distribution of glucose transporter SGTP4 at the apical surface of intramammalian-stage Schistosoma mansoni.," *Proceedings of the National Academy of Sciences of the United States of America*, **93**(8): 3642–6.

Smith, D. B. and Johnson, K. S. (1988), "Single-step purification of polypeptides expressed in Escherichia coli as fusions with glutathione S-transferase.," *Gene*, **67**(1): 31–40.

Southgate, V. R., van Wijk, H. B. and Wright, C. A. (1976), "Schistosomiasis at Loum, Cameroun; Schistosoma haematobium, S. intercalatum and their natural hybrid.," *Zeitschrift für Parasitenkunde (Berlin, Germany)*, **49**(2): 145–59.

Spear, R. C. (2012), "Internal versus external determinants of Schistosoma japonicum transmission in irrigated agricultural villages.," *Journal of the Royal Society, Interface / the Royal Society*, **9**(67): 272–82.

Stich, A. H., Biays, S., Odermatt, P., Men, C., Saem, C., Sokha, K., *et al.* (1999), "Foci of Schistosomiasis mekongi, Northern Cambodia: II. Distribution of infection and morbidity.," *Tropical medicine & international health : TM & IH*, **4**(10): 674–85.

Stossel, T. P. (1993), "On the crawling of animal cells.," *Science (New York, N.Y.)*, **260**(5111): 1086–94.

Studier, F. W. (2005), "Protein production by auto-induction in high density shaking cultures.," *Protein expression and purification*, **41**(1): 207–34.

Studier, F. W. (2014), "Stable expression clones and auto-induction for protein production in E. coli.," *Methods in molecular biology (Clifton, N.J.)*, **1091**: 17–32.

Sturrock, R. (1993), "The parasites and their life cycles, the intermediate hosts and host-parasitic relationships.," in P. Jordan, G. Webbe and R. Sturrock (eds), *Human schistosomiasis*. CAB International, Wallingford, Oxon, UK, 1–86.

Stüven, T., Hartmann, E. and Görlich, D. (2003), "Exportin 6: a novel nuclear export receptor that is specific for profilin.actin complexes.," *The EMBO journal*, **22**(21): 5928–40.

Su, Y., Kondrikov, D. and Block, E. R. (2005), "Cytoskeletal regulation of nitric oxide synthase.," *Cell biochemistry and biophysics*, **43**(3): 439–49.

Sun, H. Q., Yamamoto, M., Mejillano, M. and Yin, H. L. (1999), "Gelsolin, a multifunctional actin regulatory protein.," *The Journal of biological chemistry*, **274**(47): 33179–82.

Tallima, H. and El Ridi, R. (2007), "Praziquantel binds Schistosoma mansoni adult worm actin," *International Journal of Antimicrobial Agents*, **29**(December 2006): 570–575.

Tchuem Tchuenté, L.-A., Southgate, V. R., Jourdane, J., Webster, B. L. and Vercruysse, J. (2003), "Schistosoma intercalatum: an endangered species in Cameroon?," *Trends in parasitology*, **19**(9): 389–93.

Terwilliger, T. C., Adams, P. D., Read, R. J., McCoy, A. J., Moriarty, N. W., Grosse-Kunstleve, R. W., Afonine, P. V, Zwart, P. H. and Hung, L. W. (2009), "Decision-making in structure solution using Bayesian estimates of map quality: the PHENIX AutoSol wizard.," *Acta crystallographica. Section D, Biological crystallography*, **65**(Pt 6): 582–601.

Terwilliger, T. C., Grosse-Kunstleve, R. W., Afonine, P. V, Moriarty, N. W., Zwart, P. H., Hung, L. W., Read, R. J. and Adams, P. D. (2008), "Iterative model building, structure refinement and density modification with the PHENIX AutoBuild wizard.," *Acta crystallographica. Section D, Biological crystallography*, **64**(Pt 1): 61–9.

Theriot, J. A. and Mitchison, T. J. (1991), "Actin microfilament dynamics in locomoting cells.," *Nature*, **352**(6331): 126–31.

Thorn, K. S., Christensen, H. E., Shigeta, R., Huddler, D., Shalaby, L., Lindberg, U., Chua, N. H. and Schutt, C. E. (1997), "The crystal structure of a major allergen from plants.," *Structure (London, England : 1993)*, **5**: 19–32.

Threadgold, L. T. and Hopkins, C. A. (1981), "Schistocephalus solidus and Ligula intestinalis: pinocytosis by the tegument.," *Experimental parasitology*, **51**(3): 444–56.

Tian, F., Lin, D., Wu, J., Gao, Y., Zhang, D., Ji, M. and Wu, G. (2010), "Immune events associated with high level protection against Schistosoma japonicum infection in pigs immunized with UV-attenuated cercariae.," *PloS one*, **5**(10): e13408.

Tilney, L. G., Bonder, E. M., Coluccio, L. M. and Mooseker, M. S. (1983), "Actin from Thyone sperm assembles on only one end of an actin filament: a behavior regulated by profilin.," *The Journal of cell biology*, **97**(1): 112–24.

Tran, M. H., Pearson, M. S., Bethony, J. M., Smyth, D. J., Jones, M. K., Duke, M., *et al.* (2006), "Tetraspanins on the surface of Schistosoma mansoni are protective antigens against schistosomiasis.," *Nature medicine*, **12**(7): 835–40.

Vagin, A. and Teplyakov, A. (2010), "Molecular replacement with MOLREP.," *Acta crystallographica. Section D, Biological crystallography*, **66**(Pt 1): 22–5.

Valenta, R., Sperr, W. R., Ferreira, F., Valent, P., Sillaber, C., Tejkl, M., *et al.* (1993), "Induction of specific histamine release from basophils with purified natural and recombinant birch pollen allergens.," *The Journal of allergy and clinical immunology*, **91**(1 Pt 1): 88–97.

Valle, C., Troiani, A. R., Festucci, A., Pica-Mattoccia, L., Liberti, P., Wolstenholme, A., Francklow, K., Doenhoff, M. J. and Cioli, D. (2003), "Sequence and level of endogenous expression of calcium channel beta subunits in Schistosoma mansoni displaying different susceptibilities to praziquantel.," *Molecular and biochemical parasitology*, **130**(2): 111–5.

Van Haastert, P. J. M. and Devreotes, P. N. (2004), "Chemotaxis: signalling the way forward.," *Nature reviews. Molecular cell biology*, **5**(8): 626–34.

Van Hellemond, J. J., Retra, K., Brouwers, J. F. H. M., van Balkom, B. W. M., Yazdanbakhsh, M., Shoemaker, C. B. and Tielens, A. G. M. (2006), "Functions of the tegument of schistosomes: clues from the proteome and lipidome.," *International journal for parasitology*, **36**(6): 691–9.

Van Holde, K. E., Johnson, W. C. and Ho, P. S. (1998), *Principles of Physical Biochemistry van Holde, Kensal E; Johnson, Curtis; Ho, Pui Shing: 0130464279*. New Jersey: Prentice Hall.

Van Remoortere, A., van Dam, G. J., Hokke, C. H., van den Eijnden, D. H., van Die, I. and Deelder, A. M. (2001), "Profiles of immunoglobulin M (IgM) and IgG antibodies against defined carbohydrate epitopes in sera of Schistosoma-infected individuals determined by surface plasmon resonance.," *Infection and immunity*, **69**(4): 2396–401.

Verheyen, E. M. and Cooley, L. (1994), "Profilin mutations disrupt multiple actin-dependent processes during Drosophila development.," *Development (Cambridge, England)*, **120**(4): 717–28.

Vervaet, N., Kallio, J. P., Meier, S., Salmivaara, E., Eberhardt, M., Zhang, S., *et al.* (2013), "Recombinant production, crystallization and preliminary structural characterization of Schistosoma japonicum profilin," *Acta Crystallographica Section F: Structural Biology and Crystallization Communications*, **69**(11): 1264–1267.

Vinson, V. K., Archer, S. J., Lattman, E. E., Pollard, T. D. and Torchia, D. a. (1993), "Three-dimensional solution structure of Acanthamoeba profilin-I," *Journal of Cell Biology*, **122**(6): 1277–1283.

Vinson, V. K., Archer, S. J., Lattman, E. E., Pollard, T. D. and Torchia, D. A. (1993), "Three-dimensional solution structure of Acanthamoeba profilin-I.," *The Journal of cell biology*, **122**(6): 1277–83.

Vogl, A. W. (1989), "Distribution and function of organized concentrations of actin filaments in mammalian spermatogenic cells and Sertoli cells.," *International review of cytology*, **119**: 1–56.

Von Lichtenberg, F. (1987), "Consequences of infections with schistosomes.," in D. Rollinson and A. Simpson (eds), *The biology of schistosomes from genes to latrines*.

Walker, A. J. (2011), "Insights into the functional biology of schistosomes.," *Parasites & vectors*, **4**: 203.

Wallar, B. J. and Alberts, A. S. (2003), "The formins: active scaffolds that remodel the cytoskeleton.," *Trends in cell biology*, **13**(8): 435–46.

Wang, Y., Fu, T., Howard, A., Kothary, M. H., Mchugh, T. H. and Zhang, Y. (2013), "Crystal Structure of Peanut (Arachis hypogaea) Allergen Ara h 5," 6–11.

Webb, J. L., Harvey, M. W., Holden, D. W. and Evans, T. J. (2001), "Macrophage nitric oxide synthase associates with cortical actin but is not recruited to phagosomes.," *Infection and immunity*, **69**(10): 6391–400.

Weber, G. (1960), "Fluorescence-polarization spectrum and electronic-energy transfer in proteins.," *The Biochemical journal*, **75**: 345–52.

Webster, J. P., Oliviera, G., Rollinson, D. and Gower, C. M. (2010), "Schistosome genomes: a wealth of information.," *Trends in parasitology*, **26**(3): 103–6.

Wegner, A. (1976), "Head to tail polymerization of actin.," *Journal of Molecular Biology*, **108**: 139–150.

Whitmore, L. and Wallace, B. A. (2008), "Protein secondary structure analyses from circular dichroism spectroscopy: methods and reference databases.," *Biopolymers*, **89**(5): 392–400.

Wilson, M. S., Mentink-Kane, M. M., Pesce, J. T., Ramalingam, T. R., Thompson, R. and Wynn, T. A. (2006), "Immunopathology of schistosomiasis.," *Immunology and cell biology*, **85**(2): 148–54.

Wilson, R. A. and Barnes, P. E. (1974), "The tegument of Schistosoma mansoni: observations on the formation, structure and composition of cytoplasmic inclusions in relation to tegument function.," *Parasitology*, **68**(2): 239–58.

Winder, S. J. and Ayscough, K. R. (2005), "Actin-binding proteins.," *Journal of cell science*, **118**(Pt 4): 651–4.

Witke, W. (2004), "The role of profilin complexes in cell motility and other cellular processes.," *Trends in cell biology*, **14**(8): 461–9.

Witke, W., Podtelejnikov, A. V, Di Nardo, A., Sutherland, J. D., Gurniak, C. B., Dotti, C. and Mann, M. (1998), "In mouse brain profilin I and profilin II associate with regulators of the endocytic pathway and actin assembly.," *The EMBO journal*, **17**(4): 967–76.

Witke, W., Sutherland, J. D., Sharpe, A., Arai, M. and Kwiatkowski, D. J. (2001), "Profilin I is essential for cell survival and cell division in early mouse development.," *Proceedings of the National Academy of Sciences of the United States of America*, **98**(7): 3832–6.

Wu, Z.-D., Lü, Z.-Y. and Yu, X.-B. (2005), "Development of a vaccine against Schistosoma japonicum in China: a review.," *Acta tropica*, **96**(2-3): 106–16.

Xu, Y., Moseley, J. B., Sagot, I., Poy, F., Pellman, D., Goode, B. L. and Eck, M. J. (2004), "Crystal structures of a Formin Homology-2 domain reveal a tethered dimer architecture.," *Cell*, **116**(5): 711–23.

Yang, W., Jones, M. K., Fan, J., Hughes-Stamm, S. R. and McManus, D. P. (1999), "Characterisation of a family of Schistosoma japonicum proteins related to dynein light chains.," *Biochimica et biophysica acta*, **1432**(1): 13–26.

Yarmola, E. G. and Bubb, M. R. (2006), "Profilin: emerging concepts and lingering misconceptions.," *Trends in biochemical sciences*, **31**(4): 197–205.

You, H., Gobert, G. N., Duke, M. G., Zhang, W., Li, Y., Jones, M. K. and McManus, D. P. (2012), "The insulin receptor is a transmission blocking veterinary vaccine target for zoonotic Schistosoma japonicum.," *International journal for parasitology*, **42**(9): 801–7.

Zhang, L.-H., McManus, D. P., Sunderland, P., Lu, X.-M., Ye, J.-J., Loukas, A. and Jones, M. K. (2005), "The cellular distribution and stage-specific expression of two dynein light chains from the human blood fluke Schistosoma japonicum.," *The international journal of biochemistry & cell biology*, **37**(7): 1511–24.

Zhang, S. M., Lv, Z. Y., Zhou, H. J., Zhang, L. Y., Yang, L. L., Yu, X., Zheng, H. and Wu, Z. D. (2008), "Characterization of a profilin-like protein from Schistosoma japonicum, a potential new vaccine candidate," *Parasitology Research*, **102**: 1367–1374.

Zhang, W., Li, J., Duke, M., Jones, M. K., Kuang, L., Zhang, J., Blair, D., Li, Y. and McManus, D. P. (2011), "Inconsistent protective efficacy and marked polymorphism limits the value of Schistosoma japonicum tetraspanin-2 as a vaccine target.," *PLoS neglected tropical diseases*, **5**(5): e1166.

Zhang, Y., Taylor, M. G. and Bickle, Q. D. (1998), "Schistosoma japonicum myosin: cloning, expression and vaccination studies with the homologue of the S. mansoni myosin fragment IrV-5.," *Parasite immunology*, **20**(12): 583–94.

Zhang, Z., Xu, H., Gan, W., Zeng, S. and Hu, X. (2012), "Schistosoma japonicum calcium-binding tegumental protein SjTP22.4 immunization confers praziquantel schistosomulumicide and antifecundity effect in mice.," *Vaccine*, **30**(34): 5141–50.

Zhou, Y. and Podesta, R. B. (1989), "Surface spines of human blood flukes (Schistosoma mansoni) contain bundles of actin filaments having identical polarity.," *European journal of cell biology*, **48**(1): 150–3.

Zigmond, S. H. (2004), "Formin-induced nucleation of actin filaments.," *Current opinion in cell biology*, **16**(1): 99–105.

9 Appendix

9.1 Publications

Recombinant production, crystallization and preliminary structural characterization of *Schistosoma japonicum* profilin

Nele Vervaet, Juha Pekka Kallio, Susanne Meier, Emilia Salmivaara, Maike Eberhardt, Shuangmin Zhang, Xi Sun, Zhongdao Wu, Petri Kursula and Inari Kursula

Acta Cryst. (**2013**). F**69**, 1264–1267

9.2 Risk and safety statements

Following is the list of potentially hazardous materials, and respective hazard and precautionary statements as introduced by the Globally Harmonised System of Classification and Labeling of Chemicals (GHS).

Compound	Chemical Abstracts Service No.	Hazard statements	GHS hazard	Precautionary statements
Ampicillin	69-52-3	H334, H317	GHS08	P280, P261, P302+P352, P342+P311
β-mercaptoethanol	60-24-2	H301, H310, H330, H315, H318, H410	GHS05, GHS06, GHS09	P280 P273, P302+P352, P304+P340, P305+P351+P338+P310
$CaCl_2$	10043-52-4	H319	GHS07	P280, P305+P351+P338
Citric acid	5949-29-1	H319	GHS07	P305+P351+P338
DTT	3483-12-3	H302, H315, H319, H335	GHS07	P280, P301+P312, P302+P352, P403+P233
EDTA	60-00-4	H319	GHS07	P264,P280, P305+P351+P338
Ethanol	64-17-5	H225	GHS02	P210
Ethidium bromide	1239-45-8	H302, H330, H341	GHS06, GHS08	P260, P281, P284, P310
Hydrochloric acid>25%	7647-01-0	H314, H335	GHS05, GHS07	P261, P280, P310, P305+P351+P338
Imidazole	288-32-4	H301, H314, H361	GHS05, GHS06,	P260, P281, P303+P361+P353,

			GHS08	P301+P330+P331, P305+P351+P338, P308+P313
Isopropanol	67-63-0	H225, H319, H336	GHS02, GHS07	P210, P233, P305+P351+P338
Kanamycin	25389-94-0	H360	GHS08	P281, P260, P308+P313
NaOH	1310-73-2	H290, H314	GHS05	P280, P303+P361+P353, P301+P330+P331, P305+P351+P338, P310, P406
SDS	151-21-3	H228, H302, H311, H315, H319, H335	GHS02, GHS06	P210, P261, P280, P312, P305+P351+P338
TCEP	51805-45-9	H314		P280, P305+P351+P338, P310
Tris	1185-53-1	H315, H319, H335	GHS07	P261, P305++P351+P338

9.2.1 GHS hazard statements

H225	Highly flammable liquid and vapor
H228	Flammable solid
H290	May be corrosive to metals
H301	Toxic if swallowed
H302	Harmful if swallowed
H310	Fatal in contact with skin
H311	Toxic in contact with skin
H314	Causes severe skin burns and eye damage
H315	Causes skin irritation
H317	May cause an allergic skin reaction
H318	Causes serious eye damage
H319	Causes serious eye irritation
H330	Fatal if inhaled
H332	Harmful if inhaled
H334	May cause allergy or asthma symptoms or breathing difficulties if inhaled
H335	May cause respiratory irritation
H336	May cause drowsiness or dizziness
H341	Suspected of causing genetic defects
H350	May cause cancer
H360	May damage fertility or the unborn child
H361	Suspected of damaging fertility or the unborn child
H372	Causes damage to organs through prolonged or repeated exposure
H410	Very toxic to aquatic life with long lasting effects

9.2.2 GHS precautionary statements

P201	Obtain special instructions before use
P210	Keep away from heat/sparks/open flames/hot surfaces – No smoking
P233	Keep container tightly closed
P260	Do not breathe dus/fume/gas/mist/vapors/spray
P261	Avoid breathing dus/fume/gas/mist/vapors/spray
P264	Wash thoroughly after handling
P273	Avoid release to the environment

P280	Wear protective gloves/protective clothing/eye protection/face protection
P281	Use personal protective equipment as required
P284	Wear respiratory protection
P310	Immediately call a POISON CENTER or doctor/physician
P312	Call a POISON CENTER or doctor/physician
P406	Store in a corrosive resistant/… container with a resistant inner liner
P501	Dispose of contents/container to…
P301+P312	IF SWALLOWED: Call a POISON CENTER or doctor/ physician if you feel unwell
P302+P352	IF ON SKIN: Wash with soap and water
P304+P340	IF INHALED: Remove victim to fresh air and keep at rest in a position comfortable for breathing
P304+P341	IF INHALED: If breathing is difficult, remove victim to fresh air and keep at rest in a position comfortable for breathing
P308+P313	IF exposed or concerned: Get medical advice/attention
P342+P311	IF experiencing respiratory symptoms: Call a POISON CENTER or doctor/physician
P403+P233	Store in a well-ventilated place. Keep container tightly closed
P301+P330+P331	IF SWALLOWED. Rinse mouth. Do NOT induce vomiting
P303+P361+P353	IF ON SKIN (or hair): Remove/take off immediately all contaminated clothing. Rinse skin with water/shower
P305+P351+P338	IF IN EYES: Rinse cautiously with water for several minutes. Remove contact lenses if present and easy to do – continue rinsing

9.2.3 GHS and hazard symbols

Hazard symbol	GHS symbol	Category
		Explosive
	 GHS03	Oxidizing
	 GHS02	Flammable (extremely – highly)
	 GHS06	Toxic
	 GHS07	Harmful
	 GHS05	Corrosive

GHS09

Dangerous to the environment

GHS08

Health hazard

9.3 Buffers used in the high-throughput thermal stability assay

1	2	3	4	5	6	7	8	9	10	11	12
Sodium Acetate pH 3,5				**MES pH 6,0**				**Imidazole pH 8,5**			
0mM	50mM	150mM	500mM	0mM	50mM	150mM	500mM	0mM	50mM	150mM	500mM
NaCl	NaCl	NaCl	NaCl	NaCl	NaCl	NaCl	NaCl	NaCl	NaCl	NaCl	NaCl
Sodium Acetate pH 4,0				**MES pH 6,5**				**Bicine pH 9,0**			
0mM	50mM	150mM	500mM	0mM	50mM	150mM	500mM	0mM	50mM	150mM	500mM
NaCl	NaCl	NaCl	NaCl	NaCl	NaCl	NaCl	NaCl	NaCl	NaCl	NaCl	NaCl
Citric acid pH 4,0				**Imidazole pH 6,5**				**Glycine pH 9,5**			
0mM	50mM	150mM	500mM	0mM	50mM	150mM	500mM	0mM	50mM	150mM	500mM
NaCl	NaCl	NaCl	NaCl	NaCl	NaCl	NaCl	NaCl	NaCl	NaCl	NaCl	NaCl
Sodium Acetate pH 4,5				**MOPS pH 6,5**				**Glycine pH 10,0**			
0mM	50mM	150mM	500mM	0mM	50mM	150mM	500mM	0mM	50mM	150mM	500mM
NaCl	NaCl	NaCl	NaCl	NaCl	NaCl	NaCl	NaCl	NaCl	NaCl	NaCl	NaCl
Sodium Acetate pH 5,0				**MES pH 7,0**							
0mM	50mM	150mM	500mM	0mM	50mM	150mM	500mM				
NaCl	NaCl	NaCl	NaCl	NaCl	NaCl	NaCl	NaCl				
Citric acid pH 5,0				**HEPES pH 7,0**							
0mM	50mM	150mM	500mM	0mM	50mM	150mM	500mM				
NaCl	NaCl	NaCl	NaCl	NaCl	NaCl	NaCl	NaCl				
Citric acid pH 5,5				**HEPES pH 7,5**							
0mM	50mM	150mM	500mM	0mM	50mM	150mM	500mM				
NaCl	NaCl	NaCl	NaCl	NaCl	NaCl	NaCl	NaCl				
Sodium Acetate pH 6,0				**Imidazole pH 8,0**							
0mM	50mM	150mM	500mM	0mM	50mM	150mM	500mM				
NaCl	NaCl	NaCl	NaCl	NaCl	NaCl	NaCl	NaCl				

10 Erklärung

Erklärung über frühere Promotionsversuche

Hiermit erkläre ich, Nele Vervaet, dass vorher keine weiteren Promotionsversuche unternommen worden sind, oder an einer anderen Stelle vorgelegt wurden.

Hamburg, 17. Juli 2015

Nele Vervaet

Eidesstattliche Versicherung

Hiermit erkläre ich an Eides Statt, dass die vorliegende Dissertationsschrift selbständig und allein von mir unter den angegebenen Hilfsmitteln angefertigt wurde.

Hamburg, 17. Juli 2015

Nele Vervaet